2010

Numerical models for natural fibre composites with stochastic properties

Virk, Amandeep Singh

Numerical models for natural fibre composites with stochastic properties

by

Amandeep Singh Virk

A thesis submitted to the University of Plymouth
in partial fulfilment for the degree of

Doctor of Philosophy

School of Marine Science and Engineering

Faculty of Science and Technology

September 2010

Amandeep Singh Virk

Numerical models for natural fibre composites with stochastic properties

Abstract

Natural fibres are increasingly being considered as the reinforcement for polymer matrix composites as they are perceived to be sustainable being a renewable resource. However, they suffer from higher variability in mechanical properties and concerns about their long-term durability in a moist environment.

In this study the physical properties of the jute fibres were characterised, the fibre length distribution was determined and the fibre cross-section was analysed using digital images. It was observed that the true fibre area followed a log-normal distribution. The fibre area distribution for different geometrical shapes was estimated and the error in the estimated area of assumed fibre cross-section was also determined to assess the applicability of the assumed cross-section.

The mechanical properties of the jute technical fibres from a single batch from South Asia were determined; fibre tensile tests were carried out at ten different gauge lengths between 6 mm and 300 mm and the Young's modulus, strain to failure and ultimate tensile strengths were determined individually. A strong correlation was observed between the fibre strength/fracture strain and fibre gauge length. It was found as the gauge length increases the fibre strength/fracture strain drops. The fibre failure (Strength/Strain) was modelled using Weibull distribution and three statistical models were developed to relate the fibre strength/fracture strain to the fibre gauge length. Examination of tensile test data reveals that the coefficient of variation (CoV) for failure strain is consistently lower than the CoV for fracture stress (strength), as the failure strain is weakly influenced by the fibre cross-section. Hence, failure strain is the more consistent failure criterion and it is recommended to use failure strain as the key design criterion for natural fibre composites in order to improve reliability in the design of these materials.

Different authors have tried to model natural fibre reinforced polymer elastic modulus using micromechanical models and have suggested that further study should include fibre angle and length distribution factors to improve the micromechanical prediction.

This thesis further seeks to validate a novel methodology for the prediction of the tensile modulus and strength of natural fibre composites through careful consideration of each of the parameters in the rule of mixtures along with consideration of the statistical variation inherent in reinforcements extracted from plants.

The tensile modulus and strength of jute fibre reinforced composites manufactured from well characterised fibres was measured experimentally. Six well established micromechanical models were used to predict the composite elastic modulus. Two micromechanical models were used to predict composite strength. For both mechanical properties, the inclusion of a fibre area correction factor to account for the non-circular cross-section of the fibre resulted in an improved prediction of the respective mechanical properties.

Table of Contents

List of Appendices

Appendix – A (on CD Rom)

A1 – Composites Part A: Applied Science and Manufacturing, 2010, 41(10), 1329-1335.

A2 – Composites Part A: Applied Science and Manufacturing, 2010, 41(10), 1336-1344.

A3 – Journal of Natural Fibres, 7(3), 2010, 216-228.

A4 – Materials Science and Technology, 2010, 26(x), yyy-zzz.

A5 – Composites Science and Technology, June 2010, 70(6), 995-999.

A6 – Composites Part A: Applied Science and Manufacturing, November 2009, 40(11), 1764-1771.

A7 – Materials Science and Technology, October 2009, 25(10), 1289-1295.

Appendix – B

B1 – Maximise the likelihood method

B2 – Confidence bounds on the Weibull parameters

B3 – Anderson-Darling (AD) goodness of fit test

B4 – Coefficient of variation for Weibull Distribution

B5 – Dyeing jute fibres

B6 – Specimen tensile test results

B7 – Specimen axial Poisson's ratio

B8 – Micrograph fibre volume fraction

B9 – Micrograph fibre angle distribution parameters

B10 – Fibre orientation factor calculated from fibre distribution

B11 – Weibull plots of raw data

B12 – Weibull distribution literature survey

List of Figures

List of Tables

Glossary

The natural fibres glossary could be found at

http://www.tech.plym.ac.uk/sme/MATS324/MATS324A9 FibreGlossary.htm

Nomenclature

a	Slope of Weibull shape parameter
a_n	Proportion of fibres making θ angle to applied load
a_x	Size of super-ellipse in x-axes
b	Intercept of Weibull shape parameter
b_y	Size of super-ellipse in y-axes
c	Slope of Weibull scale parameter
d	Intercept of Weibull scale parameter
E_1	Composite modulus in fibre direction (GPa)
E_2	Composite modulus in direction transverse to the fibre direction (GPa)
E^*	Composite modulus (GPa)
E_f	Fibre modulus (GPa)
E_m	Matrix modulus (GPa)
l	Fibre test gauge length (mm)
l_0	Fibre reference length (mm)
L	Fibre length (mm)
m	Shape parameter for super-ellipse in x-axes
n	Shape parameter for super-ellipse in y-axes
r_0	Fibre radius
R	Half of inter-fibre spacing
T_A	Fibre area
T_L	Fibre length (mm)
V_f	Fibre volume fraction
V_m	Matrix volume fraction
x_i	Cartesian coordinate
y_i	Cartesian coordinate
β	Weibull distribution shape parameter
β_{Linear}	Weibull distribution shape parameter for linear model
β_{Log}	Weibull distribution shape parameter for natural log model
β_{MDS}	Weibull distribution shape parameter for multiple data set model

ε	Error in the estimated super-ellipse shape parameter
η	Weibull distribution scale parameter (MPa)
η_d	Fibre diameter distribution factor
η_l	Length distribution factor
η_{Linear}	Weibull distribution scale parameter for linear model (MPa)
η_{Log}	Weibull distribution scale parameter for natural log model (MPa)
η_{MDS}	Weibull distribution scale parameter for multiple data set model (MPa)
η_o	Fibre orientation distribution factor
η_p	Weibull distribution predicted scale parameter (MPa)
η_w	Weibull distribution scale parameter for weak-link scaling (MPa)
θ	Angle of applied load to fibres
κ	Fibre area correction factor
$\lambda_{T'}$	Log-normal distribution scale parameter
μ'	Log-normal distribution location parameter
$\mu_{apparent}$	Geometric mean of apparent fibre area
μ_{geo}	Geometric mean
μ_N	Normal distribution location parameter (mean)
μ_{true}	Geometric mean of true fibre area
v_f	Fibre Poisson's ratio
v_m	Matrix Poisson's ratio
ξ	Reinforcing efficiency
σ	Fibre strength (MPa)
σ_c	Unidirectional composite tensile strength (MPa)
σ_{cu}	Ultimate composite tensile strength (MPa)
σ_f	Fibre tensile strength (MPa)
σ_{geo}	Geometric standard deviation
σ_N	Normal distribution scale parameter (standard deviation)
σ_{max}	Matrix tensile strength (MPa)
$(\sigma_m)_{\varepsilon f}$	Matrix stress at strain equal to fibre failure strain (MPa)
φ_x	Fibre angle (degree)
Γ	Gamma function

Abbreviation

CDF	Cumulative Distribution Function
CDFWLS	Cumulative Distribution Function with Weak-Link Scaling
CLAHE	Contrast-Limited Adaptive Histogram Equalization
CLSM	Confocal Laser Scanning Microscope
CoV	Coefficient of Variation
CSA	Cross-Sectional Area
FACF	Fibre Area Correction Factor
GOFN	Goodness Of Fit Number
LIM	Linear Interpolation Model
MDS	Multiple Data Set
MLE	Maximum Likelihood parameter Estimation
NLIM	Natural Logarithmic Interpolation Model
PDF	Probability Density Function
$RoM_{\|\|}$	Rule of Mixture
SD	Standard Deviation
WLSM	Weak-Link Scaling Model

Acknowledgements

This research project would not have been possible without the support of many people.

The author is immensely thankful to his supervisors Dr John Summerscales and Dr Wayne Hall (Griffith School of Engineering – Griffith University) for continuingly assisting, supporting and guiding him throughout the research degree. The author is also grateful for the comments of Dr Miggy Singh on the MPhil-to-PhD transfer report.

The author is thankful to the University of Plymouth for the financial assistance to conduct this research. The author is also thankful to Fine Tubes Ltd. for providing the software for the research.

The author is also grateful for assistance with experiments and/or for helpful discussions. The following people should be acknowledged: Terry Richards, Greg Nash, Nilmini Dissanayake, Richard Cullen and David Harman. The omission of any appropriate name here does not constitute a deliberate rebuff. The author is also grateful to anonymous referees for their respective comments on the manuscripts of journal papers.

The author would like to offer his gratitude to his grandparents, Nana ji, parents and sisters for their love, understanding and encouragement throughout my lifetime. The author would also like to thank Anu for the affection and support. Special thanks also to all his friends who always have been there. Above all the author would like to thank God for everything.

Author's Declaration

At no time during the registration for the degree of Doctor of Philosophy has the author been registered for any other University award. This study has been financed by University of Plymouth.

Relevant scientific seminars and conferences were attended. Papers were presented at some of these meetings and subsequently refereed and published in journals. The details are on the following pages.

Signed Amandeep Singh Virk

Date 6-12-2010

Word count – 17000

Training attended:

Introduction to statistics, July 2008

Presentation skills, 2009

Transfer report, 2009

Introduction to programming in C++, September 2007

Introduction to Abaqus, September 2007

Journal papers:

1. J Summerscales, N Dissanayake, W Hall and AS Virk, A review of bast fibres and their composites. Part 1: fibres as reinforcements, Composites Part A: Applied Science and Manufacturing, 2010, 41(10), 1329-1335.
2. J Summerscales, N Dissanayake, W Hall and AS Virk, A review of bast fibres and their composites. Part 2: composites, Composites Part A: Applied Science and Manufacturing, 2010, 41(10), 1336-1344.
3. AS Virk, W Hall and J Summerscales, Physical characterisation of jute technical fibres: fibre dimensions, Journal of Natural Fibres, 7(3), 2010, 216-228.
4. AS Virk, W Hall and J Summerscales, Modelling tensile properties of jute fibres, Materials Science and Technology, 2010, 26(x), yyy-zzz (corrected proofs now on-line).
5. AS Virk, W Hall and J Summerscales, Failure strain as the key design criterion for fracture of natural fibre composites, Composites Science and Technology, June 2010, 70(6), 995-999.
6. AS Virk, W Hall and J Summerscales, Multiple data set (MDS) weak-link scaling analysis of jute fibres, Composites Part A: Applied Science and Manufacturing, November 2009, 40(11), 1764-1771.
7. AS Virk, W Hall and J Summerscales, Tensile properties of jute fibres, Materials Science and Technology, October 2009, 25(10), 1289-1295.

Conferences:

1. 'Bio-Composites'-The Next Generation of Composite, 25 September 2008.
2. ICCM-17, 27-31 July 2009.
3. SAMPE/BCS Annual Students' Seminar, 24 November 2009, Presented paper "Failure strain as the key design criterion for fracture of natural fibre composites".

1. Introduction

Natural fibres can be divided into three groups, vegetable, animal or mineral fibres. Vegetable fibres can be wood (further subdivided into softwood or hardwood) or non-wood (bast, leaf or seed-hair) fibres [1]. Bast fibres are those "obtained from the cell layers surrounding the stems of various plants" [2]. Natural bast fibres are increasingly being considered as the reinforcement for polymer matrix composites as they are perceived to be sustainable being a renewable resource. Natural fibres, and their use as the reinforcement in composites, have recently been reviewed by John and Thomas [3], Hill and Hughes [4] and Summerscales et al [5, 6] (the author of this thesis is a co-author of the latter two references which are included at Appendix A1-A2). Natural bast fibres are composed primarily of cellulose. Cellulose micro fibrils have a potential Young's modulus of ~140 GPa [7] which is comparable to that of man-made aramid [Kevlar/Twaron] fibres at ~125 GPa. Natural fibre offers some additional benefits of being a lower cost and lower density material with higher specific mechanical properties. Natural fibres are non-hazardous and nonabrasive which leads to fewer health and safety issues. Using natural fibres as composite reinforcement could reduce our dependence on non-renewable resources, lower pollutant emission and green house gas emission. Being biodegradable natural fibres can be disposed of easily at the end of product life or energy can be recovered by incineration of the composite. Initial results from a quantitative life cycle assessment have been presented by Dissanayake et. al. [8, 9]. Furthermore, natural fibre composites present good acoustic insulation properties [10].

For the fibre reinforced polymer-matrix composites, the strength and stiffness of the reinforcing fibres dominate the structural performance of the composite. Five main factors influence this fibre contribution: the mechanical (elastic) properties of the fibres; the fibre-resin interactions; the fibre volume fraction; the fibre orientation and length of the fibres in the composite.

However, natural fibres suffer from higher variability in mechanical properties and concerns about their long-term durability in a moist environment as they absorb moisture. The fibre properties depend on the conditions during growth, maturity at harvest, fibre processing technique and the moisture content of the fibres. Poor wettability and inadequate adhesion between natural fibres and matrix leads to under-utilisation of the fibre potential. The non-uniform fibre cross-section adds to the high variability in the fibre mechanical properties.

This high variability in their mechanical properties is one of the factors constraining the widespread use of natural fibres as the reinforcement in polymer matrix composites. Moreover this variability leads to difficulty in accurately predicting the composite properties using existing micromechanical models. Thus, an in-depth understanding of the natural variation of the fibre physical and mechanical properties is necessary for these fibres to emerge as a realistic alternative to synthetic fibre reinforcements for structural composites.

The bast fibres which are currently attracting the most interest are flax and hemp (in temperate climates) or jute and kenaf (in tropical climates). Jute is relatively low-cost and a commercially available fibre. The investigation therefore aims to enhance understanding of the stochastic nature of jute fibres with reference to the focus on natural fibre reinforced polymer matrix composite structures and to improve the prediction of the mechanical properties (specifically tensile modulus and strength).

2. Experiments

Jute technical fibres from a single source in South Asia were used throughout the study. The jute fibres were in sliver form (processed using carding technique to give 90-95% uniaxial orientation) as shown in Figure 1. The physical and mechanical properties of the jute fibres were characterised. Then the fibres were used to manufacture composite plates to evaluate the composite properties and compare experimental properties with micromechanics model predictions to assess the applicability of the models.

Figure 1: Jute fibres sliver

2.1. Fibre physical characterisation

2.1.1. Fibre length distribution

The fibre length distribution of the jute fibres in this batch of fibres was determined according to ISO 6989 - 'Method A' [11]. The lengths of the fibres were measured and recorded individually under a light tension using a steel rule. The length of 700 jute fibres were recorded.

2.1.2. Fibre cross-sectional area distribution

The fibre cross-sectional area is an important physical property which is used to calculate the fibre mechanical properties (modulus and strength) therefore, accurate determination of the fibre cross-sectional area is important. The 'true' cross sectional area of jute fibres was determined by digital image analysis of 106 fibre cross-sections. Random samples of jute technical fibres were considered for this study. The fibre samples were bonded to a cellulose acetate sheet using epoxy adhesive for accurate fibre alignment and for ease of fibre handling. The cellulose acetate sheet with the jute fibres was cast into potting compound (epoxy resin). The cast jute fibre samples were ground flat in stages on 180, 240, 400, 600, 800, 1200 and 2500 grit paper and then subsequently polished with 6 µm and then 1 µm diamond. The potted sample was washed thoroughly with dilute detergent in an ultrasonic bath between each stage. The cross-section of each fibre was examined using an Olympus LEXT OLS3000 Confocal Laser Scanning Microscope (CLSM serial number – 6E23013) and LEXT OLS image analysis software version 6.03. Figure 2 shows the cross section of two typical technical fibres.

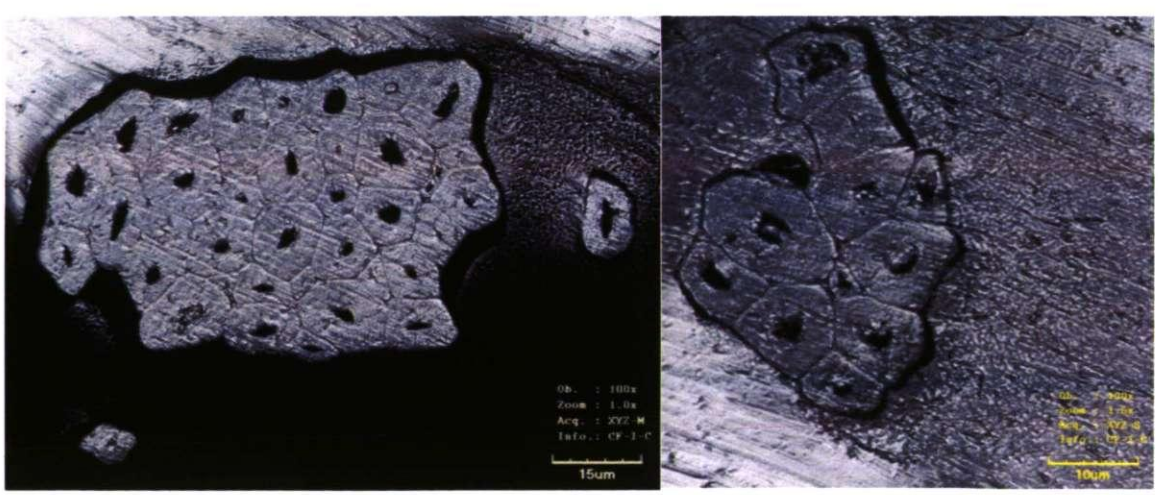

Figure 2: Typical fibre cross sections

The digital images acquired using CLSM were processed using Matlab R2008a [12-14]. The outline of the fibre was selected manually to leave only the area of interest (fibre cross-section) in the digital image (see Figure 3). The fibre cross sectional area was calculated using the vertices [15] of the remaining image.

$$Area = \frac{1}{2}\sum_{i=1}^{N}(x_{i+1}+x_i)(y_{i+1}-y_i) \qquad (1)$$

where x_i and y_i are coordinate values of i^{th} vertices and N is number of vertices.

The Canny edge detection method [12-14] was used to detect the fibre edges, by looking for local maxima of the intensity gradient of the original greyscale image masked to remove area of insignificance. A Gaussian filter was used to smooth the noise in the masked image then a gradient was calculated using the derivative [12-14]. The Canny Edge Image (CEI) was translated and rotated to align the maximum fibre dimension with the horizontal axis (x-axis) of the coordinate system and to place the origin of the coordinate system at the midpoint of the maximum fibre dimension. The maximum and minimum fibre coordinate in ordinate (y-axis) were determined. The fibre image was translated in ordinate to make the absolute value of maximum and minimum fibre coordinates in y-axes equal.

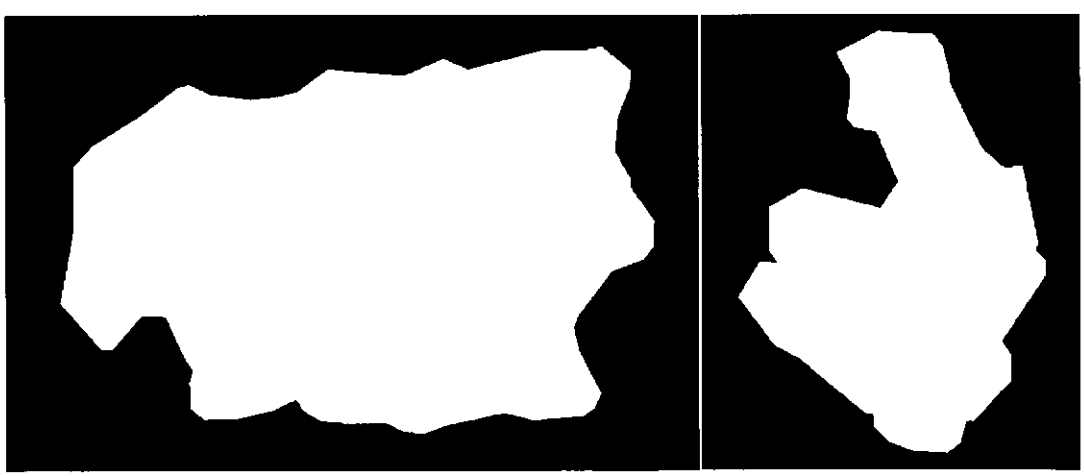

Figure 3: The mask used to identify true fibre shape and area of fibres shown in Figure 2

Two circles were overlaid on the Canny edge image. The maximum x- and y-coordinate values were used to define the radius of the major and the minor circles

respectively (Note: the minor circle diameter is formed by the projected width of the fibre at 90 degrees to the maximum projected width of the fibre: it is not the smallest circle which can be inscribed in the fibre image). The area of the major and minor circles was determined. The major and minor circles are concentric.

An ellipse was constructed to bound the outer shape of the fibre. The maximum coordinate values in *x* and *y* axes were used to define the semi-major axis and semi-minor axis of the ellipse respectively. The area of the ellipse was determined.

The convex hull [16] is the shape formed by a continuous line which follows a straight path between each projection of the shape such that no concave region remains. The convex hull was calculated from the Canny edge image to bound the outer shape of each fibre as shown in Figure 4. The convex hull area was determined using Equation 1 [15] to characterise the fibre area.

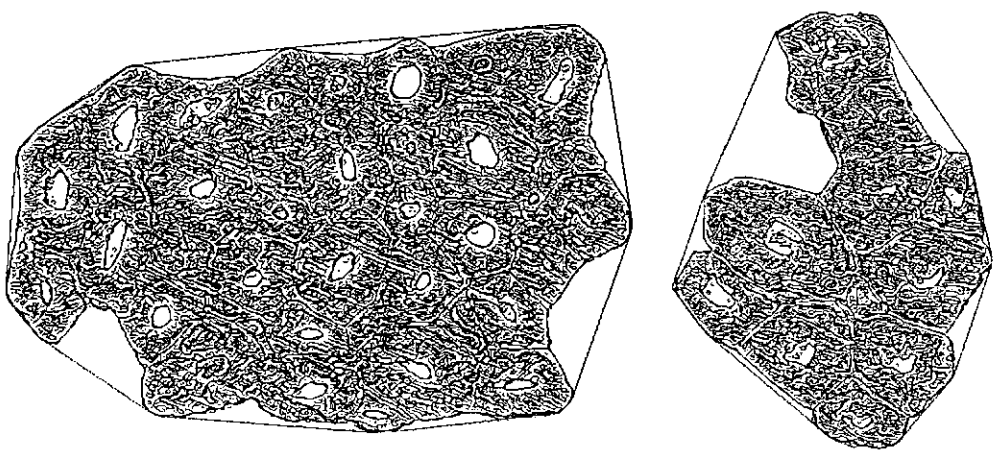

Figure 4: Convex Hull of true fibre shape for the fibres in Figure 2

A super-ellipse [17] was used to bind the outer shape of the fibre. The super-ellipse is defined by Equation 2:

$$\left|\frac{x}{a_x}\right|^m + \left|\frac{y}{b_y}\right|^n = 1 \qquad (2)$$

where a_x and b_y define the size of the super-ellipse, m and n define the shape of the super-ellipse. The parameters a_x, b_y, m and n are all positive numbers. The size parameters, a_x and b_y of the super-ellipse were given by the maximum coordinate value in abscissa and ordinate respectively (these are the diameters of the major and minor circles and are concentric with those circles). The shape parameters, m

and n of the super-ellipse were estimated from the fibre convex hull by minimising 'ε' in Equation 3, using the Nelder-Mead simplex search method [18, 19]:

$$\varepsilon = \sum_{i=1}^{N} abs\left[\left\{\left|b_y\right|\bullet\left(1-\left|\frac{x_i}{a_x}\right|^m\right)^{1/n}\right\}-\left|y_i\right|\right] \tag{3}$$

where a_x and b_y define the size of the super-ellipse, N is number of vertices of the convex hull, x_i and y_i are the coordinates of the convex hull vertices. The super-ellipse parameters were estimated from the fibre convex hull to reduce the computational effort. The area bound by the super-ellipse was determined.

Figure 5 shows the fibre major and minor circle, ellipse, convex hull and super ellipse overlaid on the same graph.

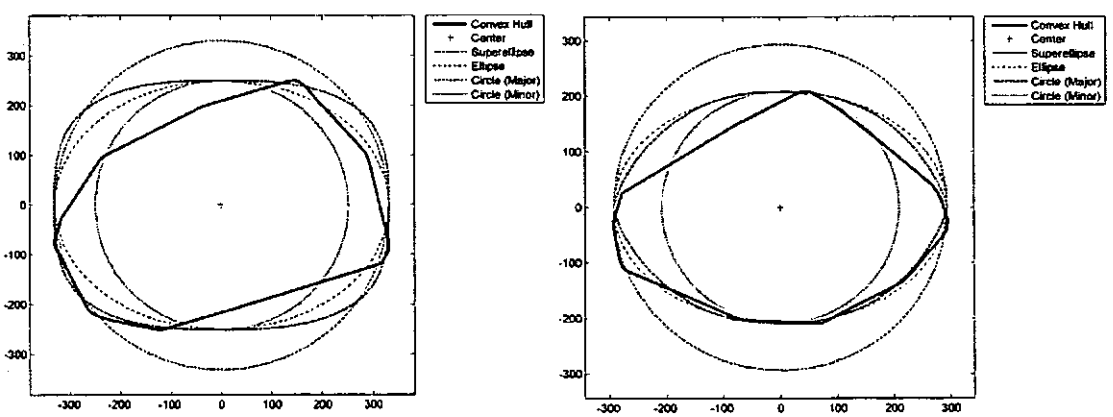

Figure 5: The five shapes fitted to the convex hull of the fibres shown in Figure 2

2.2. Fibre mechanical properties

The tensile properties of retted technical jute fibres (extracted from a 127 mm wide roll with an areal weight of 880 gm/m^2) were assessed. Jute technical fibres were mounted on test cards (based on Grafil Test 101.13 [20]) with Devcon® 2 Ton® epoxy adhesive for ease of handling and subsequent tensile testing. A schematic representation of the test card is shown in Figure 6. Ten gauge lengths were considered, i.e. 6 mm, 10 mm, 20 mm, 30 mm, 50 mm, 100 mm, 150 mm, 200 mm, 250 mm and 300 mm. These gauge lengths were selected based on an analysis of the fibre lengths found in a representative sample of the jute. The fibres gauge lengths from 6 mm to 300 mm, covered 93.3% of fibre lengths, estimated by

integrating the fibre length distribution (log-normal) probability density function between 6 and 300 mm (see section 3.1.1).

At least one hundred individual fibres were tested at each of five gauge lengths (6 mm, 10 mm, 20 mm, 30 mm, 50 mm) and at least fifty individual fibres were tested at each of five additional gauge lengths (100 mm, 150 mm, 200 mm, 250 mm and 300 mm). A total of 785 fibre tests were carried out. The fibre length was measured to an accuracy of ±1 mm at each end. Above 50 mm gauge length fewer fibres were tested because they are more difficult to find within the material supplied and it was observed that the spread of test results decreased as the fibre gauge length increased.

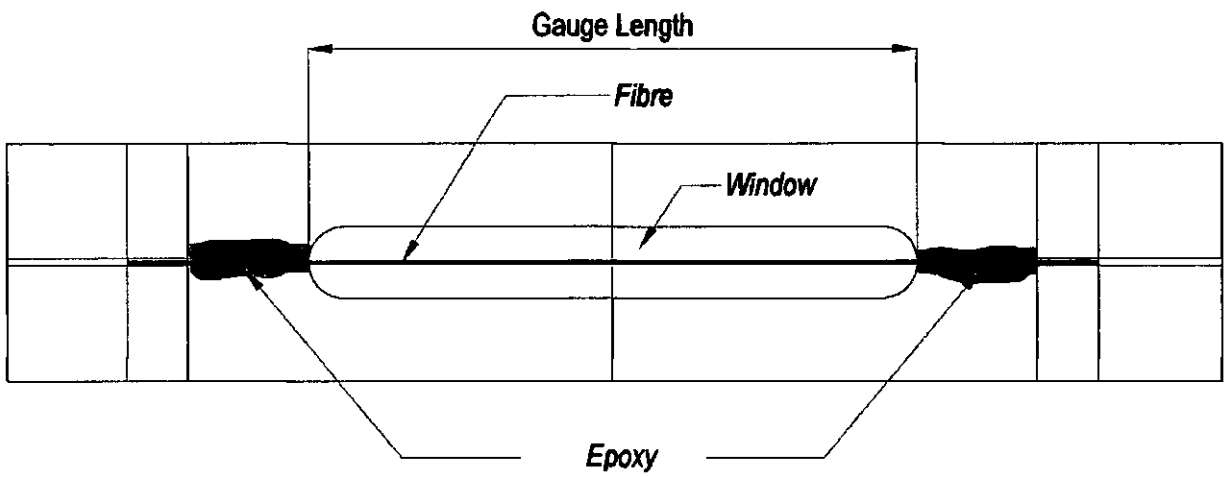

Figure 6: Single fibre mounted on a test card

Before testing, measurements of fibre 'diameter' were taken at 1 mm intervals along the fibre length within the window of the test card for fibres with gauge length ≤ 50 mm and at 10 mm intervals for fibres with gauge lengths ≥ 100 mm using an Olympus BX60MF optical microscope (serial number – 5M04733) and analySIS™ image analysis software. The apparent cross-sectional area of each fibre was calculated from the mean fibre 'diameter' assuming a circular cross-section.

Table 1 shows the mean fibre diameters and standard deviations at each fibre length.

Note that "diameters" here is used as in the textile industry to represent the characteristic dimension normal to the principal axis of the fibre. The textile industry normally measure fibre fineness as a linear density in dtex (grams/10 km). However, for engineering purposes in the stress analysis of composites we need stress in

Pascal (N/m^2). The conversion between units is not straightforward because of the difficulty of identifying an accurate density for the (primarily) cellulose material and the presence of lumen (central void space) in the fibres. Typical section of a fibre is shown in Figure 2. Clearly the fibre is not circular and thus the assumption of a circular cross-section is therefore one error source in the calculation of the mechanical properties below. The potential error is likely to scale with the measured fibre diameter.

Table 1: Mean fibre diameters (standard deviations in parentheses).

Fibre Length [mm]	*Diameter [µm]*
6	53.89 (13.96)
10	57.67 (10.99)
20	61.06 (13.48)
30	59.59 (13.67)
50	61.53 (18.62)
100	64.34 (13.93)
150	61.07 (9.91)
200	64.59 (12.32)
250	62.67 (11.54)
300	61.23 (10.83)
All	**60.16 (13.79)**

Fibre dimension measurements and mechanical testing were conducted between 16 April and 19 September 2008. The mean test temperatures were in the range 11-20°C±1°C and 43-100%RH±7%.

The fibre test specimens mounted in the test cards shown in Figure 6 were secured in the tensile test machine grips. The test card was cut at the middle with scissors before starting the tensile test. The tests were carried out on an Instron 3345 K1669 universal testing machine with an Instron 500N load cell (model 2519-104, serial number – 52967), according to Grafil method 101.13 [20], modified to account for different fibre lengths at a constant strain rate of 0.01 min^{-1} for all the fibre gauge lengths. The test is broadly similar to ASTM D3379-75 [21].

The load cell was calibrated with dead weights up to 2N force: a consistent error of less than 5% of the target force was observed.

2.3. Statistical strength and fracture strain distribution

2.3.1. Weibull point estimate

The natural and man-made fibres exhibit considerable strength and failure strain variations. Weibull statistics are often used to characterise the statistical distribution of the fibre strengths. Reviews have been published of Weibull statistics for the probabilistic strength of materials [22], for their use in relation to filament strengths [23], for fracture theories [24] and for fibrous composite materials [25]. A brief literature review of the Weibull distribution is given in Appendix B12. Therefore, the failure strength and failure strain distribution of natural fibres were described by two-parameter Weibull distributions [26-31]. The two-parameter Weibull Probability Density Function (PDF) [32, 33] is:

$$f(\sigma) = \frac{\beta}{\eta}\left(\frac{\sigma}{\eta}\right)^{\beta-1} e^{-\left(\frac{\sigma}{\eta}\right)^{\beta}} \tag{4}$$

where β is the shape parameter (Weibull modulus), η is the scale parameter (characteristic strength or strain) and σ is measured fibre strength. **Note:** σ can be substituted by ε for failure strain throughout the following text.

Integration of the PDF yields the two-parameter Weibull Cumulative Distribution Function (CDF):

$$F(\sigma) = 1 - e^{-\left(\frac{\sigma}{\eta}\right)^{\beta}} \tag{5}$$

The Weibull distribution parameters in Equations 4 and 5 for each of the ten gauge lengths were calculated using the Maximum Likelihood parameter Estimation (MLE) method [34] detailed in Appendix B1.

2.3.2. Weak-Link Scaling Model (WLSM)

The fibre tensile properties are limited by the presence of critical flaws. If a fibre comprises a series of elements (or links) then the strength of that fibre is governed by the weakest link. A longer fibre contains more links than a shorter one and the probability of a critical flaw therefore increases with fibre length, resulting in longer fibres having a lower tensile strength (on average) [35]. This follows from Griffith's

crack theory [35]. The strength at one fibre length is often scaled to estimate the strength at a different length. This physical model is often referred to as the principle of 'weak link scaling'. The relationship of the strength (or failure strain) to the fibre length is modelled using the Weibull Cumulative Distribution Function with Weak-Link Scaling [26-31] (CDFWLS):

$$F(\sigma) = 1 - e^{-\frac{l}{l_0}\left(\frac{\sigma}{\eta_w}\right)^{\beta}} \tag{6}$$

where η_w is the scale parameter (characteristic strength) for the Weibull distribution with weak link scaling, l is the designated fibre length and l_0 is the reference length. For simplicity, the reference length is generally normalised to 1. The distribution parameters were estimated using MLE method.

The relationship between the characteristic strength (or strain) for the two-parameter Weibull CDF calculated using Equation 5 and Weibull CDFWLS computed using Equation 6 can be found by equating these two equations, to give:

$$F(\sigma) = 1 - \exp\left\{-\frac{l}{l_0}\left(\frac{\sigma}{\eta_w}\right)^{\beta}\right\} = 1 - \exp\left\{-\left(\frac{\sigma}{\eta}\right)^{\beta}\right\} \tag{7}$$

Equation 7 can be simplified to:

$$\frac{\eta_w}{\eta} = \sqrt[\beta]{\frac{l}{l_0}} \tag{8}$$

where η_w is the scale parameter (characteristic strength) for the Weibull distribution with weak-link scaling (Equation 6), η is the scale parameter (characteristic strength) for the standard Weibull distribution (Equation 5), l is the fibre test length and the reference length l_0 was chosen to be 1 mm for mathematical convenience.

Weak-link scaling predictions assume the characteristic strength can be scaled for any fibre length from a single weak link (characteristic strength) point estimate at a chosen fibre test gauge length. The appropriate length, l, is used in Equation 8 to yield the corresponding prediction of η. To distinguish between predicted and measured estimates of η, we use η_p for a predicted value and hence Equation 8 is rewritten as:

$$\frac{\eta_w}{\eta_p} = \sqrt[\beta]{\frac{l}{l_0}} \tag{9}$$

2.3.3. Multiple Data Set (MDS) Weak-link scaling model

The relationship between the strength (and failure strain) distribution and the fibre length can be improved when two or more strength or fracture strain data sets (at different fibre lengths) are used to better estimate β and η_w. These parameters for two or more strength or fracture strain data sets can be estimated by the MLE method [34]. The PDF for Weibull distribution with weak link scaling is obtained from the derivative of the CDF (Equation 6) with respect to failure stress.

$$f(\sigma)=\frac{d}{d\sigma}F(\sigma)$$

$$f(\sigma)=\frac{l}{l_0}\frac{\beta}{\eta_w}\left(\frac{\sigma}{\eta_w}\right)^{\beta-1}e^{-\frac{l}{l_0}\left(\frac{\sigma}{\eta_w}\right)^{\beta}} \tag{10}$$

The Likelihood function for Multiple Data Sets (MDS) Weibull PDF with weak-link scaling is given by:

$$L(\sigma|\beta,\eta_w,l_0)=\sum_{i=1}^{k}\prod_{r=1}^{n}\left\{\left(\frac{l_i}{l_0}\right)\left(\frac{\beta}{\eta_w}\right)\left(\frac{\sigma_r}{\eta_w}\right)^{\beta-1}e^{-\frac{l_i}{l_0}\left(\frac{\sigma_r}{\eta_w}\right)^{\beta}}\right\} \tag{11}$$

where i is data set number, k is the number of gauge lengths and l_i is the fibre test gauge length for data set i.

For computational convenience the log-likelihood function is used:

$$\Lambda(\sigma|\beta,\eta,l_0)=\sum_{i=1}^{k}\left[n_i\ln\left(\frac{l_i}{l_0}\right)+n_i\ln\left(\frac{\beta}{\eta_w}\right)+\sum_{r=1}^{n}\ln\left\{\left(\frac{\sigma_r}{\eta_w}\right)^{\beta-1}\right\}-\sum_{r=1}^{n}\left\{\frac{l_i}{l_0}\left(\frac{\sigma_r}{\eta_w}\right)^{\beta}\right\}\right] \tag{12}$$

The log-likelihood function is maximised by Newton's method [19, 36, 37] to estimate the distribution parameters for the MDS weak-link scaling model.

2.3.4. Empirical Models

In contrast to the physical-based models (weak link scaling, MDS-weak link scaling), empirical or phenomenological models can be developed from a (limited) database of experimental results. A number of authors have used the principle of weak link scaling in an attempted to fully characterise the statistical distribution of synthetic and natural fibre properties but have found limited success [26, 38, 39]. Therefore, two empirical models: (a) a linear and (b) a Natural Logarithmic Interpolation Model (NLIM) for the estimation of the fibre properties were developed to better model the effect of fibre length on the strength and fracture strain of a fibre.

2.3.4.1. Linear Interpolation Model (LIM)

For the linear model the shape parameter, β, and the scale parameter, η in Equation 4 are replaced by the linear relationship between the fibre length given by Equation 13,

$$\begin{aligned}\beta &= aL_i + b \\ \eta &= cL_i + d\end{aligned} \tag{13}$$

where *a* and *c* are the slope, and *b* and *d* are the intercept for the shape parameter and scale parameter respectively. L_i is given fibre length.

Replacing the shape parameter and the scale parameter in the *PDF* by the linear relationship yields,

$$f(\sigma) = \left(\frac{aL_i + b}{cL_i + d}\right)\left(\frac{\sigma}{cL_i + d}\right)^{aL_i+b-1} e^{-\left(\frac{\sigma}{cL_i+d}\right)^{aL_i+b}} \tag{14}$$

Thus, the Weibull Likelihood function is,

$$L(\sigma|a,b,c,d) = \sum_{i=1}^{k}\prod_{r=1}^{n}\left(\left(\frac{aL_i + b}{cL_i + d}\right)\left(\frac{\sigma_r}{cL_i + d}\right)^{aL_i+b-1} e^{-\left(\frac{\sigma_r}{cL_i+d}\right)^{aL_i+b}}\right) \tag{15}$$

And the log-likelihood function is,

$$\Lambda = \sum_{i=1}^{k}\left\{n_i \times \ln\left(\frac{aL_i + b}{cL_i + d}\right) + \sum_{r=1}^{n}\ln\left\{\left(\frac{\sigma_r}{cL_i + d}\right)^{aL_i+b-1}\right\} - \sum_{r=1}^{n}\left(\frac{\sigma_r}{cL_i + d}\right)^{aL_i+b}\right\} \tag{16}$$

The parameters for the linear relationship are estimated by maximising the log-likelihood function using Newton's method [19, 36, 37].

The distribution parameters were estimated for the strength and fracture strain by maximising the log-likelihood function for all of the experimental observations at all of the fibre lengths.

2.3.4.2. Natural-Logarithmic Interpolation Model (NLIM)

As in previous section, parameters for a logarithmic relation between the shape parameter or the scale parameter and the fibre length can be optimised. The linear relations between shape and scale parameter and fibre length are simply replaced with the logarithmic functions,

$$\begin{aligned}\beta &= a\ln(L_i) + b \\ \eta &= c\ln(L_i) + d\end{aligned} \tag{17}$$

The parameters for the natural logarithmic relationship were also estimated by maximising the log-likelihood function using Newton's method [19, 36, 37] for the strength and fracture strain experimental observation at all of the fibre lengths.

2.4. Jute/Epoxy Composite

2.4.1. Dyeing Fibres

Jute fibres are primarily composed of cellulose [40] and do not show up in micrographic samples when clear resin is used. Procion MX cold fibre reactive dye was used [40-42] to colour the fibres black following the procedure described by Milner [42] detailed in Appendix B5. The matrix was pigmented white (giving a Luminosity Contrast Ratio of 21) [43]. High contrast allows digital image analysis to easily separate the foreground information (fibres) from the background information (matrix) in micrographs.

2.4.2. Comparison of tensile properties of un-dyed and dyed fibres

A total of 104 dyed fibres were tested according to Grafil method 101.13 [20], at a constant strain rate of 0.01 min^{-1} to determine the effect of dyeing on the fibre mechanical properties. Single fibres having 50 mm gauge length were mounted on the test cards. The apparent fibre diameter (projected width) was measured at 1 mm intervals along the fibre gauge length to calculate a mean apparent fibre diameter. The cross-sectional area of each fibre was calculated from the mean apparent fibre diameter assuming circular cross-section to calculate the stress in the fibre. The test is broadly similar to ASTM D3379-75 [21]. The mean mechanical properties of dyed fibres and as-received fibres (50 mm gauge length) [section 3.2.1] are shown in Table 2.

Table 2: Mean Young's modulus, fibre strength and fracture strain (standard deviations in parentheses).

	Dyed Fibres	***As-received Fibres***
Elastic Modulus [GPa]	29.56 (7.4)	28.3 (8.8)
Strength [MPa]	378.2 (151)	336.3 (132)
Strain to failure [%]	1.16 (0.35)	1.11 (0.34)

No significant change in the mechanical properties of the fibres was observed after dyeing as the variation in the properties was less than one-third of a standard deviation. Wilcoxon rank sum test was performed on the fibre tensile test data. The test accepted the null hypothesis that the data is from independent samples having identical continuous distributions with equal medians [44].

2.4.3. Manufacturing of composite plate

Composite plates were manufactured by resin infusion with a flow medium/distributor mesh [45-49] using as received (three plates) and dyed jute fibres (one plate) with no pigment or white pigment respectively. The epoxy was pigmented white[1] to improve the contrast ratio between dyed fibres and the matrix. A flat glass plate was used as a mould. The reinforcement was laid directly on the pre-released mould surface. To achieve uniform test plate thickness pre-released Perspex sheet was placed on top of reinforcement fibres and spacers were inserted between the glass plate and the Perspex sheet to control the composite plate thickness as shown in Figure 7.

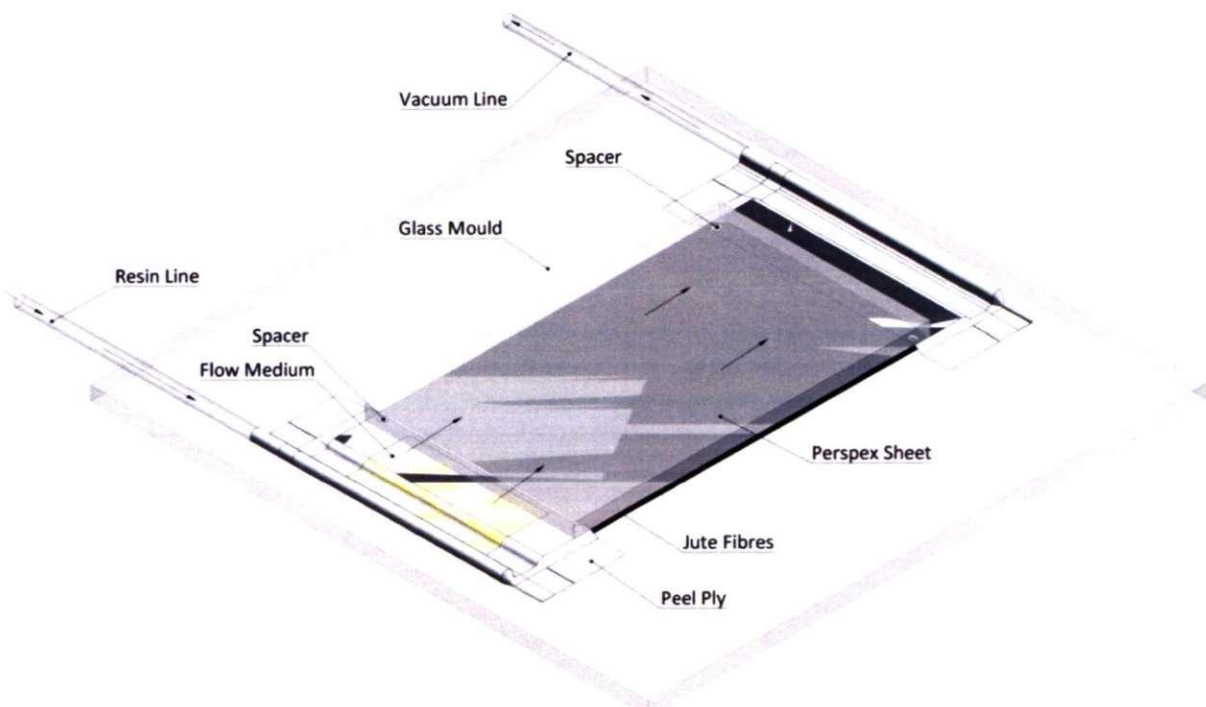

Figure 7: Resin infusion arrangement

[1] West System 501 White Pigment for epoxy.

The peel ply was laid near the resin and vacuum line ends to assist in removing the cured plate. This arrangement was bagged and a vacuum of 10-15 mbar drawn before the resin was infused along the fibre direction. The infusion resin system was Sicomin^{TM} 8100 epoxy resin and SD8822 hardener mixed in 100/31 ratio by weight [50].

The infused plates were cured for 24 hours at ambient temperature and then post-cured at 60 °C for 16 hours in an oven according to the resin manufacturer's recommendation.

2.4.4. Mechanical properties of the composites

The tensile test specimens were machined parallel to the fibre direction from the resin infused plates as shown in Figure 8a using a diamond slitting saw [6]. The tensile test specimens machined from the pigmented epoxy plate were further used to characterise composite fibre volume fraction and fibre angle distribution. The specimen ends were reinforced by gluing ±45° glass fabric / epoxy end tabs as shown in Figure 8b, to encourage sample failure within the gauge length [51-54].

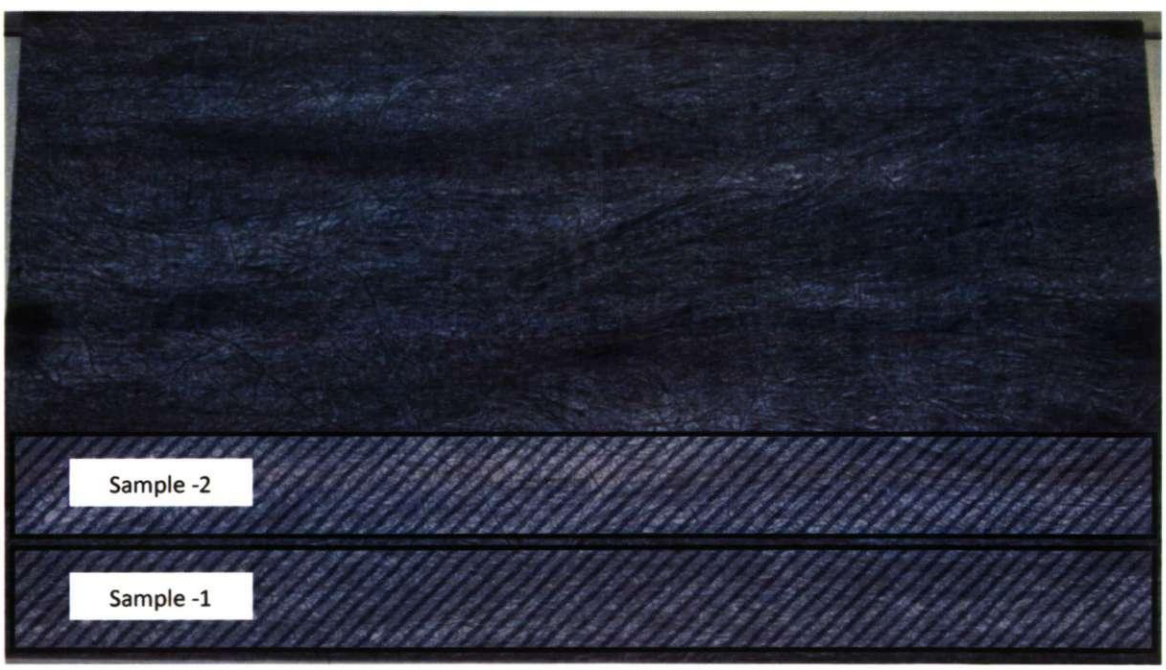

(a)

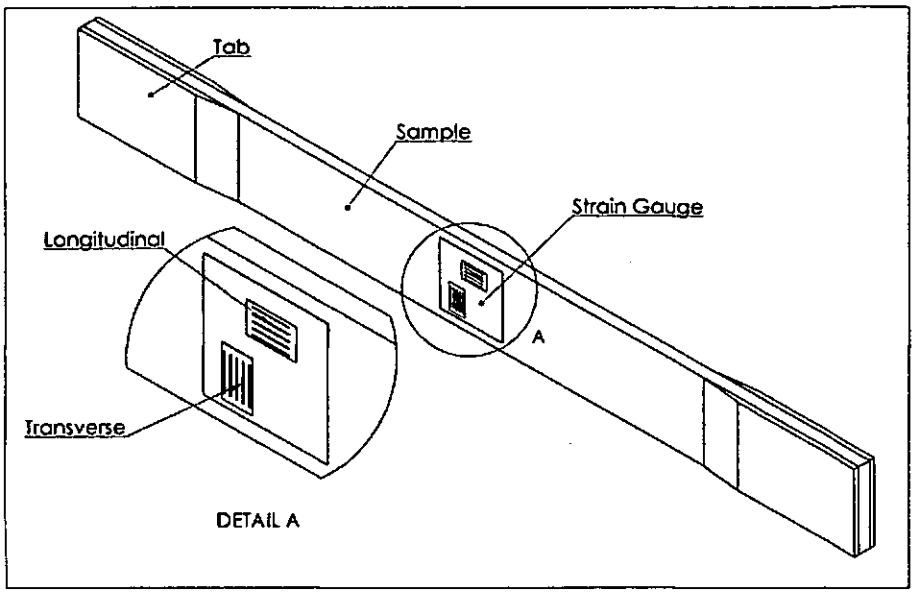

(b)

Figure 8: Resin infused plate: (a) Sample location; (b) Schematic of tensile test specimen

The test specimen was machined and tested according to ASTM D3039 standards [53]: 250 mm long with 150 mm gauge length, 25 mm wide and average thickness of 3.5 mm. Bidirectional 0°/90° strain gauge was bonded on each surface of the specimen with cyanoacrylate adhesive according to the method detailed in [55] to evaluate the axial strain and transverse strain during loading. The strain gauge rosettes (Vishay Micro-Measurements & SR4, CAE-06-250UT-350, 6 mm gauge length, 350 Ω grid resistance and 2.1 nominal gauge factor) were bonded at the centre of the specimen gauge length as shown in Figure 8b. Each strain gauge was wired using three-wire quarter bridge strain gauge circuit to measure the strain [56].
The prepared specimens were tensile tested at ambient temperature (10°C and 70% RH) on an Instron 5582 universal testing machine with an Instron 100kN load cell (serial number – UK185) at a constant cross-head speed of 2 mm/min [53]. The tensile strain in the specimen was measured with a 50 mm gauge length Instron 2630-113 extensometer (serial number – 77). The axial and transverse strain gauge measurements were recorded every second until failure using Vishay P3 strain indicator and recorder. A total of 24 specimens were tested, 6 specimens from each plate. 10 test samples failed within the gauge length (Sample 5b failed near the tab therefore strength and fracture strain result are discarded for the sample but the

modulus is included as this parameter only depends on the initial slope of the stress strain curve).

The tensile modulus, strength and failure strain for each specimen were calculated according to ASTM D3039 and the respective failure modes were recorded. The axial strain range of 1000 με (0.1%) to 3000 με (0.3 %) was used to calculate tensile modulus [53]. A typical stress-strain curve with the calculated modulus overlaid on the plot is shown in Figure 9a.

The Poisson's ratio was calculated from the recorded strain gauge measurements according to ASTM E 132-4 [57] standard, Figure 9b shows a typical axial and transverse strain measurement for a specimen. The final Poisson's ratio of each specimen was calculated as the average of the two paired strain gauge measurements (bonded to opposite surfaces of each specimen).

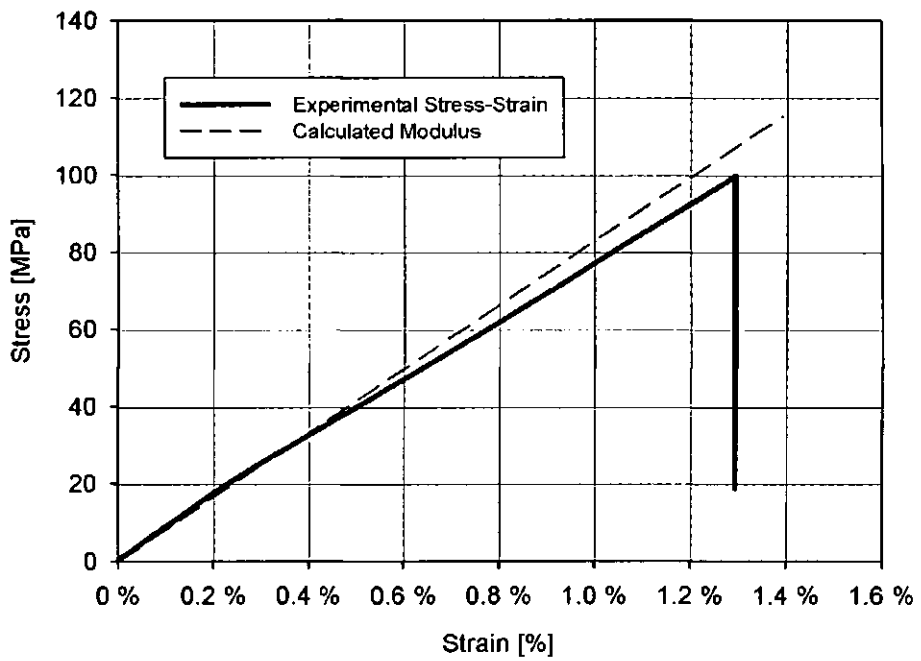

(a)

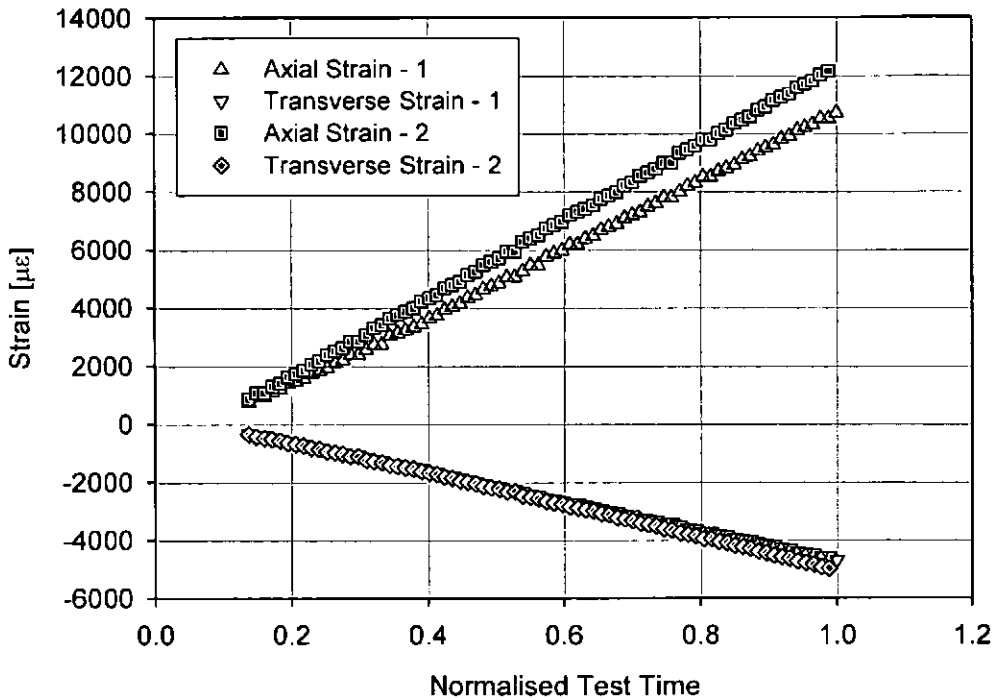

(b)

Figure 9: (a) Typical jute fibre reinforced composite stress–strain curve; (b) Typical axial and transverse strain gauge measurement for a specimen

2.4.5. Micro-structural characterisation

The fibre volume fraction and the fibre angle distribution of the jute fibre reinforced composite tensile test specimens were estimated using photomicrographic techniques [54]. The microscopy samples were taken from each tested specimen near the fracture location as shown in Figure 10. The composite fibre volume fraction was estimated by casting the fibre volume fraction samples in the potting compound perpendicular to the fibre axis to examine the specimen/fibre cross-section. The fibre angle distribution was estimated from the surfaces parallel to the fibre axis (i.e. those in contact with the top and bottom mould surfaces). The samples were ground flat in stages on 180, 240, 400, 600, 800, 1200 and 2500 grit paper. The fibre volume fraction cast samples were subsequently polished with 6 μm and then 1 μm diamond. The samples were washed thoroughly with dilute detergent in an ultrasonic bath between each stage.

Figure 10: Location of microscopy samples from a typical test sample

The polished samples were examined using Olympus BX60MF optical microscope (serial number – 5M04733) and analySIS image analysis software. The sample micrographs were captured at 100X and 50X magnification for fibre volume fraction and fibre angle distribution respectively. Multiple images were captured under polarised light (which provided better contrast) and then stitched together to generate a compound macro-image from contiguous micrographs. Analysis of a large area gives a better overall estimate for both the fibre volume fraction and the fibre angle distribution.

The sample size analysed for the volume fraction and fibre angle distribution were 7.81 mm X 2.95 mm (11440 X 4324 pixels) and 27.60 mm X 12.16 mm (19900 X 8764 pixels) respectively. Figure 11a and Figure 11b show typical micrographs of the polished samples for the fibre volume fraction and the fibre angle distribution evaluation respectively.

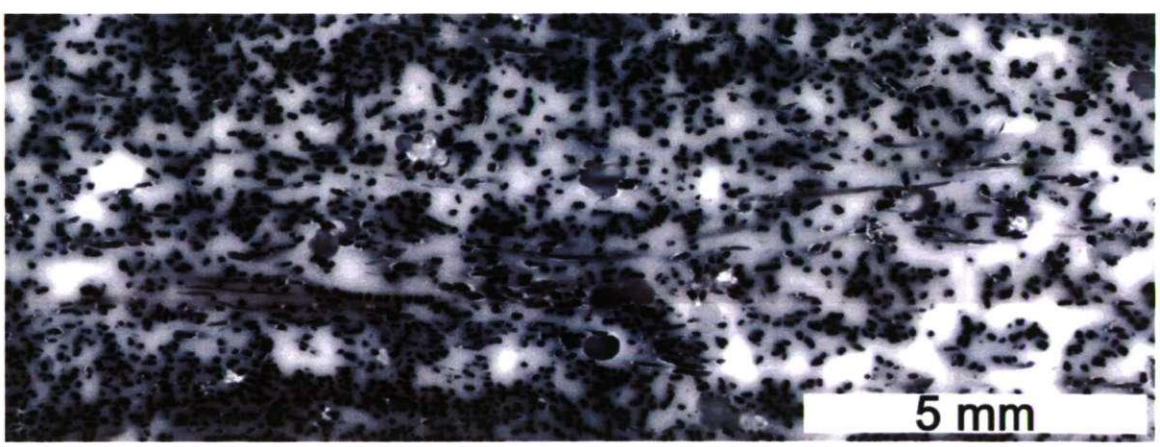

(a)

(b)

Figure 11: Sample micrograph: (a) Typical fibre volume fraction sample; (b) Typical fibre orientation sample

The black features in the micrographs are jute fibres. The acquired digital images were processed using Matlab R2008a [12-14]. The micrograph images were converted to 8-bit (0-255) greyscale image and the contrast of the greyscale images was enhanced by scaling the intensity value of the image so that it covered the entire dynamic range.

2.4.5.1. Fibre volume fraction

An algorithm for automatic fibre volume fraction measurement was written in Matlab. The region of interest on the digital image was selected manually and the area of the selected region was recorded. The micrograph digital image was then smoothed using 5 X 5 averaging filter to reduce noise in the image. The intensity histogram of the selected region of the image was calculated [12, 13] after smoothing. Figure 12a shows the intensity histogram for the micrograph shown in Figure 11a. The intensity which forms the base of the valley of the histogram [12] was selected as the threshold intensity for converting greyscale image to binary image. The generated binary image was morphologically closed (dilation followed by erosion) and opened (erosion followed by dilation) to remove internal voids and small features respectively [12]. The resulting image is shown in Figure 12b. The fibre area was calculated from the binary image and fibre volume fraction was estimated as the ratio of the fibre area to the area of the recorded region of interest.

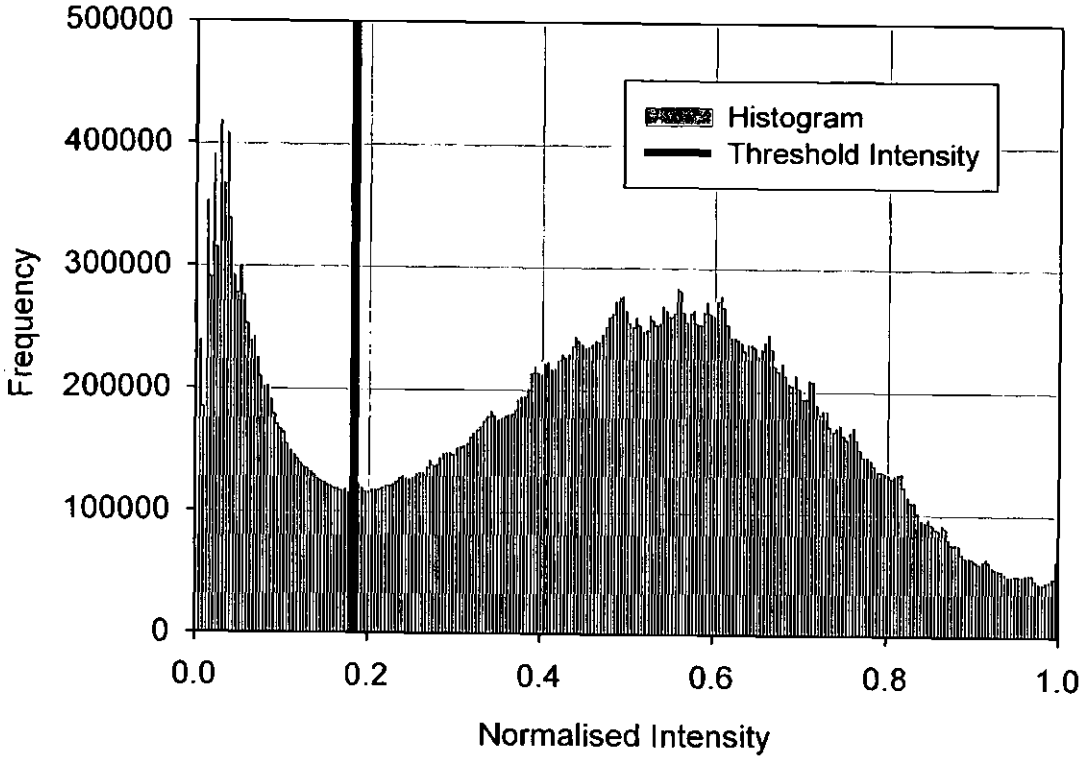

(a)

(b)

Figure 12: Fibre volume fraction: (a) Intensity histogram of the sample; (b) Binary image to estimate volume fraction for the image at Figure 11a

The precision of the volume fraction estimation algorithm was investigated using a software generated calibration image for which the fibre volume fraction was 18%. The calibration image shown in Figure 13 was generated using AutoCAD.

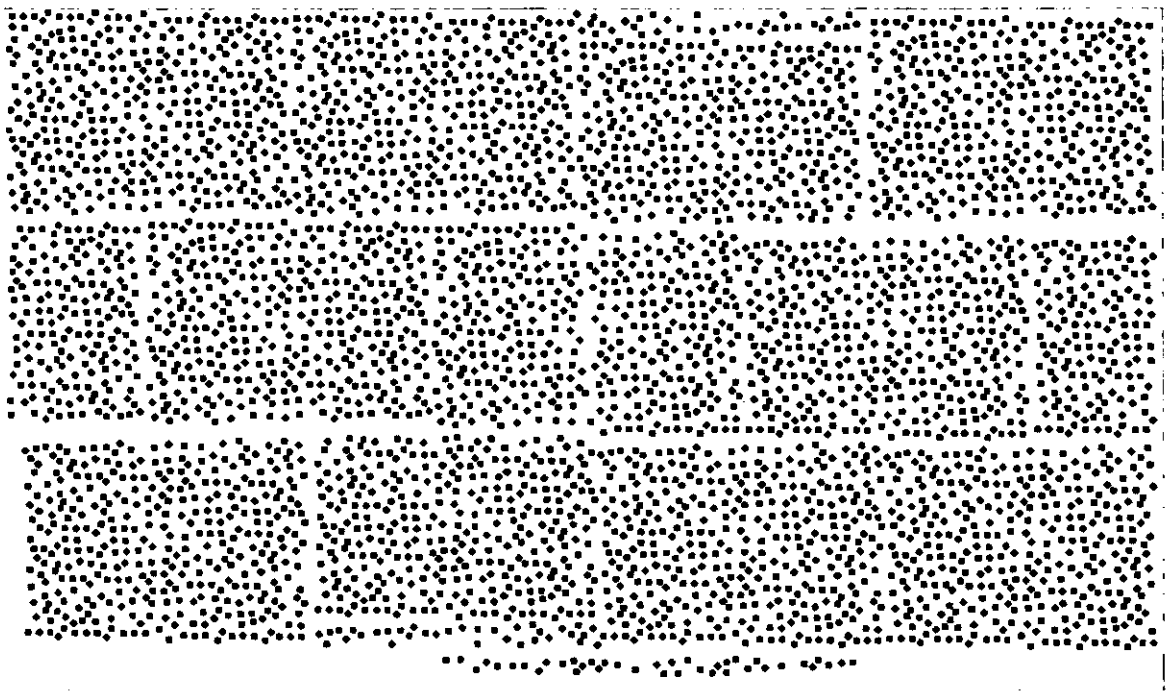

Figure 13: Software generated Fibre volume fraction image

The algorithm estimated the fibre volume fraction for the calibration image to be 18.6%. The calibration image has rogue pixels (noise) which increase the fibre volume fraction above the target value.

2.4.5.2. Fibre angle distribution

To estimate the fibre angle distribution the micrograph image contrast was enhanced by means of Contrast-Limited Adaptive Histogram Equalization (CLAHE) [14, 58]. Using a 350 X 350 pixel tile to calculate the intensity histogram, CLAHE improves the contrast near the fibre matrix interface in the micrograph images. The enhanced contrast near the fibre and the matrix helps to distinguish each fibre in the image thus gives a better binary image [12]. The enhanced micrograph image was thresholded using 70% of the intensity specified by Otsu's method [12, 13] and converted to binary image. The binary image was morphologically closed (erosion / dilation) and opened (dilation / erosion) to remove internal voids and small features respectively [12-14]. The resulting image is shown in Figure 14.

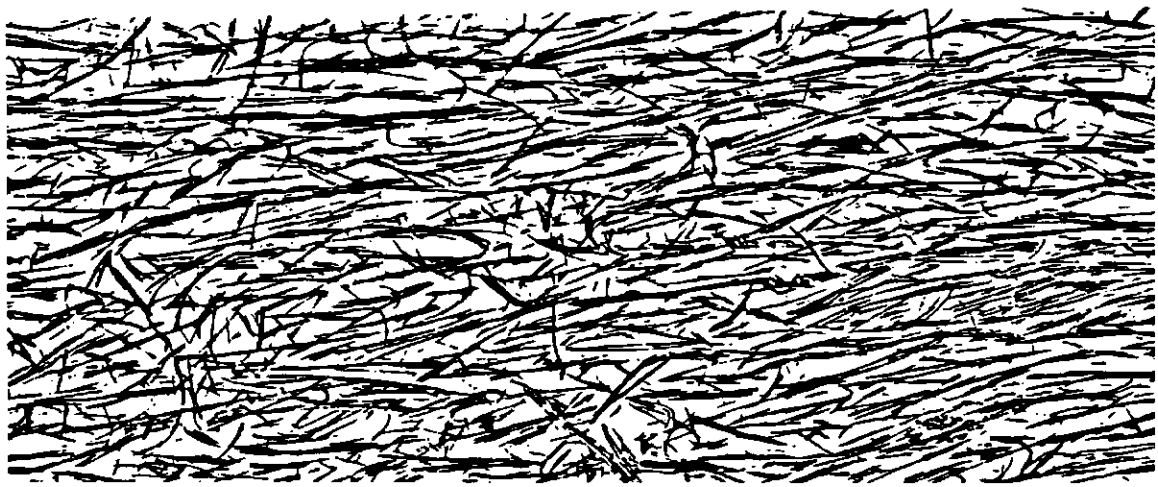

Figure 14: Typical binary image to estimate fibre orientation derived from Figure 11b

A 15 X 15 pixel array seed point was positioned on a regular grid pattern on the micrograph image. A set of 20022 seed points were used for each binary image (213 horizontal X 94 vertical seed points with 93 pixels spacing between each seed point on both axes). The resulting grid pattern is similar to that shown in Figure 15a. The seed points which completely lie on the fibre (the sum of the intensity of the micrograph pixels masked by the seed point is zero [i.e. black = 0]) were selected and overlaid with a masking image to cover the fibre in the micrograph as shown in Figure 15b. The length and thickness of the masking image were 1000 X 15 pixels respectively. The intensity of the pixels enclosed by each masking image was summed and recorded before the masking image was rotated in 1 degree steps through 180 degrees as shown in Figure 15b. The fibre rotation angle and the sum of intensities were recorded at each step. The angle with the minimum sum of intensity at each seed point was accepted as the fibre angle for that seed point.

The ratio of fibre area enclosed by the masking image to the total masking image area was calculated for each seed point. If the ratio of the areas was less than 0.9 then the angle estimated for that seed point was discarded. Typically about 1900 data points remain. As shown in Figure 15b seed points 'a', 'b' and 'c' completely lie on the fibre but the ratio of area for seed point 'a' and 'c' was less than 0.9 therefore they were discarded.

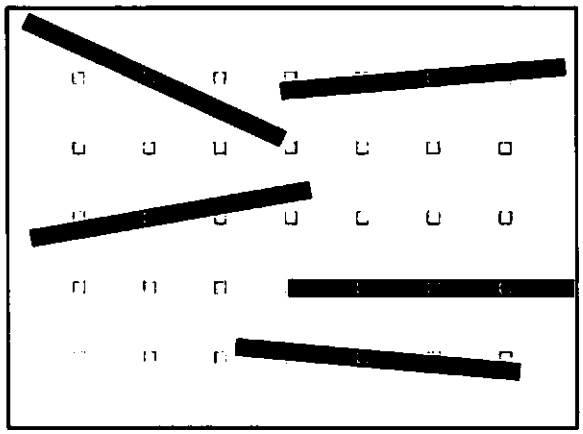

Reinforcement Fibre

■ - Selected Seed Point
□ - Discarded Seed Point

(a)

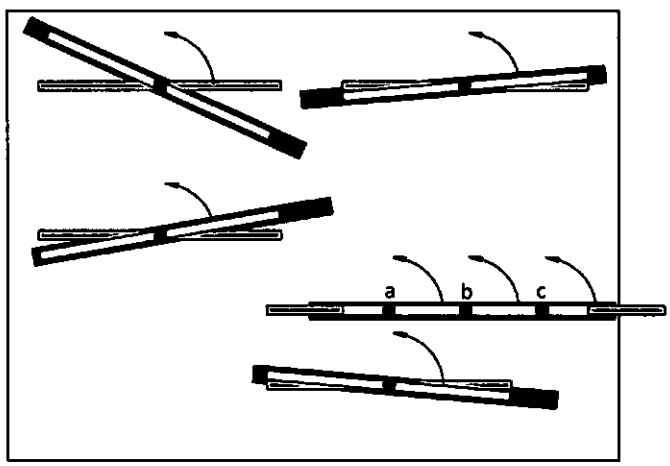

Reinforcement Fibre

Masking Image

Minimum Intensity Angle

■ - Selected Seed Point

(b)

Figure 15: Schematic representation of fibre angle estimation procedure

Figure 16 shows the fibre angle distribution estimated for the image shown in Figure 11b (grey scale) and Figure 14 (binary image).

The measured fibre angles for the sample image followed a Normal distribution [32, 33]. The normal probability density function is:

$$f(x) = \frac{1}{\sigma_N \sqrt{2\pi}} e^{\left(-\frac{(\varphi_x - \mu_N)^2}{2\sigma_N^2}\right)} \qquad (18)$$

Where φ_x is the fibre angle, μ_N is the mean fibre angle (location parameter) and σ_N is the standard deviation (scale parameter).

The mean and standard deviation (distribution parameters) for the fibre angles measured on each micrograph was recorded.

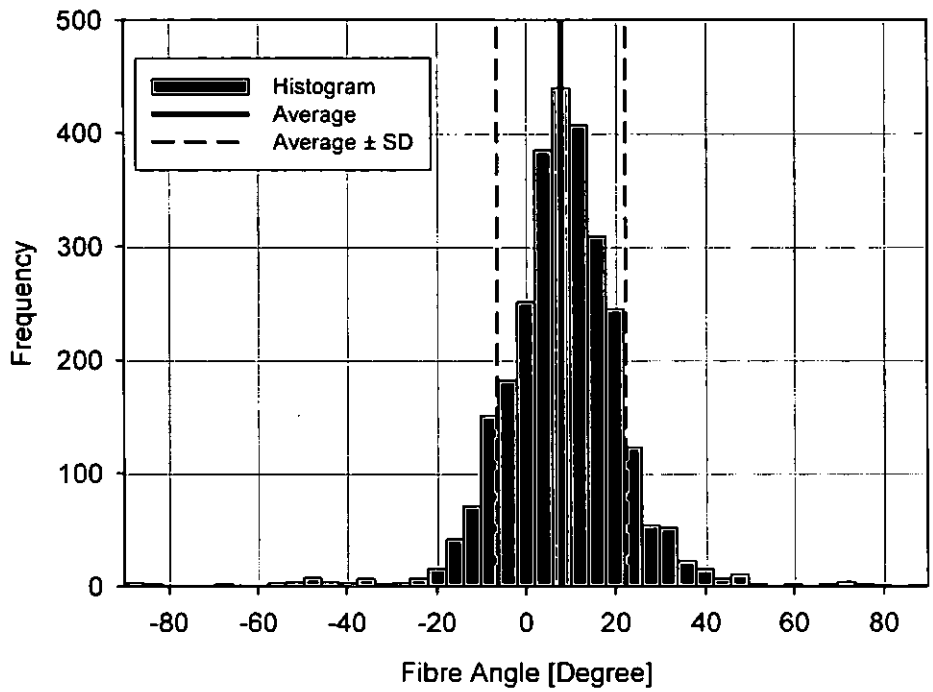

Figure 16: Histogram of estimated Fibre angle distribution

The precision of the fibre angle measurement algorithm was investigated on software generated images for which the fibre angle distribution was known. Images were generated using the normal fibre angle distribution given in Table 3. A typical software generated image is shown in Figure 17.

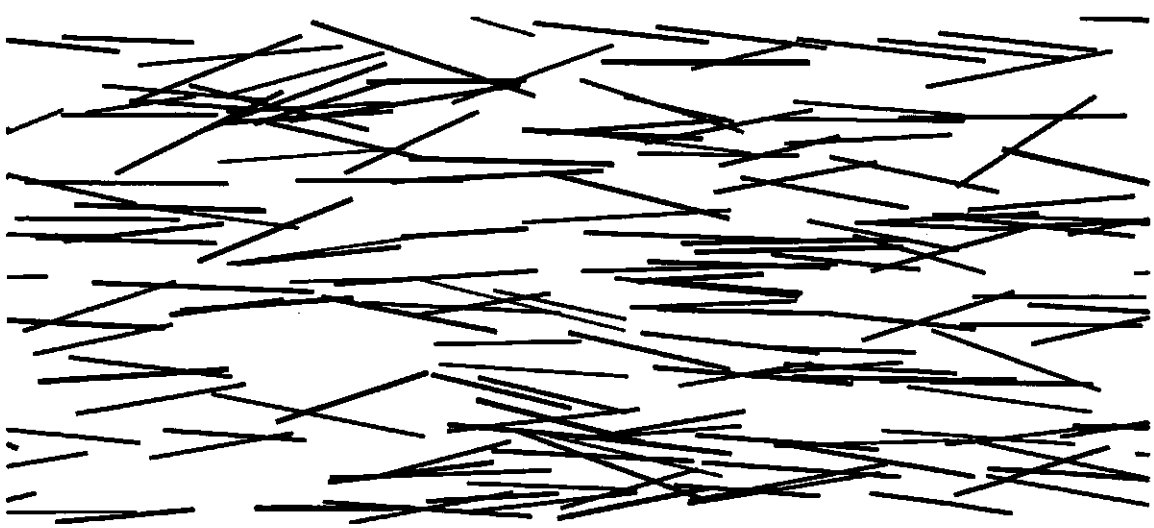

Figure 17: Software generated Fibre angle distribution image

The estimated fibre angle distribution parameters for the software generated images are given in Table 3 for different ratios of the enclosed fibre area to the masking image area. The fibre angle distribution parameters estimated by the fibre angle measurement algorithm were within 1° of the specified fibre angle distribution.

Table 3: Specified fibre angle distribution for the image and estimated angle distribution by angle measurement algorithm

	Specified		***Estimated***		***Estimated***		***Estimated***		***Estimated***	
Area Ratio			***0.80***		***0.85***		***0.90***		***0.95***	
Image	***Mean***	***SD***	***Mean***	***SD***	***Mean***	***SD***	***Mean***	***SD***	***Mean***	***SD***
1	0	10.0	0.44	11.20	0.48	11.19	0.47	11.23	0.43	11.28
2	5	10.0	5.77	10.86	5.71	10.84	5.72	10.86	5.80	10.92
3	0	20.0	0.22	20.43	0.27	20.44	0.25	20.42	0.28	20.48
4	2	20.0	2.20	20.28	2.10	20.25	2.15	20.30	2.17	20.30
5	5	20.0	5.59	19.86	5.69	19.87	5.67	19.90	5.78	19.91

SD - Standard Deviation

2.5. Modelling

2.5.1. Micromechanical model

The elastic properties of a composite can be predicted by micromechanical models based on the properties of the individual constituent materials of the composite and their geometrical characteristics. Better prediction of the mechanical properties of natural fibre composites will help our understanding of the effect of the constituents on the final properties of the material. Using micromechanical models, the composite properties can be optimised for a given application by varying the composition of the composite. Six different micromechanical models will be used to predict the elastic modulus and two models used to predict the strength of jute fibre reinforced composite.

2.5.1.1. Models for composite modulus prediction

2.5.1.1.1. The simplest micromechanical model used to predict the composite elastic modulus parallel to the principal axis is Rule of Mixture ($RoM_{||}$). It is a parallel spring model based on the assumption that the fibres and matrix will experience

equal strain during loading in fibre direction. The $RoM_{||}$ equation [59] for the modulus of a continuous unidirectional fibre composite in the fibre direction is,

$$E_1 = E_f V_f + E_m V_m \tag{19}$$

Where E_1 is composite modulus in fibre direction, E_f and E_m are fibre and matrix modulus respectively and V_f and V_m are fibre and matrix volume fraction.

$RoM_{||}$ provides the upper bound for the composite modulus [60] when,

$$v_m = v_f \tag{20}$$

Where v_m and v_f are matrix and fibre axial Poisson's ratio respectively.

The composite modulus in the direction transverse to the fibre direction is given by $RoM_{\perp}$. This series spring model assumes that the fibres and matrix experience the same stress when the composite is loaded in the direction transverse to the fibres. The $RoM_{\perp}$ equation [59] is,

$$E_2 = \frac{E_f E_m}{E_f V_m + E_m V_f} \tag{21}$$

Where E_2 is composite modulus in the direction transverse to the fibres.

$RoM_{\perp}$ gives the lower bound for the composite modulus [60].

2.5.1.1.2. Halpin - Tsai. Halpin and Tsai [61] developed a semi-empirical method to predict the composite properties. Halpin-Tsai method tries to make a sensible interpolation between upper and lower bounds of composite properties. Halpin-Tsai equation is,

$$E^* = E_m \left(\frac{1 + \xi \eta_{H-T} V_f}{1 - \eta_{H-T} V_f} \right) \tag{22}$$

Where

$$\eta_{H-T} = \frac{E_f - E_m}{E_f + \xi E_m} \tag{23}$$

E^* is composite modulus, E_f and E_m are fibre and matrix modulus respectively, V_f is fibre volume fraction and ξ is reinforcing efficiency (which depends on fibre geometry, packing arrangement and loading condition).

The reinforcing efficiency ξ can be calculated using Equation 24 [62] from the experimental test result, where composite modulus, E^* and fibre volume fraction, V_f are known.

$$\xi = \frac{E_f\left(E^* - E_m\right) - V_f E^*\left(E_f - E_m\right)}{Em\left\{\left(E_f - E^*\right) - V_m\left(E_f - E_m\right)\right\}} \tag{24}$$

and V_m is matrix volume fraction which is equal to $1\text{-}V_f$ assuming a zero void fraction. Value of reinforcement efficiency, ξ can vary from 0 to ∞. When $\xi = \infty$ Halpin-Tsai equation becomes $RoM_{||}$ and for $\xi = 0$ Halpin-Tsai equation is reduced to $RoM_{\perp}$ [60]. The higher reinforcement efficiency, ξ signifies that fibres are contributing to the composite stiffness. Halpin-Tsai method offers the advantage of being simple (easy to use in design process) and offers more exact prediction but normally requires empirical data to determine ξ.

2.5.1.1.3. Cox. The modulus for discontinuous fibre composite can be estimated using Cox Shear-Lag model [63]. The $RoM_{||}$ is modified by including a length factor, which is a function of fibre length, fibre and matrix properties, fibre geometry and placement. The modified $RoM_{||}$ equation [63-65] is

$$E = \eta_l E_f V_f + E_m V_m \tag{25}$$

$$\eta_l = 1 - \frac{\tanh\left(\beta_{cox} l/2\right)}{\beta_{cox} l/2} \tag{26}$$

$$\beta_{cox} = \sqrt{\frac{2\pi G_m}{E_f A_f \ln\left(R/r_0\right)}} \tag{27}$$

Where η_l is fibre length distribution factor, l is fibre length, G_m is matrix shear modulus, A_f is fibre cross sectional area, r_0 and R are the fibre radius and half of inter-fibre spacing respectively.

For square and hexagonal fibre arrangement and fibre of circular cross section the fibre volume fraction is given by Equation 28 and 29 respectively.

$$V_f = \frac{\pi r_0^{\,2}}{4R^2} \tag{28}$$

$$V_f = \frac{2\pi r_0^{\,2}}{\sqrt{3}R^2} \tag{29}$$

This model assumes the interface between fibre and matrix is perfect, fibre and matrix response is elastic and no axial force is transmitted through the fibre ends.

2.5.1.1.4. Stiffness of partially oriented composite can be estimated by including the fibre orientation distribution factor by Krenchel [66] in the $RoM_{||}$ equation. The resulting equation [65, 66] is,

$$E = \eta_o E_f V_f + E_m V_m \tag{30}$$

$$\eta_o = \sum_n a_n \cos^4 \theta_n \tag{31}$$

Where η_o is fibre orientation distribution factor, a_n is the proportion of the fibres making θ_n angle to the applied load.

2.5.1.1.5. Stiffness of discontinuous fibre composite with partially orientated fibres can be predicted by combining Equation 25 and 30 [63-66].

$$E = \eta_l \eta_o E_f V_f + E_m V_m \tag{32}$$

However, if η_l is unity (for long fibres) this returns the same results as Krenchel (Equation 30).

2.5.1.1.6. The modulus of natural fibres has been reported to decrease with increasing fibre diameter [67, 68]. The modulus of composite reinforced with natural fibres can be estimated by equation proposed by Summerscales et al [6]. The $RoM_{||}$ equation is extended to include a fibre "diameter" distribution factor, η_d as in Equation 33:

$$E = \eta_d \eta_l \eta_o E_f V_f + E_m V_m \tag{33}$$

When the fibres used in the composite are well characterised η_d can be taken as 1 i.e. the modulus of the batch of fibres used has been measures independently.

2.5.1.2. Models for composite strength prediction

2.5.1.2.1. Strength of the unidirectional (continuous fibre) composite can be predicted by assuming all the reinforcing fibres have identical strength and the strain in the fibres and the matrix is equal during loading. If the fibre failure strain is less than the matrix failure strain then the composite longitudinal tensile strength (parallel to the fibres) can be estimated using Kelly-Tyson Equation 34 [69],

$$\sigma_c = \sigma_f V_f + (\sigma_m)_{\varepsilon_f}(1 - V_f) \quad (34)$$

Where σ_c is unidirectional composite tensile strength, σ_f is fibre tensile strength and $(\sigma_m)_{\varepsilon_f}$ is matrix stress at the strain equal to failure strain in the fibres. Equation 34 is not true for low fibre volume fraction, therefore for low fibre volume fraction the composite strength is approximated by,

$$\sigma_c < \sigma_{m_{max}}(1 - V_f) \quad (35)$$

Where $\sigma_{m_{max}}$ is maximum matrix tensile strength.

The composite strength is given by the higher of the two values calculated using Equation 34 and 35.

The tensile strength of quasi-unidirectional composite loaded slightly off axis to the fibre direction is given by [70],

$$\sigma_{cu} = \sigma_c \sec^2 \theta \quad (36)$$

Where σ_{cu} is ultimate composite strength, σ_c is unidirectional composite tensile strength and θ is angle between the fibre axes and the composite loading axes. The mean fibre orientation angle for the plate is 7.4° (Section 3.4.2.2) which negligibly increases (by 1.7%) the composite tensile strength therefore it is ignored in further calculations.

The mechanical properties predicted by each micromechanics model were compared to the experimental results to assess the error in the prediction. Knowing that the micromechanics models have inbuilt limitations and assumptions (i.e. they assume perfect bond between fibres and matrix, fibres are homogenous, linear elastic and regularly spaced in the composite and the matrix is also homogenous, linear elastic and void free), the micromechanics model which most closely predicts the experimental data will be deemed more appropriate for natural fibre composites.

3. Results

3.1. Fibre physical characterisation

3.1.1. Fibre length distribution

The fibre length histogram is shown in Figure 18 the data was binned in 20 mm intervals. A normal distribution fitted to the fibre length histogram could yield negative

fibre lengths which is clearly unrealistic so a log-normal distribution is selected to represent the fibre length distribution. The log-normal distribution [32, 33] offers a more realistic fit to the measured fibre length distribution. The log-normal probability density function is:

$$f(T_L') = \frac{1}{\lambda_{T'}\sqrt{2\pi}} e^{-\frac{1}{2}\left(\frac{T_L' - \mu'}{\lambda_{T'}}\right)^2} \quad (37)$$

Where, $T_L' = \ln(T_L)$, T_L is the fibre length, μ' is location parameter (mean of natural logarithms of fibre length) and $\lambda_{T'}$ is the scale parameter (standard deviation of the natural logarithms of fibre length). The log-normal distribution location and scale parameters for this batch of fibres are 4.183 and 0.976 respectively.

The arithmetic mean fibre length and standard deviation are 101.35 ± 100.44 mm. The median and mode fibre length are 67 mm and 40 mm respectively. For a skewed distribution the arithmetic mean does not report the central tendency of the data, as it is heavily influenced by a few large readings. Therefore, it is preferable to use the geometric mean [71] fibre length and standard deviation which are 65.60 mm and 2.65 respectively for this batch of fibres. One standard deviation lower bound and upper bound for geometric mean is given by Equation 38 and 39 respectively.

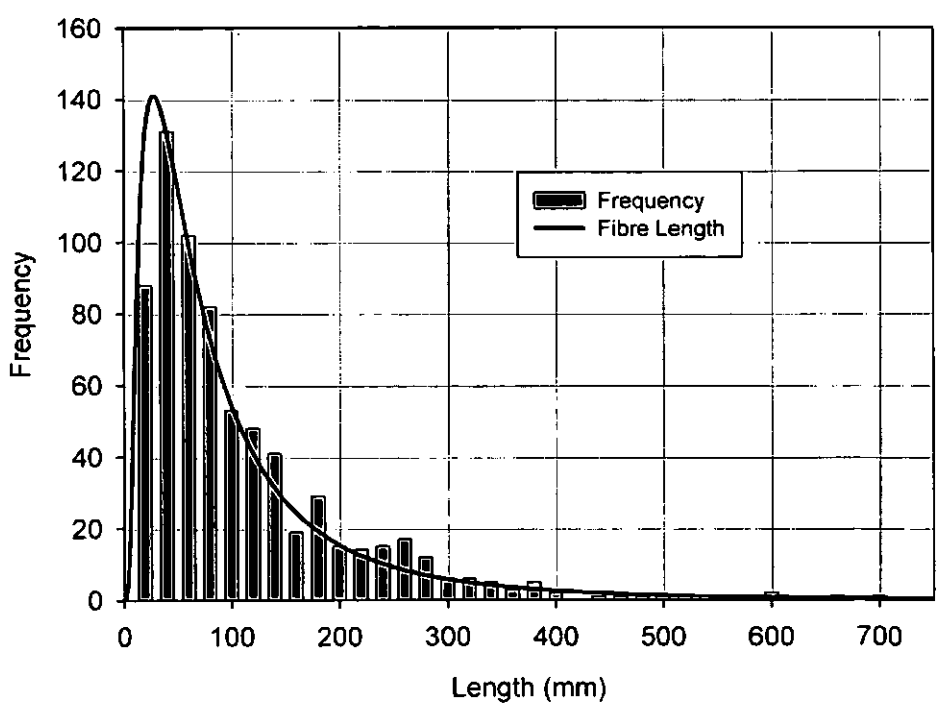

Figure 18: Fibre length distribution for 700 jute fibres.

3.1.2. Fibre true cross-section distribution

The true cross-sectional area of 106[2] individual jute technical fibres was measured and recorded. The true fibre cross-sectional area distribution (histogram) is shown in Figure 19. The central tendency of a skewed distribution is given by the geometric mean [71]. Therefore, the geometric mean, geometric standard deviation and confidence bound for true fibre area and the fibre area calculated for the assumed fibre cross-section shape are given in Table 4. One standard deviation lower bound [72], $1\sigma_L$ is given by,

$$1\sigma_L = \frac{\mu_{geo}}{\sigma_{geo}} \tag{38}$$

One standard deviation upper bound [72], $1\sigma_U$ is given by,

$$1\sigma_U = \mu_{geo}\sigma_{geo} \tag{39}$$

Where μ_{geo} is geometric mean and σ_{geo} is geometric standard deviation.

Table 4: Geometric Mean fibre Area, Geometric Standard Deviation and Confidence interval bound

Area	*Geometric Mean (μm^2)*	*1σ Lower Bound (μm^2)*	*1σ Upper Bound (μm^2)*	*Geometric Standard Deviation*	*Location Parameter*	*Scale Parameter*
True Area	1896	1122	3205	1.69	7.55	0.52
Minor Circle	1776	966	3266	1.84	7.48	0.61
Major Circle	3404	1969	5886	1.73	8.13	0.55
Ellipse	2459	1431	4225	1.72	7.81	0.54
Super Ellipse	2505	1486	4223	1.69	7.83	0.52
Convex Hull	2137	1266	3609	1.69	7.67	0.52

A log-normal distribution [32, 33] was selected to represent the fibre area distribution because a normal distribution of true fibre area could indicate negative areas which are clearly unrealistic. The log-normal probability density function is:

[2] 150 samples were prepared but only 106 samples yielded suitable quality image for analysis.

$$f(T_A') = \frac{1}{\lambda_{T'}\sqrt{2\pi}} e^{-\frac{1}{2}\left(\frac{T_A' - \mu'}{\lambda_{T'}}\right)^2} \quad (40)$$

where T_A is the fibre area, $T_A' = \ln(T_A)$, μ' is the location parameter (arithmetic mean of natural logarithms of fibre area) and $\lambda_{T'}$ is the scale parameter (standard deviation of the natural logarithms of fibre area).

The log-normal distribution location and scale parameters for the true fibre area distribution are 7.55 and 0.52 respectively. The exponent of natural logarithm of location and scale parameters give geometric mean and geometric standard deviation respectively, as reported in Table 4.

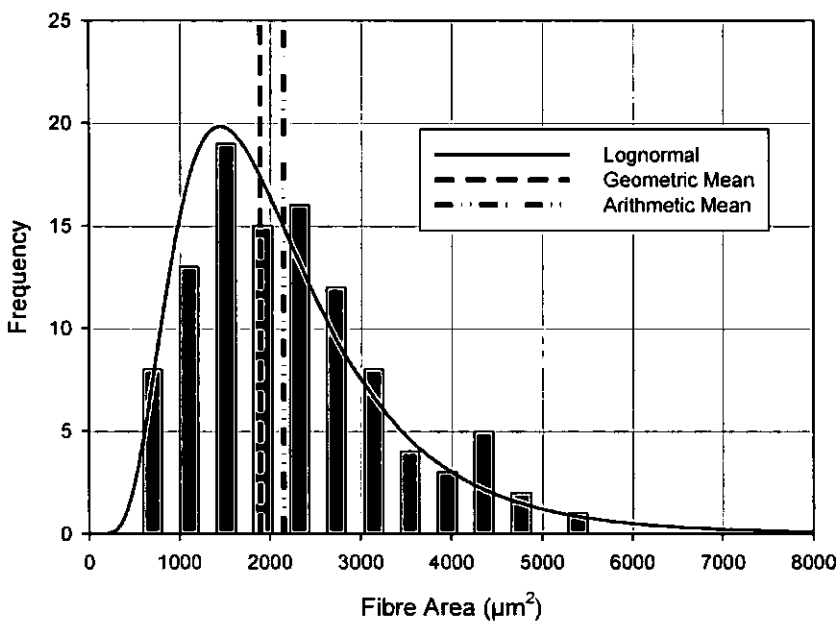

Figure 19: True fibre cross-sectional area distribution

The fibre cross-sectional area distributions for jute technical fibres assuming different cross-section shapes (circles, ellipse, super-ellipse and convex hull) are shown in Figure 20. A log-normal distribution was again selected to represent the distribution of the fibre areas. The log-normal distribution location and scale parameters for each assumed shape are given in Table 4.

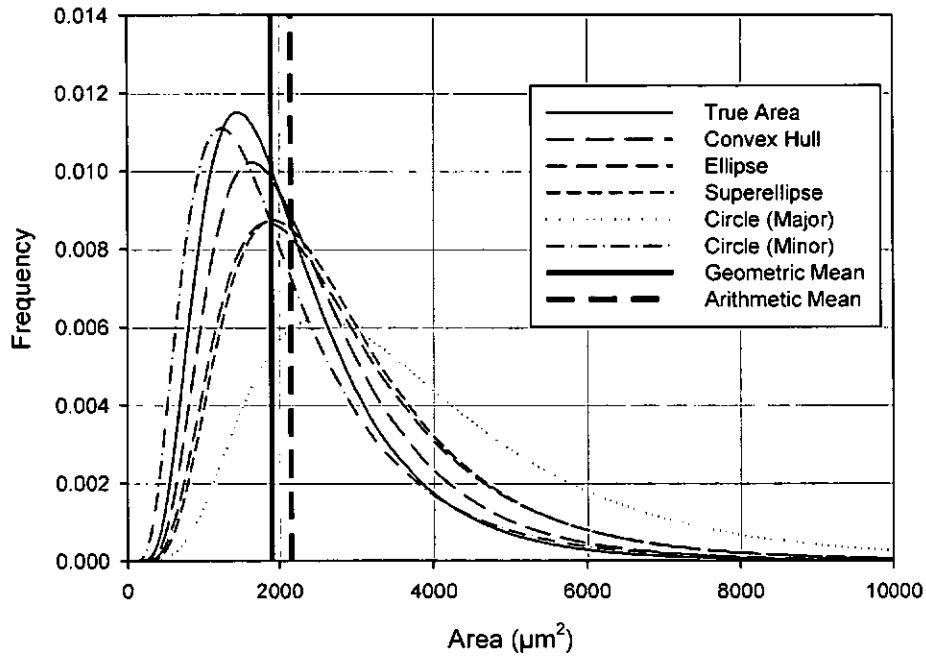

Figure 20: Log-normal plot of the area distributions (106 fibres).

A box plot of the error in the calculated fibre cross sectional area (major/minor circle, ellipse, convex hull and super-ellipse) referenced to the true fibre area is shown in Figure 21. The horizontal line bisecting the box is the median value, the box is bounded by the first and third quartiles, the whiskers indicate the 10th and 90th percentiles, whilst the dots show the 5th and 95th percentile points. The results indicate that the convex hull best represents the true fibre area with lowest range (inter-quartile range 5.2 %), but it slightly over estimates (median +12.0 %) the fibre cross-sectional area.

The major circle significantly overestimates the fibre cross-sectional area (median +76.6 %) and the spread in the estimated area was also large (inter-quartile range of 47.1 %). The minor circle slightly underestimates the fibre cross-sectional area (median -0.8 %) but the spread in the estimated area was large (inter-quartile range of 34.4 %).

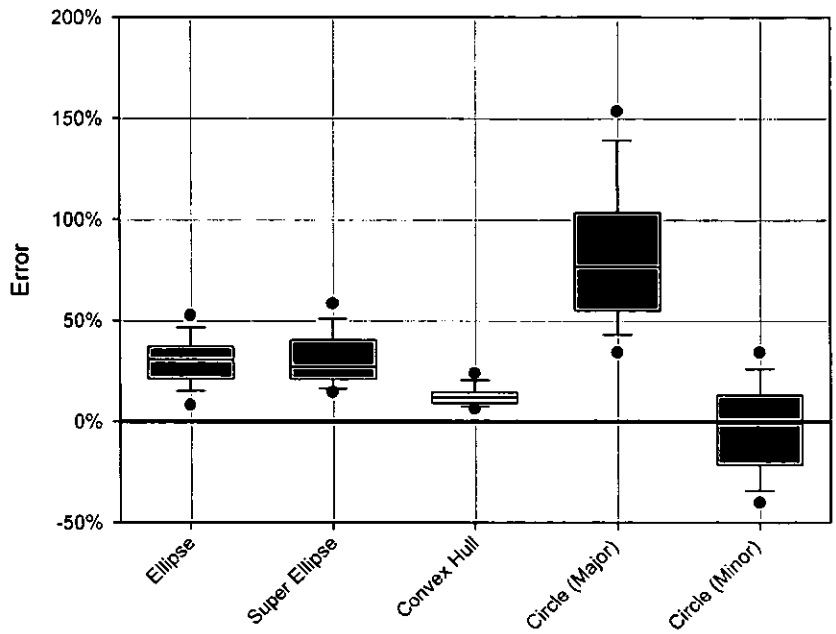

Figure 21: Error in the area measurement based on assumed shape.

Ellipse and super ellipse offered comparable spread (inter-quartile range of 15.6 % and 19.3 % respectively) in the calculated area and over estimated the fibre cross-sectional area (by +30.6 % and +27.3 % [median] respectively).

The measured projected width of a random fibre in an actual situation (e.g. to workout the cross-sectional area for tensile testing) is unlikely to be a major or minor width. Therefore, to evaluate the effect of the assumed shape and the measured projected width on the calculated fibre cross-sectional area, the fibre cross-section micrograph was rotated about the axis of the fibre and two projection widths *A* and *B* were measured from two orthogonal directions as shown in Figure 22. The fibre projected width was measured at 50 intervals by rotating image by 3.6° during each interval (i.e., a total rotation of 180°). The fibre cross-sectional area was calculated for all the projection width measurements, assuming circular cross-section with diameters *A* and *B*, and elliptical cross-section with axis *A* and *B*. The calculated cross-sectional area was compared to the true fibre cross-sectional area. The errors in the area estimated from the projection width of the fibre assuming circular and elliptical cross-section are plotted against the angle at which the measurements were recorded and are shown in Figure 22.

The fibre area calculated assuming a circular cross-section can be an underestimate or overestimate of the true fibre area depending on the angle at which the projection width is measured. The range of the error in the estimated fibre area (judged against the true area) is large, as shown in Figure 22. Thus, the area estimated assuming a circular cross-section is highly unreliable.

The elliptical cross-section gives a lower variation in the cross-sectional area compared to the circular cross-section, shown in Figure 22. The elliptical cross-section normally overestimates the fibre cross-sectional area. The minimum elliptical area calculated from the two orthogonal projection widths *A* and *B* gives the area closest to the true fibre area (minimum error).

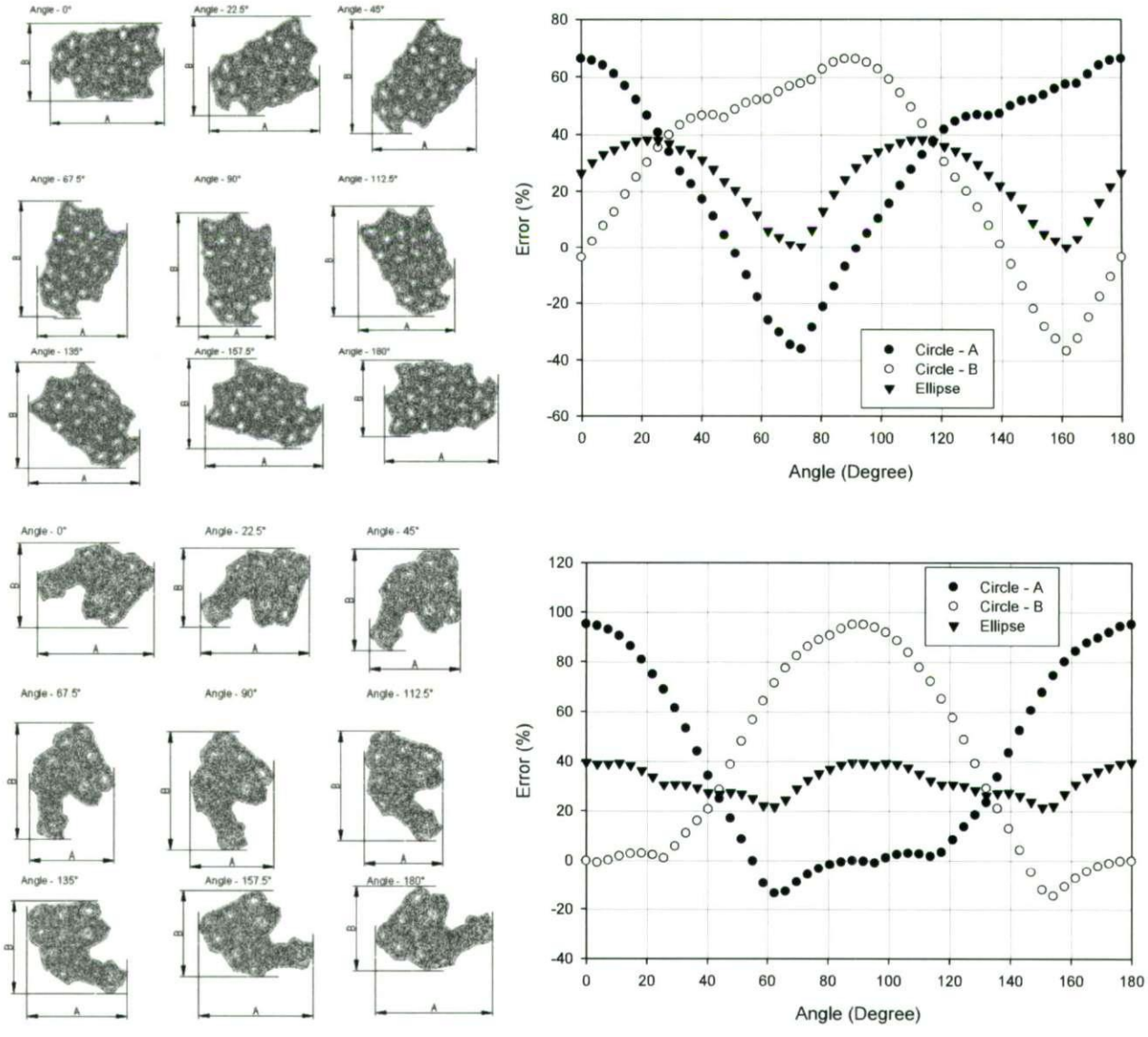

Figure 22: Error in the area measurement of the 2 fibres in Figure 2, based on assumed shape and angle of measurement

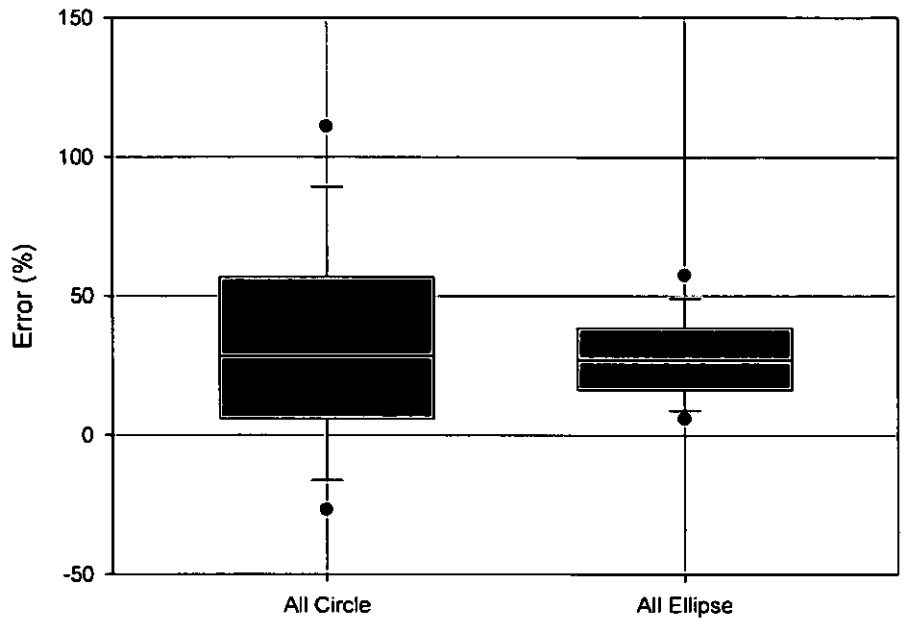

Figure 23: Error in the area measurement based on assumed shape and all the measured points

A box plot of the calculated error in the fibre cross section referenced to the true fibre area at different angles for all 106 samples assuming circular and elliptical cross section is shown in Figure 23. The same mean error in fibre cross-sectional area was observed for both the circles and the ellipse. The confidence is improved by using the ellipse as it offers a reduction in the range of the errors over 360° as shown in Figure 23.

The bounds of the error in the estimated area for the assumed fibre cross section shape (circle and ellipse) is estimated by box plotting the maximum and minimum error in area observed in each of the 106 samples analysed. The error bound is shown Figure 24. 3rd quartile of the maximum error and 1st quartile of minimum error were considered as the upper and lower bound of the error in the fibre cross-sectional area respectively. For the assumed circular cross-section, the bounds of the error are between -36.3% and +102.5%. For the elliptical cross-section, the bounds of the error are +3.8% and +50.6%. From these error bounds, it is observed that the assumed circular cross-section can underestimate or overestimate the fibre cross-sectional area, whereas an ellipse overestimates the area of the fibre. The modulus and strength of the fibre calculated using circular cross-section could be an

underestimate or overestimate depending on the fibre area. For this data set, the ellipse will always underestimate both the modulus and the strength of the fibres and also give reduced variation in the values.

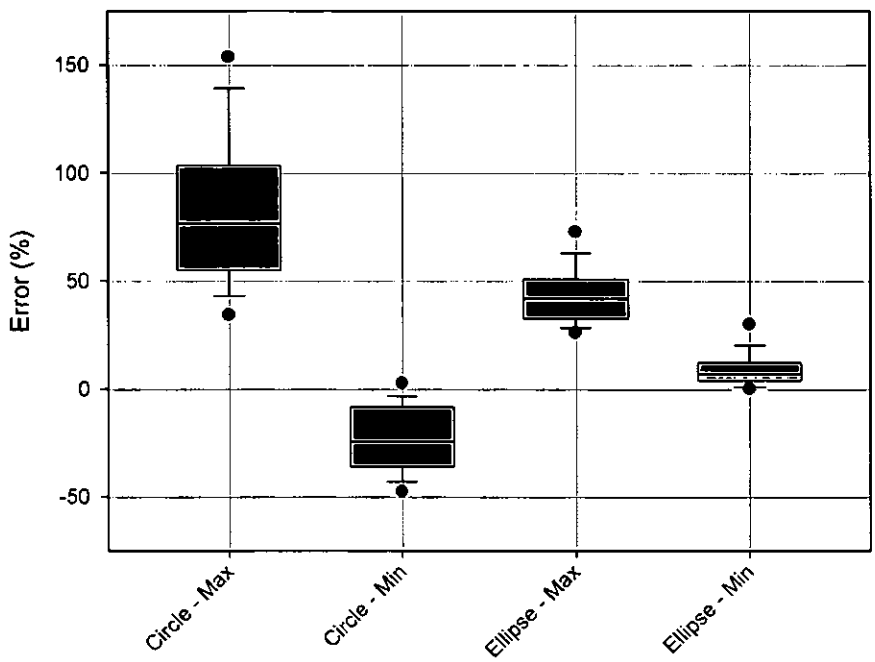

Figure 24: Bounds of the error in the area measurement based on assumed shape

3.2. Fibre mechanical properties

3.2.1. Fibre modulus, strength and fracture strain

The fibre elastic modulus was estimated from the stress and strain data (curve), using BS ISO 11566:1996 [73] assuming a linear stress-strain response. Figure 25 shows the typical tensile stress-strain curves for the jute fibre.

Box plots of the Young's moduli against fibre lengths are shown in Figure 26a. The horizontal line bisecting the box is the median value, the box is bounded by the first and third quartiles, the whiskers indicate the 10th and 90th percentiles, whilst the dots show the 5th and 95th percentile points. The results indicate that the lower bound (5th percentile points) of the fibre modulus is independent of the fibre length (solid line), but the upper bound (95th percentile points) of the fibre modulus drops with increase in fibre length (broken line). The median fibre modulus seems to be independent of fibre length and (in each case) is close to the mean value. In

descending order, the median values are given in Table 5 along with the mean and geometric mean value and standard deviation in brackets.

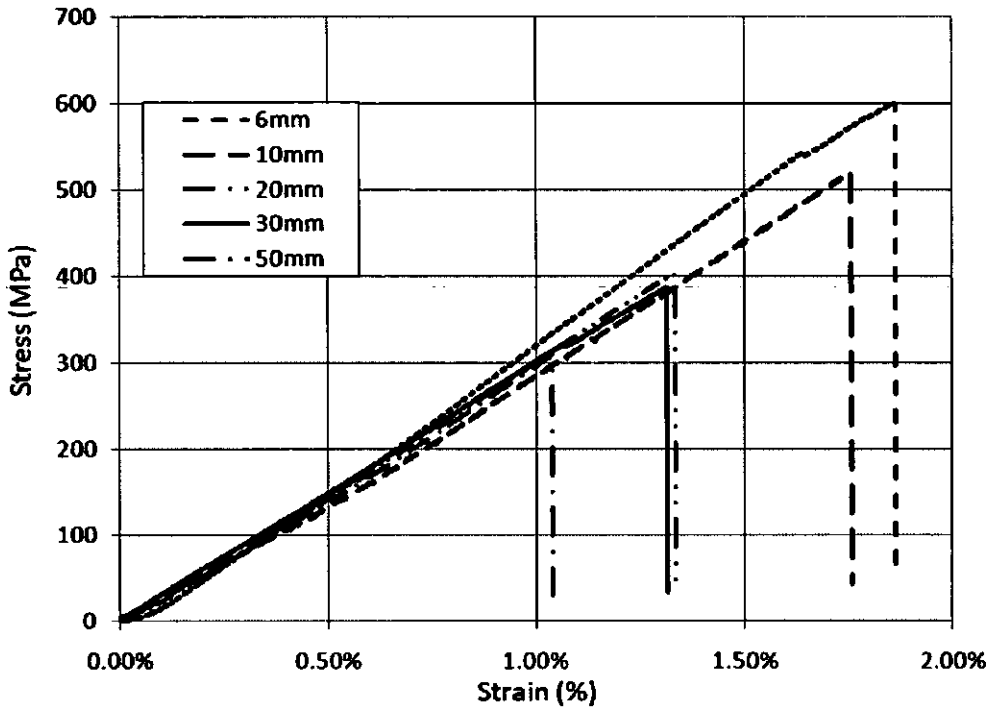

Figure 25: Typical jute fibre stress-strain curves (at a strain rate of 0.01 min^{-1})

Table 5: Jute fibre elastic modulus

Fibre Length [mm]	*Median Modulus [GPa]*	*Mean [GPa]*	*Geometric mean [GPa]*
6	32.7	32.5 (10.1)	30.7 (1.4)
30	30.7	31.0 (7.1)	30.2 (1.3)
20	30.0	31.0 (7.0)	30.2 (1.3)
50	28.7	28.3 (8.8)	26.8 (1.4)
200	28.4	27.6 (4.8)	27.2 (1.2)
100	26.7	27.1 (4.7)	26.7 (1.2)
300	26.5	26.4 (5.0)	25.9 (1.2)
150	25.9	25.8 (4.3)	25.4 (1.2)
10	25.5	26.3 (9.0)	24.7 (1.4)
250	23.6	23.4 (4.5)	23.0 (1.2)
ALL	**27.9**	**28.6 (7.8)**	**27.5 (1.3)**

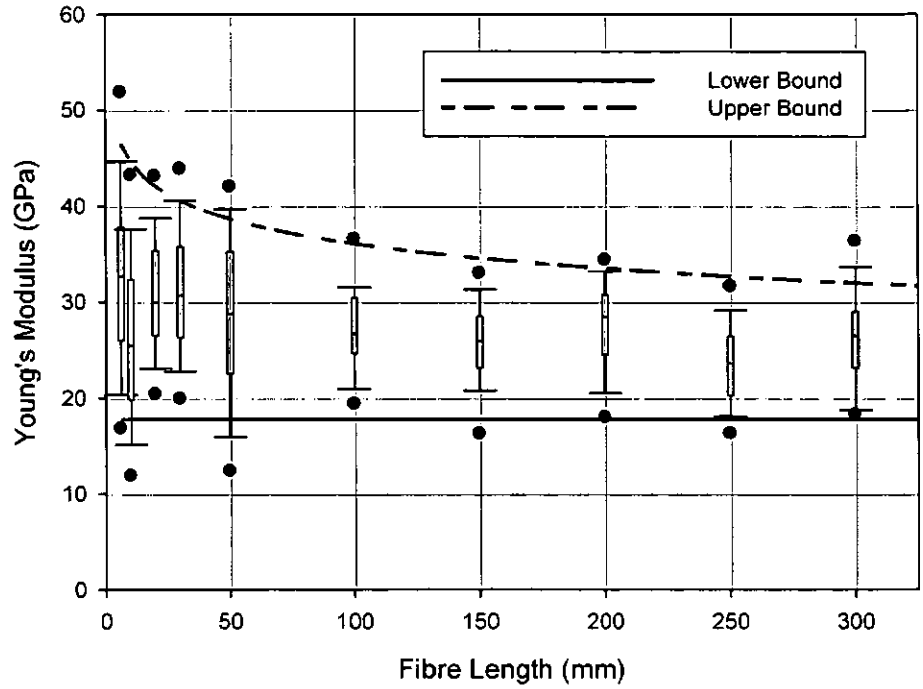
Lower Bound
Upper Bound
Young's Modulus (GPa)
Fibre Length (mm)
0
10
20
30
40
50
60
0
50
100
150
200
250
300

(a)

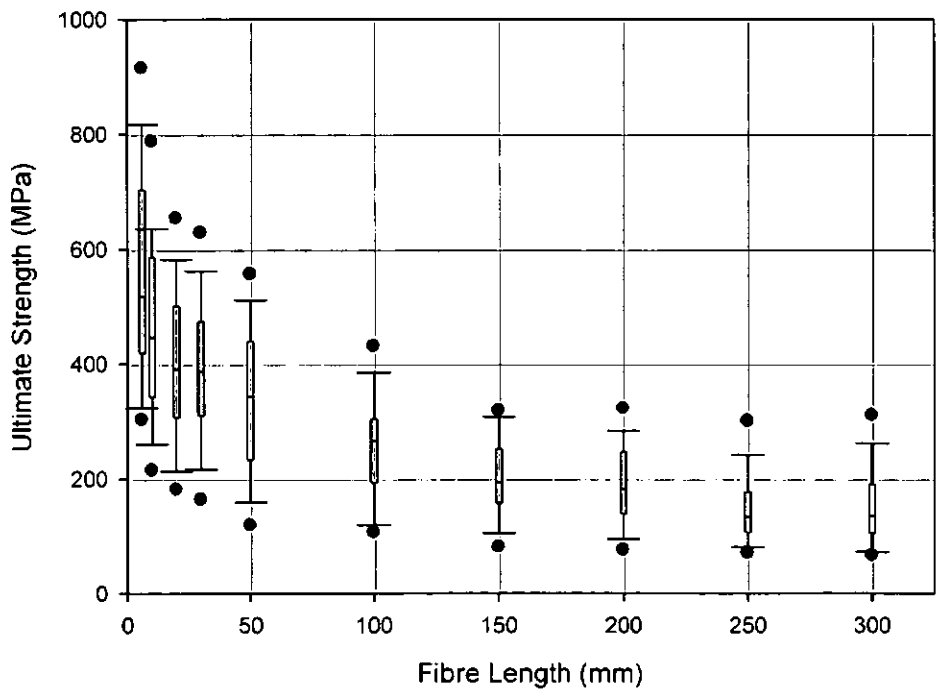
Ultimate Strength (MPa)
Fibre Length (mm)
0
200
400
600
800
1000
0
50
100
150
200
250
300

(b)

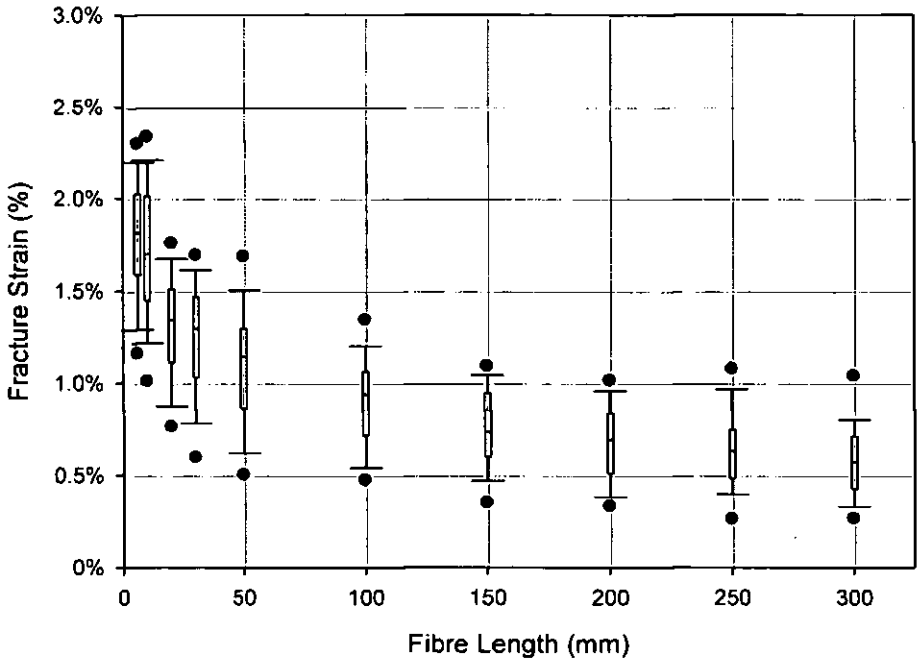

(c)

Figure 26: Tensile property variations with length: (a) Young's modulus; (b) ultimate tensile strength; and (c) fracture strain.

The box plots of the strengths and fracture strains against fibre length are shown in Figure 26b and Figure 26c respectively. The fibre strength decreases with an increase in fibre length and thus provides clear support for the concept that longer fibres are more likely to have a critical flaw than their shorter counterparts. The failure strain for longer fibres is also seen to decrease (as would be expected if the fibres have linear Hookean behaviour and notionally a constant Young's modulus). Moreover, as the fibre length increases the spread (difference between upper and lower) of the strength and failure strain data decreases and at fibre lengths above 150 mm the reduction of the experimental strength and failure strain is significantly lower than that of shorter fibres (fibre less than 50 mm).

3.3. Statistical strength and fracture strain distribution

3.3.1. Weibull point estimate

The Weibull modulus and characteristic strengths or strains were estimated using the MLE method for strength and fracture strain at individual gauge lengths. The computed tensile strength and fracture strain distribution parameters (point

estimates) are given in Table 6 and Table 7 respectively. The Weibull distribution plots are shown in Appendix B11.

Table 6: Two-parameter Weibull distribution parameters for tensile strength

Fibre Length, L [mm]	*Weibull Modulus for Strength, β*	*Characteristic Strength, η [MPa] (Equation 5)*	*Weak link Characteristic Strength, η_w [MPa] (Equation 6)*
6	3.08	624	1117
10	3.04	519	1107
20	3.18	451	1158
30	3.31	437	1222
50	2.83	378	1503
100	3.15	289	1250
150	3.29	224	1025
200	2.92	213	1307
250	2.42	172	1680
300	2.35	174	1975

Table 7: Two-parameter Weibull distribution parameters for fracture strain

Fibre Length, L [mm]	*Weibull Modulus for Strain, β*	*Characteristic Strain, η [%] (Equation 5)*	*Weak link Characteristic Strain, η_w [%] (Equation 6)*
6	6.36	1.92%	2.54%
10	4.60	1.86%	3.06%
20	5.04	1.41%	2.55%
30	4.80	1.36%	2.77%
50	3.64	1.23%	3.60%
100	4.30	1.00%	2.92%
150	4.10	0.84%	2.84%
200	3.17	0.75%	4.01%
250	3.04	0.72%	4.44%
300	3.07	0.65%	4.14%

The confidence intervals of the Weibull parameters are estimated (using the Weibull Fisher Matrix method [32, 33, 74]) to characterise the range within which the point estimates are likely to occur for a given proportion of the time [32, 75]. The 90% two-sided confidence bounds (i.e. from 5% lower bound to 95% upper bound) for tensile strength and fracture strain parameters are calculated and are given in Table 8 and Table 9 respectively. Detail of the mathematical approach for the confidence bounds are given in Appendix B2.

Table 8: Two parameter Weibull distribution parameters: confidence bound for strength

Fibre Length [mm]	*Lower Bound* β_L	*Upper Bound* β_U	*Lower Bound,* η_L *[MPa]*	*Upper Bound,* η_U *[MPa]*
6	2.73	3.47	590	660
10	2.68	3.45	490	549
20	2.81	3.60	428	476
30	2.92	3.75	415	460
50	2.49	3.23	356	402
100	2.64	3.74	268	312
150	2.76	3.93	208	240
200	2.45	3.48	196	231
250	2.06	2.84	155	189
300	1.99	2.77	157	192

Table 9: Two parameter Weibull distribution parameters: confidence bound for fracture strain

Fibre Length [mm]	*Lower Bound* β_L	*Upper Bound* β_U	*Lower Bound,* η_L *[%]*	*Upper Bound,* η_U *[%]*
6	5.60	7.23	1.87%	1.97%
10	4.06	5.21	1.79%	1.93%
20	4.44	5.73	1.36%	1.46%
30	4.21	5.46	1.32%	1.41%
50	3.20	4.13	1.17%	1.29%
100	3.61	5.14	0.95%	1.06%
150	3.44	4.90	0.79%	0.89%
200	2.68	3.75	0.70%	0.81%
250	2.57	3.59	0.67%	0.78%
300	2.60	3.63	0.60%	0.70%

3.3.2. Weak-Link Scaling Model (WLSM)

The Weibull distribution with weak-link scaling parameters is given in Table 6 and Table 7 for strength and fracture strain respectively. The Weibull modulus for the WLSM and Weibull point estimate is identical. The plots of natural logarithm of characteristic strength and fracture strain against natural logarithm of the fibre length are shown in Figure 27 and Figure 28 respectively. The point estimates for WLSM characteristic strength and fracture strain are taken from Table 6 and Table 7. The characteristic strengths and strains were predicted for each of the tested fibre lengths using Equation 9. In Figure 27 and Figure 28, only the weak-link estimates based on β and η_w for 6mm, 100mm and 300 mm lengths are presented for brevity and clarity. The slope of the linear predictions (using any individual point estimate) can be shown to equate to $-1/\beta$ and their intercept is equal to $\ln(\eta_w)$.

The predictions correlate well over a limited range of point estimates but it can be visually observed that the weak-link scaled characteristic strength (Figure 27) and strain (Figure 28) predictions do not associate well with the point estimates across the full range of the data. Moreover the accuracy of the fit is dependent upon the scaling point estimate used, and thus, weak-link scaling from a single point is considered an unreliable method. The underlying reason for this is the assumption that β for the chosen scaling point is constant for all other fibre lengths. This is not the case (see Table 6 and Table 7). However, using more than one point it should be possible to select a value of β (used to optimise the slope) and η_w (for intercept optimisation) to enhance the weak-link scaling correlation for the complete set of fibre lengths. We now need to establish the number of point estimates needed for an acceptable fit.

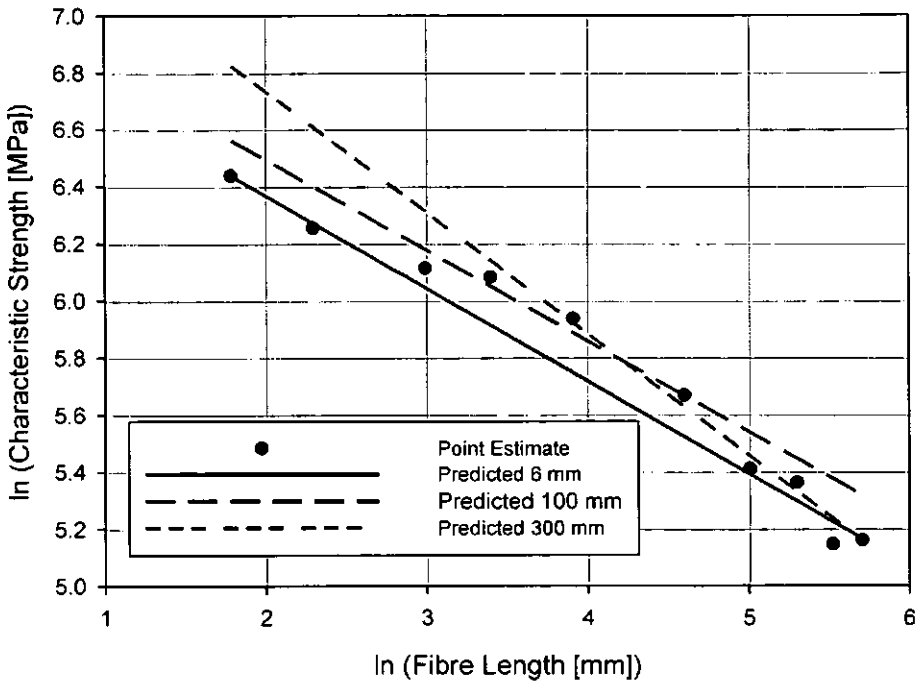

Figure 27: Weak link scaling prediction for strength

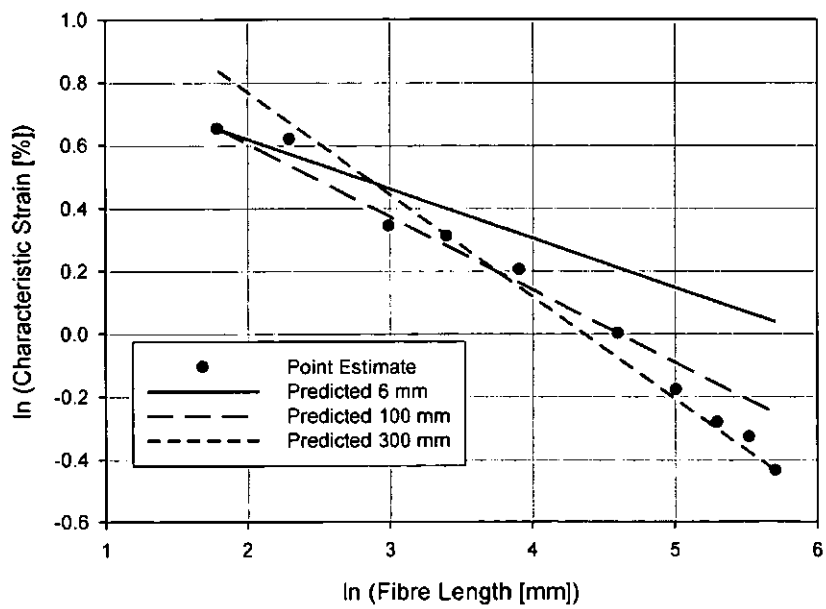

Figure 28: Weak link scaling prediction for fracture strain

3.3.3. Multiple Data Set (MDS) Weak-link scaling model

The MDS weak link distribution parameters are given in Table 10 and Table 11 for strength and fracture strain respectively. The characteristic strengths (or strain) are scaled using Equation 9.

Table 10: MDS weak link Weibull estimates for strength

Fibre Length	*Weibull Modulus, β*	*Characteristic Strength, η_w [MPa]*
6 and 300	3.03	1157
6, 50 and 300	3.00	1269
6, 100 and 300	3.11	1170
All	3.00	1243

Table 11: MDS weak link Weibull estimates for fracture strain

Fibre Length	*Weibull Modulus, β*	*Characteristic Strain, η_w [%]*
6 and 300	4.02	2.86%
6, 50 and 300	3.98	3.08%
6, 100 and 300	4.15	2.88%
All	3.92	3.12%

The predicted characteristic strength and strain curves (plotted on a natural logarithm scale) are shown in Figure 29 and Figure 30. The point estimates for characteristic strength and fracture strain are taken from Table 10 and Table 11. From a visual inspection, the fit to the point estimates (using the MDS weak-link scaling for two and three points) is more consistent than for the standard weak-link scaling method based on a single point estimate. The MDS two and three point methods seem (in all cases) to produce a realistic slope.

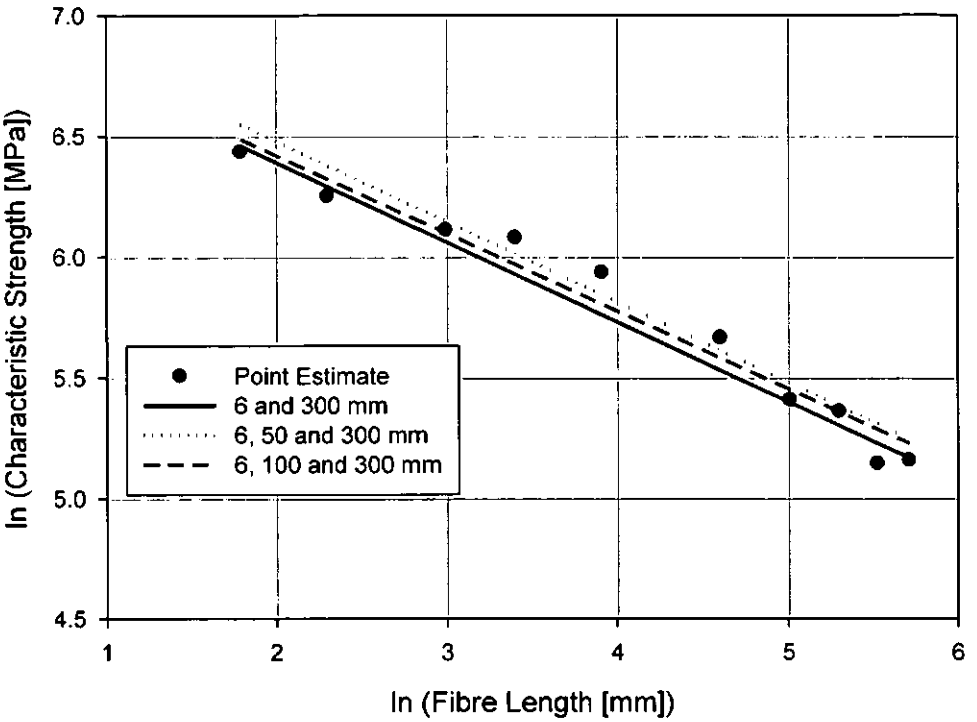

Figure 29 : MDS Weak link scaling prediction for strength

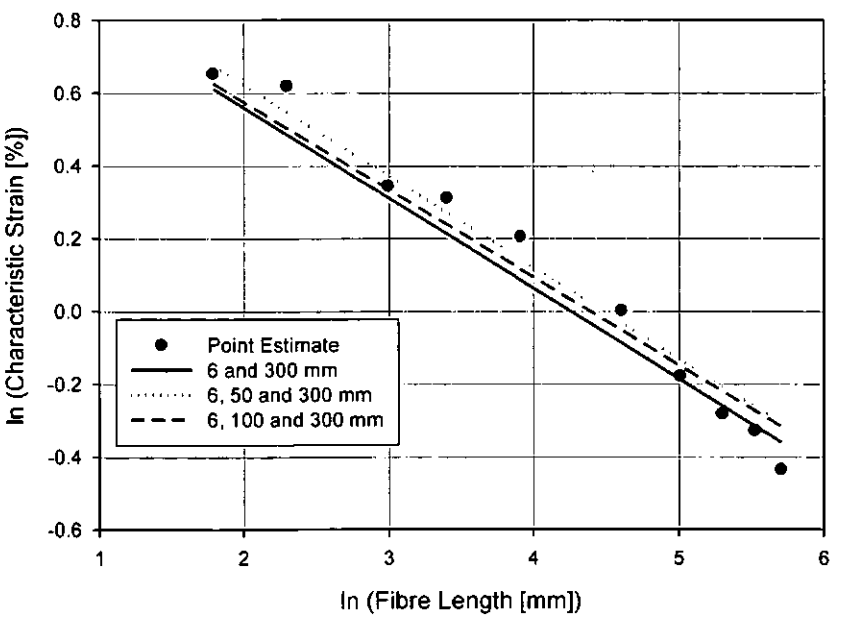

Figure 30 : MDS Weak-link scaling prediction for fracture strain

3.3.4. Empirical Models

3.3.4.1. Linear Interpolation Model (LIM)

The LIM equations for Weibull modulus and characteristic stress or strain for the strength and fracture strain respectively were estimated and plotted against the fibre length (Figure 31 and Figure 32).

3.3.4.2. Natural-Logarithmic Interpolation Model (NLIM)

The NLIM distribution parameters are plotted in Figure 31 and Figure 32 along with the Weibull point estimates (Table 6 and Table 7) against the fibre length for tensile strength and fracture strain respectively. The confidence intervals of the Weibull parameters (90% two-sided confidence bounds) are also shown in Figure 31 and Figure 32. The linear interpolation model and logarithmic interpolation model results are overlaid to illustrate the fit, where β is the shape parameter (Weibull modulus) and η is the scale parameter (Characteristic strength or strain) for two parameter Weibull distribution. In Figure 31 and Figure 32, the NLIM line clearly follows a similar trend to the data, whereas the linear model is not able to capture the trend. MDS model is also included to compare it with empirical models.

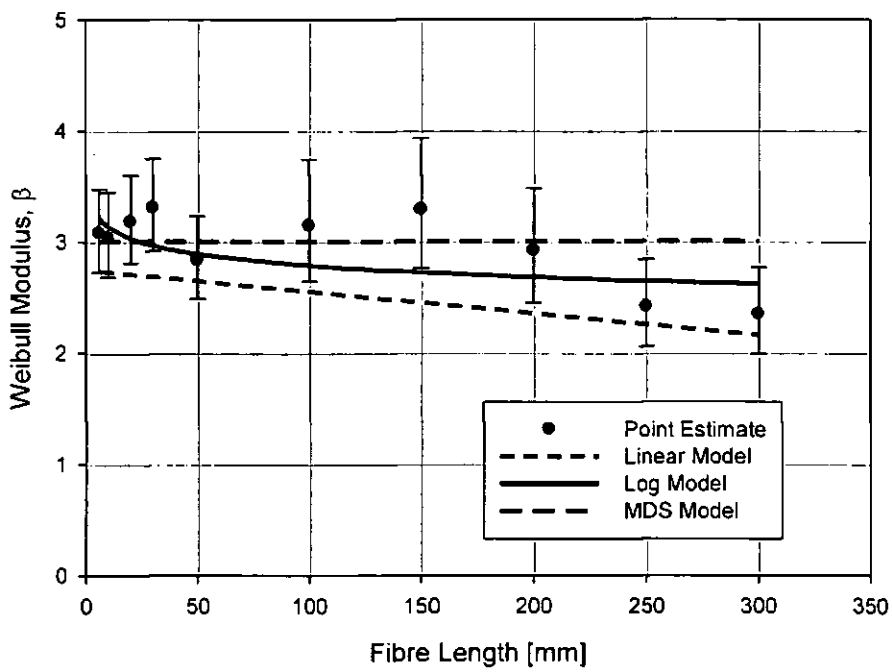

(a)

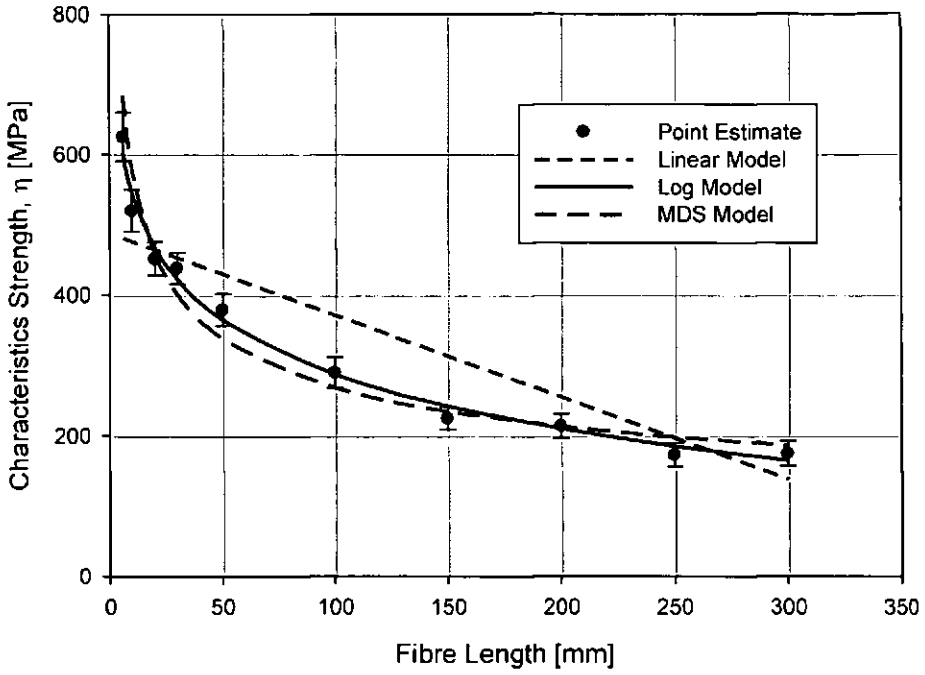

(b)

Figure 31: Tensile strength: (a) Weibull modulus versus fibre length

$\beta_{Linear} = -0.00196 \times fibre\,length + 2.747$, $\beta_{Log} = -0.152 \ln(fibre\,length) + 3.487$,

$\beta_{MDS} = 3.00$

(b) Characteristic stress versus fibre length

$\eta_{Linear} = -1.166 \times fibre\,length + 487.826$, $\eta_{Log} = -111.656 \ln(fibre\,length) + 801.63$,

$\eta_{MDS} = 1243 / \sqrt[3.00]{fibre\,length}$

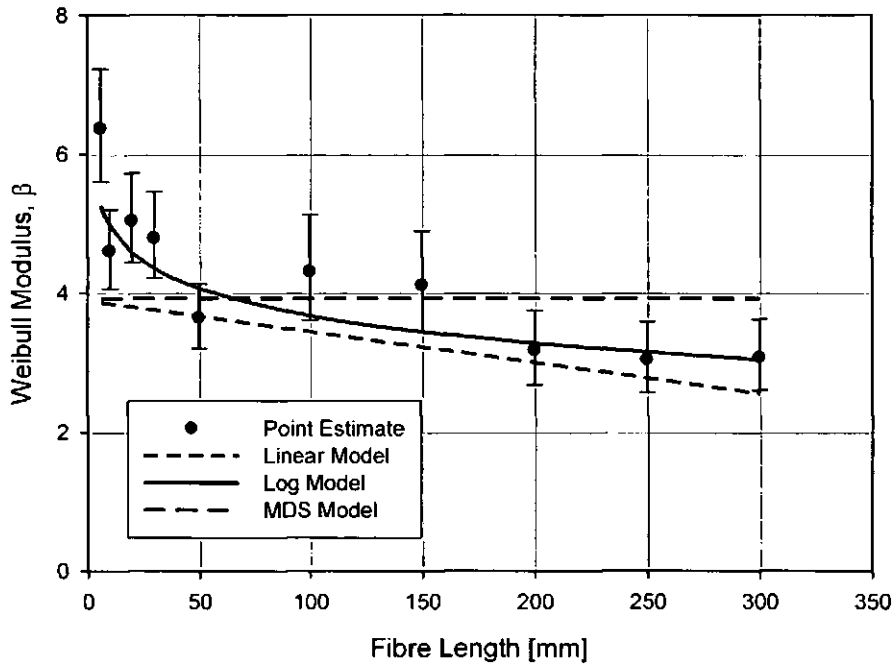

(a)

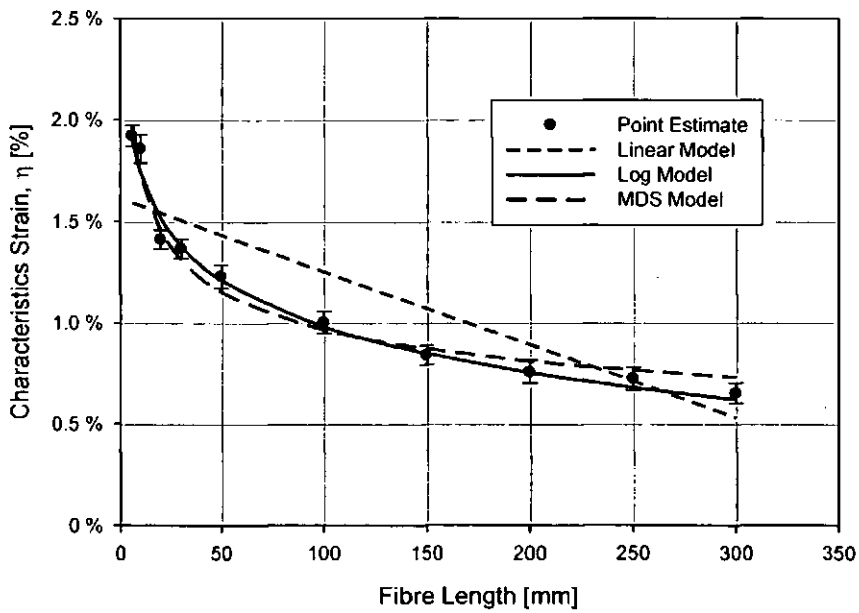

(b)

Figure 32: Fracture strain: (a) Weibull modulus versus fibre length.

$\beta_{Linear} = -0.00444 \times fibre\,length + 3.89$, $\beta_{Log} = -0.568 \ln(fibre\,length) + 6.29$, $\beta_{MDS} = 3.92$

(b) Characteristic strain versus fibre length.

$\eta_{Linear} = -3.61\text{E}-5 \times fibre\,length + 0.01612$, $\eta_{Log} = -0.0033 \ln(fibre\,length) + 0.025$,

$\eta_{MDS} = 0.0312 / \sqrt[3.92]{fibre\,length}$

3.4. Jute/Epoxy Composite

3.4.1. Mechanical properties

The average specimen dimension and the tensile test results for the specimens which failed within the gauge length are given in Table 12. The full set of specimen dimensions, the tensile test results and the failure location for each specimen which failed within the gauge length are given in Appendix B6.

Table 12: Tensile test results for jute fibre reinforced Composite

	Width [mm]	*Thickness [mm]*	*Modulus [GPa]*	*Strength [MPa]*	*Failure Strain [%]*
Average	25.13	3.46	8.06	100.5	1.34%
SD	0.14	0.43	0.84	12.1	0.14%
CoV	0.56%	12.53%	10.44%	12.04%	10.25%
Median	25.14	3.57	8.04	96.6	1.35%
Max	25.39	4.42	9.19	131.1	1.61%
Min	24.87	2.91	6.70	88.3	1.15%

CoV – Coefficient of Variation

The average modulus and average strength for plate 5 (dyed fibres) were 8.18 ± 0.6 GPa and 100.0 ± 5.7 MPa respectively.

The Poisson's ratio of the composite was calculated as the average of the Poisson's ratio given by each strain gauge rosette to counter the effect of sample bending during loading. The Poisson's ratio is not affected by the failure/fracture location of the tensile specimen therefore, results from all the tested samples (Appendix B7) are used. The Poisson's ratio was 0.42 ± 0.02 for the entire set of samples. The Coefficient of Variation (CoV) for the measured Poisson's ratio was 4 %.

3.4.2. Microstructural characterisation

3.4.2.1. Fibre volume fraction

The fibre volume fraction of the composite samples machined from the plate infused with dyed jute fibres (black) and pigmented epoxy (white) was analysed after tensile testing. At least 5 micrographs were analysed for each specimen to estimate the

average fibre volume fraction of the specimen. The calculated average fibre volume fraction for each specimen is given in Table 13. The estimated fibre volume fraction for each micrograph is given in Appendix B8.

Table 13: Fibre volume fraction and Fibre Angle distribution estimated using micrographs

	Volume Fraction		***Fibre Angle***	
Sample No.	***Average***	***SD***	***Mean***	***SD***
5a	17.5%	3.2%	5.7	15.3
5b	18.1%	2.1%	7.3	27.2
5c	20.3%	3.8%	10.5	18.4
5d	20.9%	6.1%	7.9	15.1
5e	18.0%	3.1%	6.2	16.1
5f	18.5%	5.4%	6.6	15.6
Plate (Mean)	***18.9%***	***3.9%***	***7.4***	***18.0***

The fibre volume fraction of the infused plate was calculated to be 18.9 % ± 3.9 % (mean of all samples from the plate).

3.4.2.2. Fibre angle distribution

The fibre angle distribution parameters were measured and recorded using a total of 46 micrographs for 6 tensile test specimens. The mean fibre angle and the standard deviation (distribution parameters) for each specimen are given in Table 13 and the distribution parameters for each analysed micrograph are given in Appendix B9. The mean fibre angle for the plate was 7.4° ± 18° (average of all micrographs).

3.5. Modelling

3.5.1. Fibre area correction factor

Natural fibres vary in cross-sectional area along the fibre length. To calculate the tensile properties of natural fibres, the apparent cross-sectional area of each fibre is normally calculated assuming a circular cross-section [27, 76-78] and taking the mean of multiple projected widths measured along the fibre length as the apparent fibre 'diameter' [27, 76-78]. To evaluate the effect of the assumed cross-section and

the apparent diameter on the mechanical properties of the jute fibres, single technical jute fibre tensile test data was further analysed. The apparent cross-sectional areas of 785 fibres were calculated from the mean fibre 'diameter' assuming a circular cross-section. The apparent fibre area histogram is shown in Figure 33. A log-normal distribution [32, 33] was selected to represent the apparent fibre area distribution because a normal distribution of the fibre area could indicate negative area which is clearly unrealistic. The log-normal probability density function is:

$$f(T_A') = \frac{1}{\lambda_{T'}\sqrt{2\pi}} e^{-\frac{1}{2}\left(\frac{T_A' - \mu'}{\lambda_{T'}}\right)^2} \tag{41}$$

where T_A is the fibre area, $T_A' = \ln(T_A)$, μ' is the location parameter (arithmetic mean of natural logarithms of fibre area) and $\lambda_{T'}$ is the scale parameter (standard deviation of the natural logarithms of fibre area).

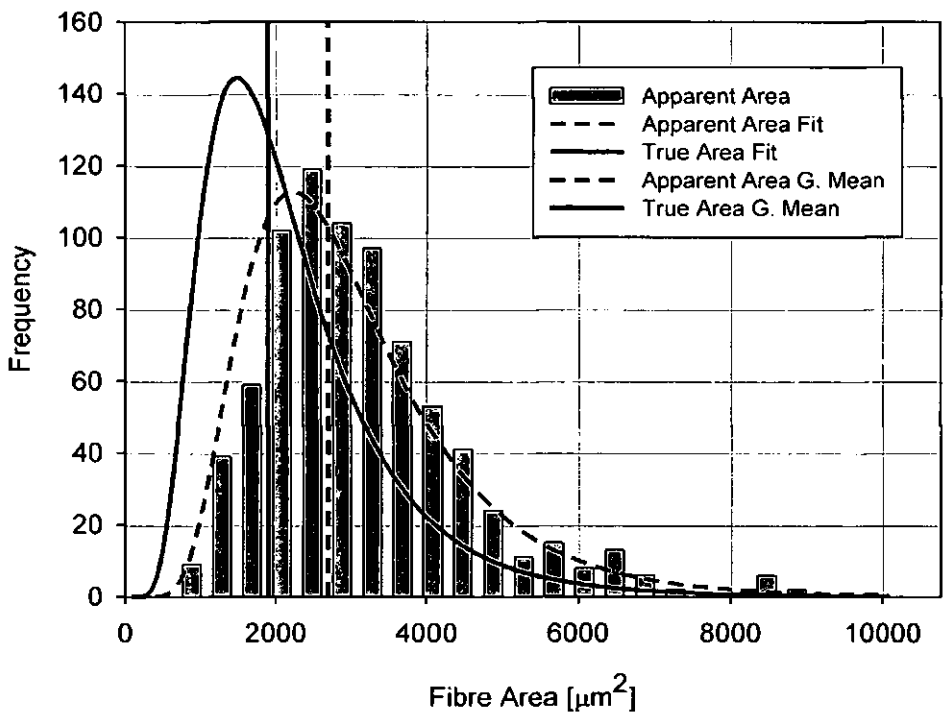

Figure 33: Apparent fibre area distribution and True fibre area distribution

The log-normal distribution location and scale parameter for the apparent fibre area distribution was 7.90 and 0.46 respectively. It was observed that the jute fibre cross-

sectional area estimated by assuming circular cross-section leads to large error in the estimated area and this error can lead to high scatter in the modulus and strength data of the fibre (as detailed in section 3.1.2).

It was also observed that the true cross sectional area of 106 jute fibres from the same batch of fibres but not the 785 tested above followed a log-normal distribution. The log-normal distribution location and scale parameters for the true cross-sectional area of the studied jute fibres were calculated to be 7.55 and 0.52 respectively. The true cross-sectional area distribution is overlaid on the apparent fibre area distribution in Figure 33. It was observed that the apparent fibre area distribution showed a negative skew (the distribution peak shifts towards the right) and the maximum peak drops when compared to true fibre area distribution. The negative skew indicates that the mechanical properties (fibre modulus and fibre strength) calculated using the apparent fibre area underestimate the mechanical properties. To counter the negative skew in the apparent fibre area distribution the location parameter of the apparent fibre area distribution (7.90) is replaced with that of the true fibre area distribution (7.55). The resulting modified apparent area distribution is shown in Figure 34.

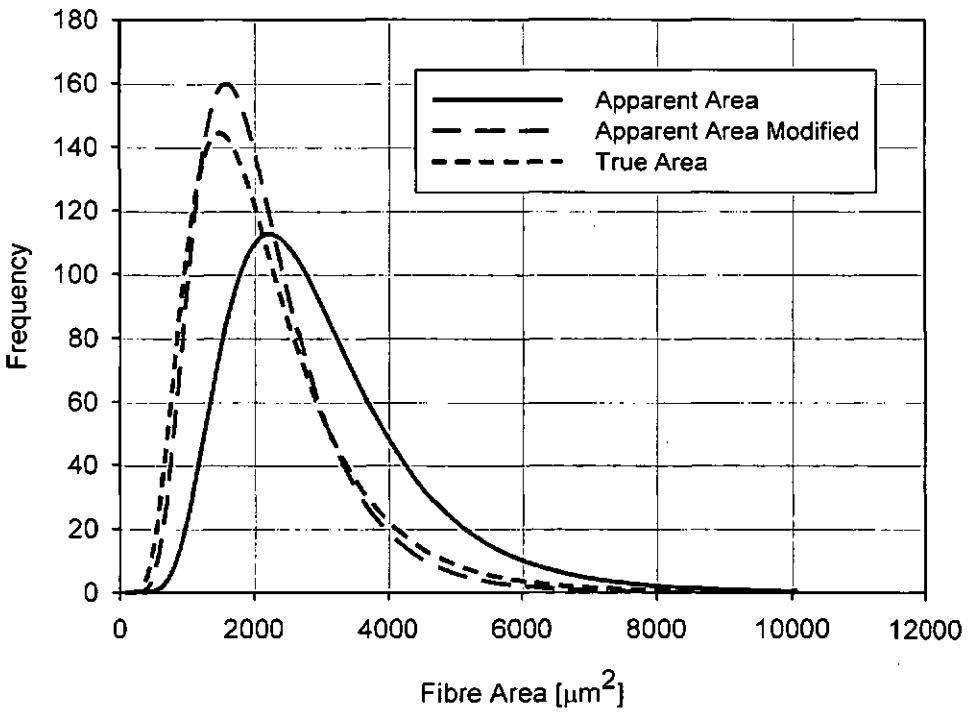

Figure 34: Modified fibre area distribution

The modified apparent area distribution is clearly a closer fit to the true fibre area distribution.

Therefore the accuracy of the mean mechanical properties based on the apparent fibre area (i.e. modulus and strength) can be improved by taking into consideration the apparent fibre area distribution, apparent stress (strength and modulus are derived from stress) and true fibre area distribution. Apparent stress and true stress are given by Equation 42 and 43 respectively.

$$\sigma_{apparent} = \frac{Force}{Area_{apparent}} \tag{42}$$

$$\sigma_{true} = \frac{Force}{Area_{true}} \tag{43}$$

By equating force in Equation 42 and 43, the true stress is given by Equation 44,

$$\sigma_{true} Area_{true} = \sigma_{apparent} Area_{apparent}$$

$$\sigma_{true} = \sigma_{apparent} \frac{Area_{apparent}}{Area_{true}} \tag{44}$$

It is difficult to calculate apparent / true fibre area ratio for individual fibres but in an average sense it can be estimated from the ratio of the location parameters of the apparent fibre area distribution and the true fibre area distribution. The location parameter of the log-normal distribution is in natural logarithmic domain therefore it is changed to the real number domain by taking the exponent of the location parameters as shown in Equation 45,

$$\kappa = \frac{Area_{apparent}}{Area_{true}} = \frac{\exp(\mu'_{apparent})}{\exp(\mu'_{true})} \tag{45}$$

The exponent of location parameter gives geometric mean of the log-normal distribution [79]. Hence, the fibre area correction factor, κ is the ratio of the geometric mean of the apparent fibre area and the true fibre area.

$$\kappa = \frac{\mu_{apparent}}{\mu_{true}} \tag{46}$$

The geometric means for the apparent fibre area and the measured true fibre area were 2697 μm^2 and 1896 μm^2 respectively thus giving a fibre area correction factor of 1.42. The fibre area correction factor, κ can be incorporated in the stiffness and strength prediction equations to improve the accuracy of the estimates.

Therefore, Equation 33 should be further extended by inclusion of the fibre area correction factor, κ to give,

$$E = \kappa \eta_d \eta_l \eta_o E_f V_f + E_m V_m \qquad (47)$$

The fibre area correction factor (given by Equation 46) can also be included in Equation 34 to account for the error in the fibre cross-sectional area measurement. The resulting equation is,

$$\sigma_{c_{max}} = \kappa \sigma_{f_{max}} V_f + (\sigma_m)_{\varepsilon_{f_{max}}} (1 - V_f) \qquad (48)$$

3.5.2. Fibre orientation factor

The fibre orientation distribution factor is given by Equation 31. In Equation 31, 'a_n' is the proportion of the fibres making θ_n angle to the applied load. The parameter 'a_n' can be calculated from the fibre angle distribution using probability density function. The fibre angle measured using micrographs followed the normal distribution, therefore 'a_n' was calculated from the normal distribution probability density function. As the normal probability density function is a continuous function the summation in Equation 31 is replaced with integration over the fibre angle from -90 to 90 degree. The resulting equation is,

$$\eta_o = \int_{-90}^{90} \left(\frac{1}{\sigma_N \sqrt{2\pi}} e^{\left(\frac{(\varphi_x - \mu_N)^2}{2\sigma_N^2} \right)} \right) \cos(\varphi_x)^4 \, d\varphi_x \qquad (49)$$

Where φ_x is fibre angle in degrees, μ_N is the mean fibre angle and σ_N is the fibre angle standard deviation.

The Equation 49 is integrated numerically using adaptive Simpson quadrature method [15] to calculate the fibre orientation distribution factor. The fibre orientation distribution factor for each micrograph was calculated using the fibre distribution parameters given in Appendix B9. The fibre orientation distribution factor for each specimen is given in Table 14. The mean fibre orientation factor for the plate was calculated to be 0.81 ±0.06.

Table 14: Fibre orientation distribution factor

Sample No.	*Fibre Orientation*
5a	0.86
5b	0.70
5c	0.77
5d	0.85
5e	0.85
5f	0.85
Plate (Mean)	***0.81***
SD	***0.06***

3.5.3. Micromechanical model

3.5.3.1. Composite modulus

The matrix and jute fibre elastic properties and fibre strength are given in Table 15 together with data for jute fibres from the literature to confirm the reported values are consistent with the works of others.

Table 15: Matrix and Fibre elastic properties

	Density [kg/m^3]	*Modulus [GPa]*	*Strength [MPa]*	*Failure Strain [%]*	*Poisson's Ratio*	*Reference*
Matrix	-	2.65	61	4.1%	0.35	[50]
Jute	-	27.9~	152-558	0.6%-1.8%	-	▲
Jute Modulus from literature	1480	25.5	442	1.8%	-	[80] ▲
	-	26.5	340	1.8%	-	[77] ▲
	1300	26.5	393-773	1.5%-1.8%	-	[81] ▲
	-	24.6	680	4.4%	-	[78] ▲
	1390	26.3	307-399	1.4%-1.6%	-	[82]
	-	30.0	540-700	-	-	[83] ▲
	1300	55.5	442	-	-	[84] #
	1300	45.0	250	-	-	[85]*

~ The modulus is calculated as the average of all the moduli reported [Table 5] at different gauge lengths assuming the fibres have circular cross-section.

▲ Fibre properties calculated assuming circular cross-sectional area from multiple linear measurements.

Composite experimental properties (tested at different fibre volume fractions) used to estimate fibre modulus and strength by extrapolating the respective properties to a fibre volume fraction of unity.

* Composite experimental properties used to estimate modulus and strength by back calculating using rule of mixture and the respective fibre volume fraction and fibre orientation factor.

The following data (given in Table 16) were reported from the experiments on jute fibres and their composites. The fibre length distribution factor for Cox model [63] (given by Equation 26) was calculated using the geometric mean of the measured fibre length, 65.60 mm and the mean apparent diameter, 60.16 μm was used to calculate the fibre cross-sectional area (assuming circular cross-section and uniform square fibre packing).

Table 16: Summary of data from experiments used in the prediction and validation of the micromechanical models

Fibre volume fraction, V_f	18.9 % ± 3.9%
Fibre angle distribution	7.4° ± 18.0°
Fibre orientation factor, η_o	0.81
Fibre diameter distribution factor, η_d	1
Fibre length distribution factor, η_l	1
Fibre area correction factor, κ	1.42
Plate modulus, E_c	8.18 ± 0.6GPa
Plate strength, σ_c	100.0 ± 5.7 MPa

The tensile modulus was predicted for 6 individual samples and for the overall plate using different micromechanics models and compared to the experimental results. The plate modulus was calculated as the average modulus of the 6 samples machined from the plate. The predicted tensile moduli using different micromechanical models are shown in Figure 35 and Table 17.

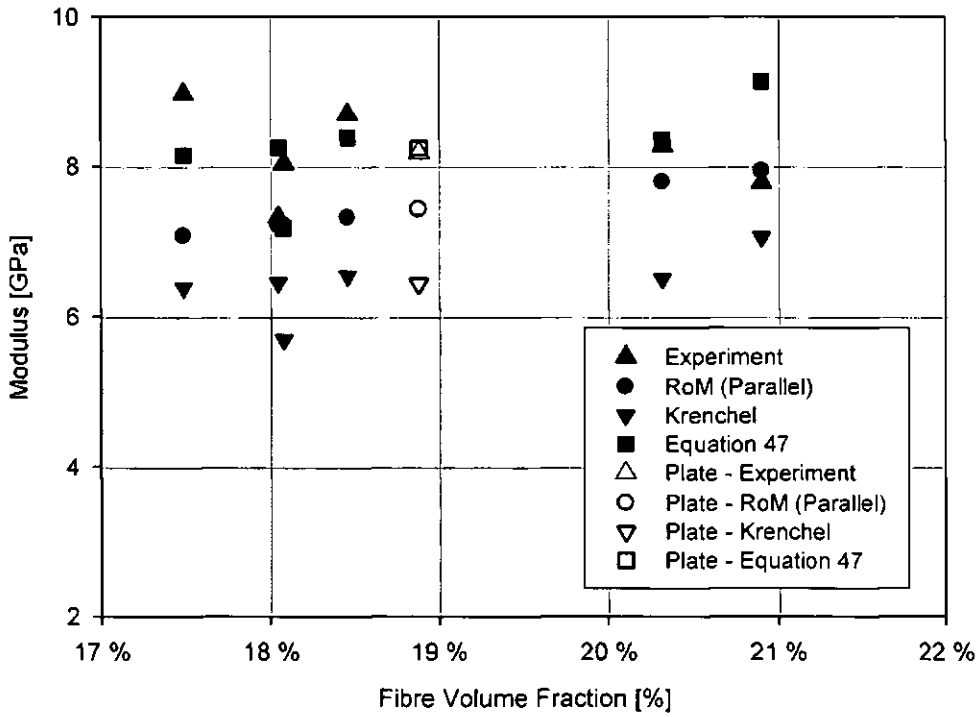

Figure 35: Experimental and predicted composite tensile modulus for individual samples (solid points) and plate average (open points)

The computed errors in the predictions are shown in Table 18. The $RoM_{||}$, $RoM_{\perp}$, Cox, Krenchel and Cox & Krenchel models all underestimated the composite modulus. The Halpin-Tsai model perfectly predicted the sample modulus but the reinforcing efficiency ξ used was calculated from the experimental modulus using Equation 24 hence it is a circular reference thus excluded. Equation 47 offers the smallest error in the predicted plate (mean) modulus.

The close correlation between the prediction of the elastic modulus and the experimentally measured values suggest that the system chosen is compliant with the assumptions of the rule-of-mixtures. The bonding between the fibres and the matrix is good.

Table 17: Predicted composite modulus

Sample	*Experiment*	*RoM (Parallel)*	*RoM (Series)*	*Cox*	*Krenchel*	*Equation 47*
5a	8.98	7.07	3.15	7.07	6.39	8.15
5b	8.04	7.22	3.17	7.22	5.70	7.18
5c	8.28	7.79	3.25	7.79	6.51	8.35
5d	7.79	7.94	3.27	7.94	7.05	9.14
5e	7.33	7.21	3.17	7.21	6.45	8.25
5f	8.70	7.32	3.18	7.32	6.54	8.38
Plate	***8.18 ± 0.6***	***7.43***	***3.20***	***7.43***	***6.44***	***8.24***

Table 18: Error in the predicted composite modulus

Sample	*RoM (Parallel)*	*RoM (Series)*	*Cox*	*Krenchel*	*Equation 47*
5a	-21.21%	-64.93%	-21.21%	-28.87%	-9.23%
5b	-10.16%	-60.59%	-10.16%	-29.15%	-10.74%
5c	-5.90%	-60.77%	-5.90%	-21.39%	0.91%
5d	1.87%	-58.05%	1.87%	-9.45%	17.28%
5e	-1.53%	-56.77%	-1.53%	-11.92%	12.63%
5f	-15.86%	-63.42%	-15.86%	-24.80%	-3.65%
Plate	***-9.27%***	***-60.95%***	***-9.27%***	***-21.32%***	***0.69%***

3.5.3.2. Composite strength

The tensile strength of the composite was predicted using Kelly-Tyson model [69]. The Kelly-Tyson model requires the tensile strength of the fibres but the natural fibres show large scatter in the tensile strength value therefore mean fibre strength was calculated from the fibre strength distribution. The tensile strength distribution of the natural fibres is described by two-parameter Weibull distributions [27, 76]. The two-parameter Weibull Probability Density Function (PDF) [32, 33] is:

$$f(\sigma) = \frac{\beta}{\eta}\left(\frac{\sigma}{\eta}\right)^{\beta-1} e^{-\left(\frac{\sigma}{\eta}\right)^{\beta}} \tag{50}$$

The mean of Weibull distribution is given by Equation 51 [33],

$$\mu = \eta\Gamma\left(\frac{1}{\beta}+1\right) \tag{51}$$

where, η is the scale parameter and β is shape parameter. Γ is gamma function given by Equation 52.

$$\Gamma(n) = \int_0^\infty e^{-x}x^{n-1}dx \tag{52}$$

However the natural fibre strength depends on the fibre gauge length [81] thus Multiple Data Set (MDS) Weak-Link Scaling model (WLS) and Natural Logarithm Interpolation Model (NLIM) were used to predict the fibre strength as these models take account of the fibre gauge length. Weibull distribution strength parameters for MDS-WLS model and NLIM are given in Table 19. The mean fibre strength used in Kelly-Tyson model was predicted at geometric mean fibre length of 65.60 mm for this batch of jute fibres. The predicted mean fibre strength using MDS and NLIM model were 275 MPa and 298 MPa respectively.

Table 19: Weibull distribution strength parameters

	Weibull Modulus, β	***Characteristic Strength, η [MPa]***
MDS Weak link	*3*	$\frac{1243}{\sqrt[3]{Fibre\ Length}}$
NLIM Model	$-0.152\ln(Fibre\ Length)+3.487$	$-111.656\ln(Fibre\ Length)+801.63$

The predicted tensile strengths of the composites are shown in Figure 36 and Table 20.

Table 20: Predicted composite strength

Sample	***Experiment***	***Kelly-Tyson NLIM***	***Kelly-Tyson MDS***	***FACF NLIM***	***FACF MDS***
5a	104.9	75.46	69.67	97.36	89.89
5b	-	77.05	71.14	99.69	92.04
5c	99.6	83.09	76.72	108.53	100.21
5d	106.8	84.66	78.17	110.82	102.33
5e	94.8	76.97	71.07	99.57	91.93
5f	94.2	78.08	72.09	101.19	93.43
Plate	***100.0 ± 5.7***	***79.22***	***73.14***	***102.86***	***94.97***

The strength prediction for the natural fibre composite was improved by including the Fibre Area Correction Factor (FACF), in the Kelly-Tyson equation. The FACF corrects the mean fibre strength to account for the true fibre area. The predicted tensile strength is shown in Figure 36 and Table 20.

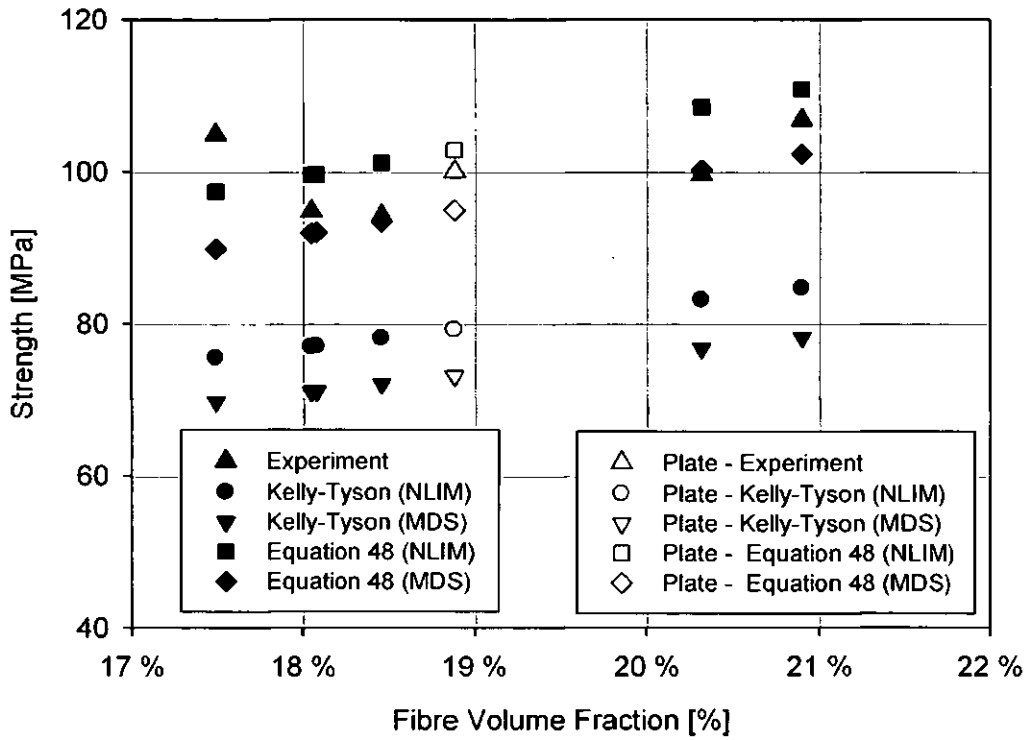

Figure 36: Experimental and predicted composite tensile Strength for individual samples (solid points) and plate average (open points)

The error in the predicted strength (Table 21) was calculated by comparing the predicted strength with the experimental strength of the composite. Equation 48 offered smallest error in the predictions.

Table 21: Error in predicted composite strength

Sample	Kelly- Tyson	Kelly- Tyson	FACF/Equation 48	FACF/Equation 48
	NLIM	***MDS***	***NLIM***	***MDS***
5a	-28.07%	-33.58%	-7.19%	-14.31%
5b	-	-	-	-
5c	-16.57%	-22.97%	8.97%	0.61%
5d	-20.73%	-26.81%	3.77%	-4.19%
5e	-18.81%	-25.03%	5.03%	-3.02%
5f	-17.12%	-23.47%	7.42%	-0.82%
Plate	***-20.83%***	***-26.90%***	***2.80%***	***-5.08%***

4. Discussion

4.1. Fibre physical characterisation

4.1.1. Fibre cross-sectional area

The jute fibre cross-section was analysed using digital images. The fibre cross-section was modelled using different geometrical shapes (major circle, minor circle, ellipse, super ellipse, convex hull) and the fibre area was estimated for each individual case. The area distribution for each case was determined and it was observed for all the assumed shapes (except for the minor circle) that the area distribution showed a negative skew (the distribution peak shifts toward right) and the maximum peak drops when compared to true area distribution. This negative skew indicates that the method overestimates the fibre area. The drop in distribution peak indicates an increase in the range of the data. Fibre area calculated using a method that over-estimates the fibre area will always underestimate the modulus and strength of the fibre. The increase in the range of the error in the area distribution contributes to the increase in the variability of the mechanical properties which are a function of the cross-sectional area (e.g. modulus and strength).

It was observed that the convex hull offered the best estimate of the fibre cross-sectional area with least spread but this measurement is not straightforward[3].

[3]The measurement might be realised with expensive micro-tomographic techniques subject to appropriate high resolution of the system.

The fibre area estimated by optical microscopy using the major projected width of the fibre as "diameter" and assuming circular cross-section will overestimate the fibre cross-sectional area.

The fibre cross-sectional area calculated assuming an elliptical cross-section gives a lower variation in the fibre area compared to circular cross-section. The minimum elliptical area calculated from the two orthogonal projection widths (*A* and *B)* gives the area closest to the true fibre area. The best practical method to estimate fibre cross-sectional area would be to measure the parameters for an ellipse. This offers a slight overestimate but with reduced spread in the data when judged relative to the commonly assumed circular cross-section of the fibre.

The assumed elliptical cross-section will yield an underestimate of modulus and strength but with reduced variation and hence will result in a safer mechanical design when the fibres are used as reinforcement in a composite.

In order to fully characterise the variation of cross-section along a fibre, the following options could assist:

- Optical, laser or electron microscopy/micrometry transverse to the major axis of the fibre. A single measurement will normally return the maximum value of the "diameter" at the monitored position. Even for measurements where the fibre is rotated, this technique is neither capable of resolving concave topological features in the surface of the fibre nor of seeing the lumen (the central void within the fibre) due to the opacity of natural fibres.
- Xu and Jayaraman [86] have conducted preliminary experiments using low (50x) magnification optical microscopy with an image-processing system for the measurement of the variations in cross-sectional shapes of sisal (leaf) fibre cross-section with the fibres mounted on a tacky support material with good optical contrast.
- Optical microscopy of fibres embedded in mounting resin with sequential polishing to expose the fibre cross section at regular intervals is fraught with difficulties as obtaining good contrast between the fibre and the resin could require processes (e.g. dyeing the fibre) which might change the characteristic under consideration. Further, this will inevitably be a tedious task!
- X-ray computer tomography - typical systems have pixel/voxel resolution of ~5μm which is inadequate for accurate analysis of fibres with diameters three-times

this value. Initial trials have been conducted with a SkyScan 1174 x-ray microtomograph [87] (6 μm resolution) which produced images with pixel resolution at a similar scale to the feature size in the batch of jute fibres studied. The SkyScan 2011 [88] state-of-the-art x-ray nanotomograph (focal spot size less than 400 nm) would be a more appropriate instrument for this task.

4.2. Fibre mechanical properties

4.2.1. Coefficient of Variation (CoV) in fibre strength and fracture strain

Most man-made fibres have a circular cross-section and when the density is known, then an effective Cross Sectional Area (CSA) can be easily determined. However, natural fibres may have an irregular cross-section which varies along the length and may include voids (lumen) within each of the individual cells. In the textile industry it is normal to define fibres by their weight per unit length. For example, denier is the mass in grams of 9 km of a fibre, filament or yarn, or the recognised SI unit, "tex", is the mass in grams of 1 km of product. It is not straightforward to convert these units into area for fibres with irregular and varying cross-sectional area.

Errors arising from the above methods lead to inaccuracies in the estimation of the CSA with consequences for the determination of fibre moduli and strengths. Accurate densities for natural fibres are difficult to determine and the presence or absence of the lumen affects both density and the effective CSA.

The variation in the mechanical properties of the 785 technical jute fibres was analysed using the Coefficient of Variation (CoV). The observed mean and standard deviation of Young's modulus, fibre strength and fracture strain at different gauge lengths is shown in Table 22. The CSA was calculated using the fibre "diameter" measured by averaging multiple readings of the transverse linear dimensions from optical microscopy with an assumption of circular cross-section.

Table 22: Mean, Standard Deviation and CoV of Young's moduli, fibre strength and fracture strain at different fibre length

	Modulus [GPa]			*Strength [MPa]*			*Fracture Strain [%]*		
Fibre Length	***Mean***	***Standard Deviation***	***CoV***	***Mean***	***Standard Deviation***	***CoV***	***Mean***	***Standard Deviation***	***CoV***
6	32.49	10.12	*0.31*	557.54	194.05	*0.35*	1.79%	0.33%	*0.19*
10	26.27	8.98	*0.34*	464.38	165.08	*0.36*	1.70%	0.41%	*0.24*
20	30.99	6.97	*0.22*	403.31	139.97	*0.35*	1.29%	0.30%	*0.24*
30	31.01	7.06	*0.23*	392.40	131.15	*0.33*	1.25%	0.31%	*0.25*
50	28.29	8.78	*0.31*	336.32	131.58	*0.39*	1.11%	0.34%	*0.31*
100	27.11	4.66	*0.17*	258.57	90.88	*0.35*	0.91%	0.24%	*0.27*
150	25.78	4.29	*0.17*	200.33	68.23	*0.34*	0.76%	0.21%	*0.28*
200	27.62	4.75	*0.17*	189.66	71.75	*0.38*	0.68%	0.23%	*0.34*
250	23.42	4.50	*0.19*	151.78	66.29	*0.44*	0.64%	0.23%	*0.35*
300	26.37	5.04	*0.19*	153.53	70.32	*0.46*	0.58%	0.20%	*0.35*

The relationship between the fibre diameter and the fibre strength irrespective of fibre gauge length, is given in Figure 37a. As the fibre diameter increases, the fibre strength decreases. Figure 37b shows the relationship between the fibre length and the strength. The fibre strength decreases with increasing fibre gauge length. The relationships between the fibre strength and either fibre diameter or fibre length are both shown to have a logarithmic trend.

Similarly, Figure 38a shows the relationship between the fibre diameter and the fibre fracture strain. Using the trendline fitted to the data within the range of fibre diameters tested, the reduction in the fracture strain as the mean fibre diameter increases is small (36%) when compared to the reduction in the fibre strength (83%). Figure 38b shows the relationship between the fibre length and the fracture strain. The fracture strain also decreases with the increasing fibre gauge length. The logarithmic trend lines represent the general variation of fracture strain with change in fibre diameter and length respectively. The fracture strain is strongly influenced by the fibre length, but it is a relatively weak function of fibre diameter as is apparent in Figure 38a for the range of lengths/diameters available in the tested sample of fibre.

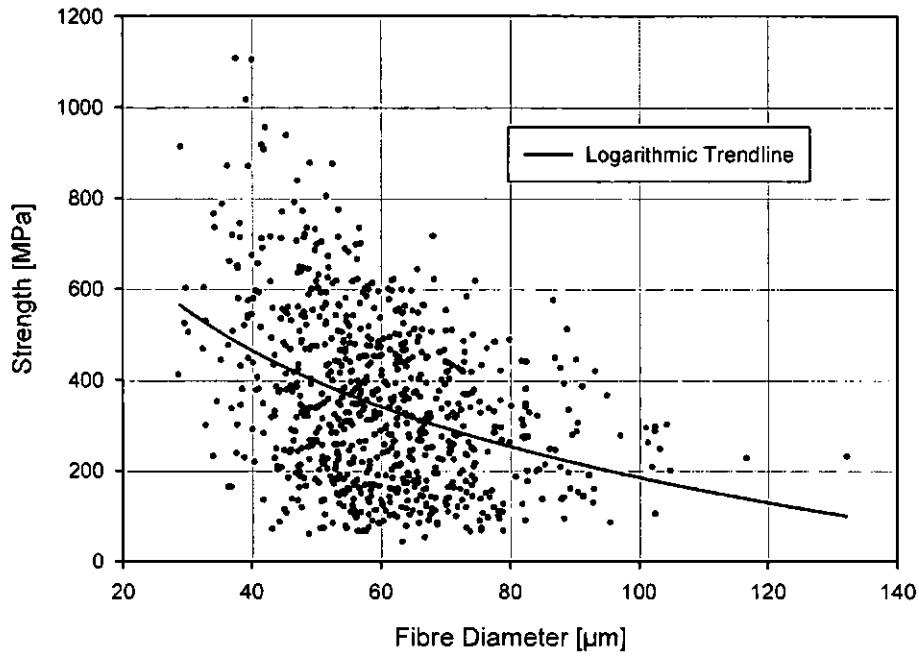

(a)

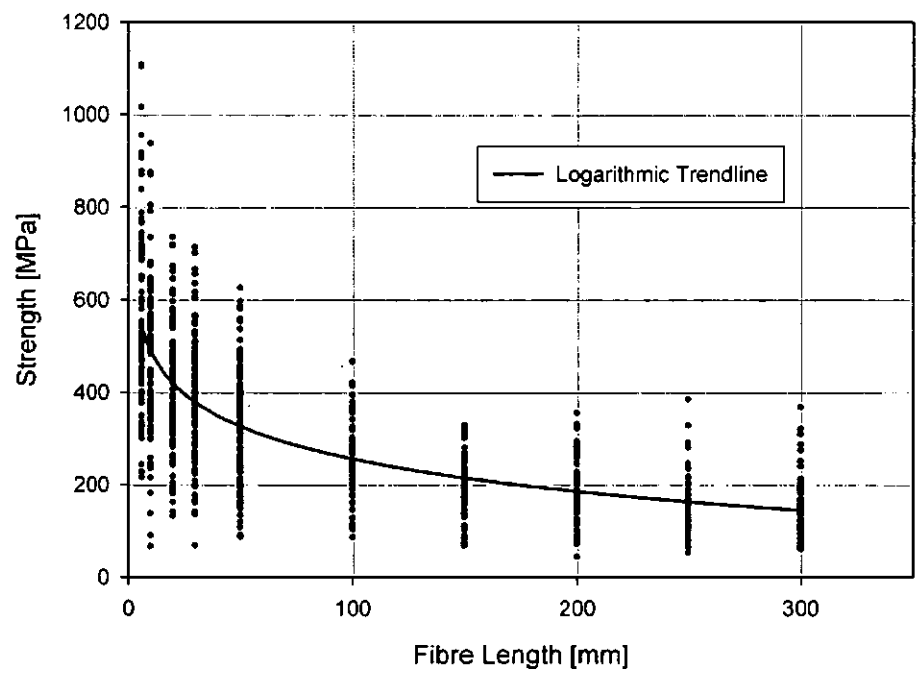

(b)

Figure 37: (a) Fibre strength against fibre diameter, (b) Fibre strength against mean fibre length

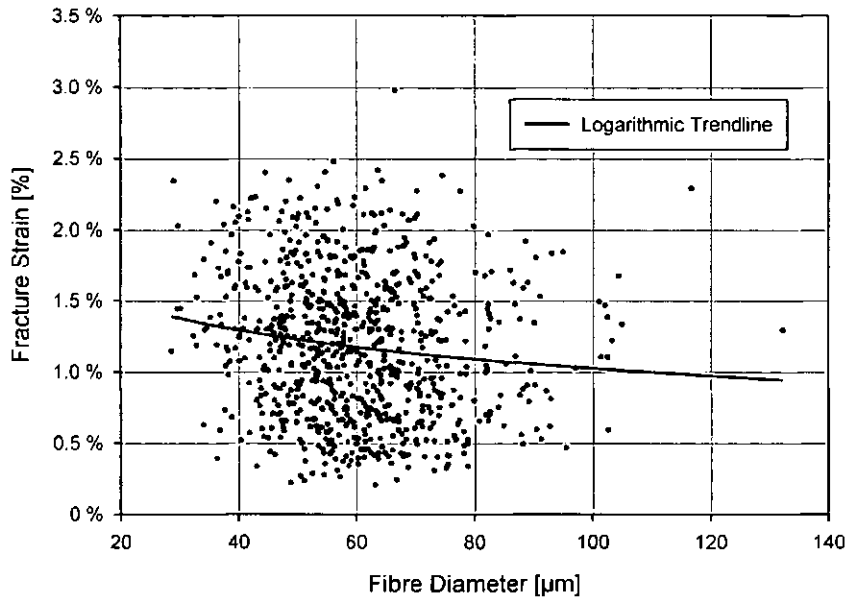

(a)

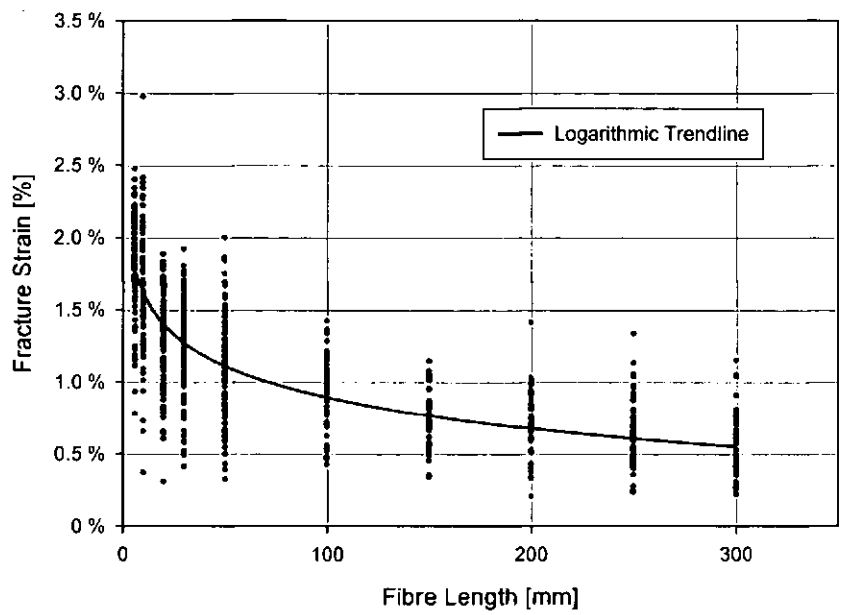

(b)

Figure 38: (a), Fibre fracture strain against fibre diameter, (b) Fibre fracture strain against mean fibre length

The normalised variation (spread) of the tensile mechanical properties of the fibres is measured by the Coefficients of Variation. The CoV is defined as the ratio of the standard deviation, σ_N to the mean, μ_N [89] given by Equation 53.

$$CoV = \frac{\sigma_N}{\mu_N} \tag{53}$$

Lower CoV value signifies smaller variations.

For Weibull distributions, the appropriate equations for CoV are given in Appendix B4. For any given data set, both equations return the same numerical value.

The calculated CoV for Young's modulus, fibre strength and fracture strain at different gauge lengths are shown in Table 22 respectively. As the fibre length increases, both the strength and fracture strain CoV increase, while the Young's modulus CoV decreased initially for the fibre length between 6 to 50 mm, however, Young's modulus CoV stays fairly constant for fibre length above 100 mm. The CoV of fracture strain was consistently lower than that of strength at each of the measured fibre lengths (Figure 39). The lower CoV of fracture strain is attributed to the fact that failure strain is independent of the measured fibre "diameter". Further, the latter parameter is difficult to determine because of the irregular and varying cross section of the fibre. The linear trend lines through the strength and fracture strain CoVs at different fibre lengths are almost parallel.

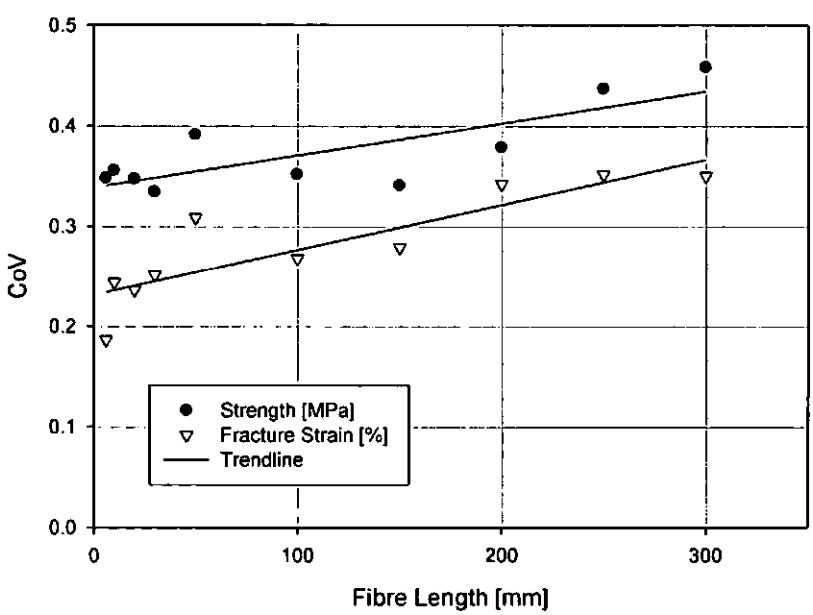

Figure 39: Strength and fracture strain CoV against fibre length

The fibre gauge length can be selected for the fibre tensile tests but the fibre diameter is an independent variable which cannot be selected. Therefore, to quantify

the effect of the fibre diameter on the strength and fracture strain the fibre diameter is grouped in classes (bins). The bin width of 10 micrometres is chosen for the fibre diameter and the resulting groups are shown in Figure 40. The average, standard deviation and CoV of fibre strength and fracture strain were calculated for each group (bin), shown in Table 23 (nb: data above 105 μm is discarded as there is only one data point in each bin). The CoV of fracture strain was consistently lower than that of strength for different fibre diameter groups as shown in Figure 41. The lower Coefficient of Variation of fracture strain signifies that it a more reliable measure of tensile properties.

Table 23: Mean, Standard deviation and CoV of Young's moduli, fibre strength and fracture strain at different fibre diameter

	Strength			*Fracture Strain*		
Diameter Group	***Mean***	***Standard Deviation***	***CoV***	***Mean***	***Standard Deviation***	***CoV***
25-35	533.03	192.95	0.36	1.46%	0.43%	0.29
35-45	506.01	240.83	0.48	1.36%	0.51%	0.38
45-55	386.03	192.46	0.50	1.21%	0.50%	0.41
55-65	329.68	160.63	0.49	1.15%	0.51%	0.44
65-75	294.01	144.44	0.49	1.14%	0.52%	0.46
75-85	248.61	123.36	0.50	1.00%	0.48%	0.48
85-95	271.75	134.57	0.50	1.12%	0.46%	0.41
95-105	247.35	85.03	0.34	1.21%	0.42%	0.35
105-115	199.14	-	-	1.33%	-	-
115-125	226.54	-	-	2.28%	-	-
125-135	230.49	-	-	1.29%	-	-

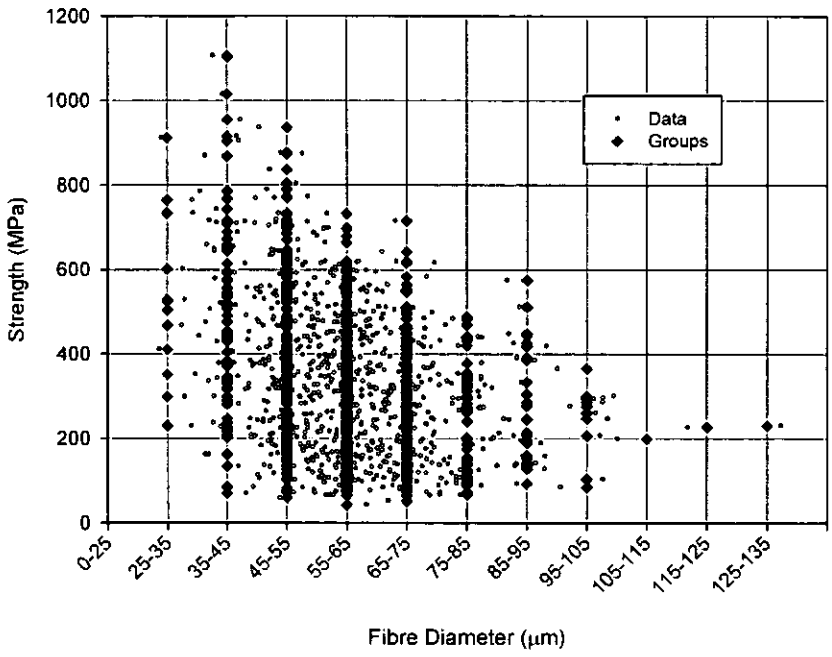

(a)

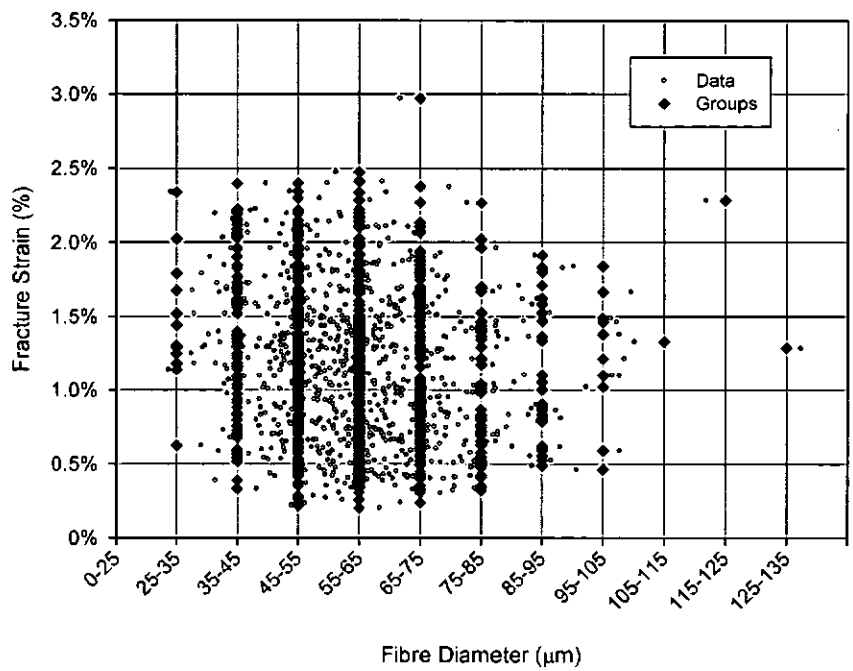

(b)

Figure 40: (a) Fibre strength against fibre diameter group, (b) Fracture strain against fibre diameter group

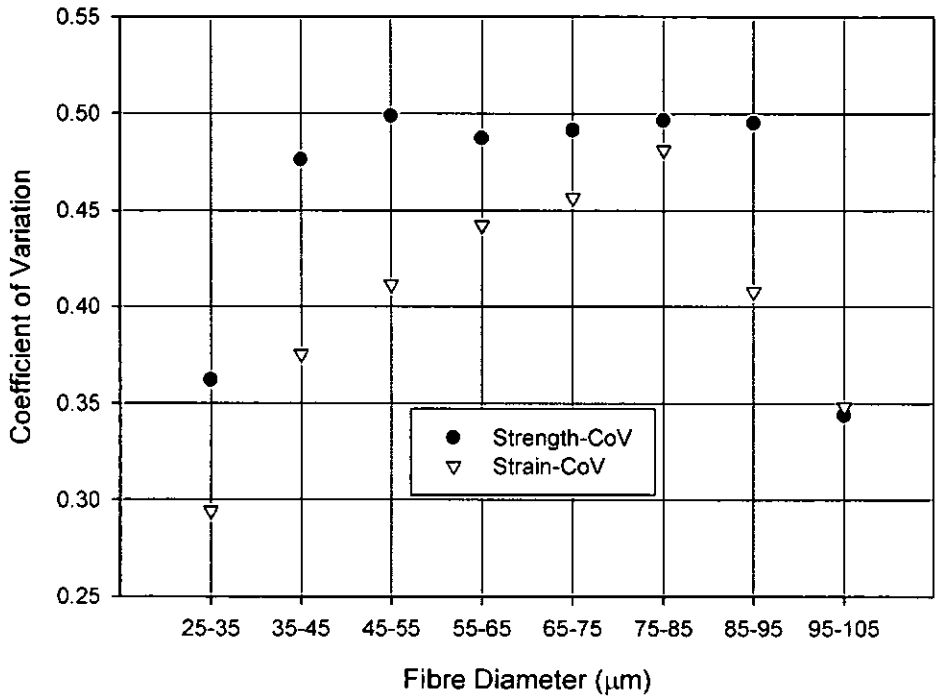

Figure 41: Strength and fracture strain CoV against fibre diameter

In order to triangulate these findings, data from other authors has been analysed (Table 24). In each case, the CoV for failure strain is lower than that for strength. The CoV for failure strain is generally of a similar magnitude to that for man-made fibres.

The modulus, strength and fracture strain are from data which do not consider Weibull distributions and where the authors use conventional mechanical testing to appropriate standards and report data mean and standard deviation values.

Table 24: Typical CoV for modulus, strength and strain to failure from the literature

	Young's modulus (GPa)	*SD*	*CoV*	*Ultimate stress (MPa)*	*SD*	*CoV*	*Strain to failure (%)*	*SD*	*CoV*	*References*
Stinging nettle	87.00	28.00	*0.32*	1594.0	640.0	*0.40*	2.11	0.81	*0.38*	[68]
Flax	54.08	15.13	*0.28*	1339.0	486.0	*0.36*	3.27	0.84	*0.26*	[90]
Flax	40.00	19.20	*0.48*	904.0	326.0	*0.36*	1.40	0.20	*0.14*	[91]
Hemp	19.10	4.30	*0.23*	270.0	40.0	*0.15*	0.80	0.10	*0.13*	[92]
Kenaf	13.40	1.60	*0.12*	153.8	41.4	*0.27*	1.18	0.24	*0.20*	[93]
Carbon- 38/III	196.53	6.60	*0.03*	2740.0	730.0	*0.27*	1.39	0.26	*0.19*	[94]
Carbon-WS/2/3	225.43	6.30	*0.03*	4700.0	1150.0	*0.24*	2.10	0.40	*0.19*	[95]
Carbon-KM3	225.24	7.40	*0.03*	2800.0	650.0	*0.23*	0.96	0.22	*0.23*	[94]
Glass	70.30	12.60	*0.18*	1950.0	550.0	0.28	2.96	0.68	0.23	[94]

4.3. Statistical strength and fracture strain distribution

4.3.1. Goodness of fit test to evaluate the fibre failure models

The Anderson-Darling Goodness Of Fit Number (GOFN) [75] (Appendix B3) is used to examine the fit of the Weibull distribution point estimates (given in Table 25 for strength and fracture strain parameters respectively) to the experimental data at each of the tested fibre lengths. A lower GOFN indicates a better fit. Summing the GOFN for the point estimates for each case across all fibre lengths shows that the minimum possible GOFN is 5.68 for tensile strength and 4.39 for fracture strain. This is the minimum possible GOFN which is used as benchmark to evaluate other Weibull models (weak-link scaling models and empirical models).

Table 25: Anderson-Darling GOFN for strength and fracture strain (Point estimates)

Fibre Length	*Strength*	*Fracture Strain*
	Point Estimate GOFN	*Point Estimate GOFN*
6	0.90	0.24
10	0.71	0.33
20	0.33	0.36
30	0.27	0.70
50	0.48	0.78
100	0.30	0.29
150	0.28	0.38
200	0.16	0.28
250	1.41	0.55
300	0.84	0.47
Sum	**5.68**	**4.39**

In each case, the accuracy of the fit to an assumed Weibull distribution is quantified and compared to the standard weak-link prediction (based on the point estimates at each fibre length under consideration as the scaling point) using the Anderson-Darling Goodness of Fit test [75]. A lower Goodness of Fit Number (GOFN) implies a closer match to the experimental data. At each fibre length, a Weibull distribution was calculated based on the β and η_p. This was done for both standard weak-link scaling at 6 mm ... 300 mm and for MDS weak-link scaling. The data was derived from Section 3.3.2 (WLSM), or from Section 3.3.3 (MDS) respectively. For each

WLSM and MDS case, a GOFN was determined for the Weibull distributions at each length. The sum of the GOFN at the ten fibre lengths was used to identify the best model. The lowest GOFN total indicated the 'best fit' model for the entire dataset. The GOFN results for strength and fracture strains are given in Table 26.

Table 26: Anderson-Darling GOFN for strength and fracture strain (Weak-link scaling)

Fibre length [mm]:	*GOFN Strength (Sum)*	*GOFN Fracture Strain (Sum)*
Standard Weak-link Model		
6	48.0	418.0
10	59.3	136.1
20	36.8	113.5
30	76.5	94.9
50	69.8	43.8
100	50.3	48.7
150	61.9	60.1
200	33.9	39.2
250	52.3	57.6
300	79.3	43.8
MDS Weak-link Model		
6 and 300	41.4	58.3
6, 50 and 300	35.3	33.8
6, 100 and 300	34.8	48.2
All (6 mm ... 300 mm)	33.0	32.1

As mentioned above (see Section 3.3.2), weak-link scaling assumes that β is constant for all fibre lengths. The change in the Weibull modulus for fracture strain is greater than for ultimate strength and as a result, the fit for strength is generally the better of the two. The MDS models tend to be significantly better for both strength and fracture strain than the standard weak-link method and thus are the preferred option. The MDS models based on the point estimates at three sets of fibre lengths give a closer fit to the experimental data (across the full range of fibre lengths) than

the two point estimate model. The three point estimate model based on the 6 mm, 50 mm and 300 mm fibre lengths produces an almost optimum fit (defined by the 'All' MDS model) for both strength and strain, whilst the model based on 6 mm, 100 mm and 300 mm fibre lengths produces an almost optimum fit for strength but not for fracture strain.

The Anderson-Darling Goodness Of Fit Number (GOFN) [75] is calculated to examine the fit, of (a) linear interpolated Weibull distribution parameters and (b) the logarithmic interpolated Weibull distribution parameters (given in Table 27 for strength and fracture strain parameters respectively) to the experimental data at each of the tested fibre lengths. The sum of the GOFNs obtained for the logarithmic model (12.06 for strength and 14.39 for fracture strain) indicate an exceptional fit. GOFNs reported based on 'standard' weak-link scaling models are dependent on the scaling fibre length. The Multiple Data-Set (MDS) weak link model reports the sum of the GOFNs of 33.0 and 32.1 for strength and fracture strain (when considering test data sets at all fibre gauge lengths) which is significantly higher than the logarithmic GOFN values above.

The NLIM produces a significant improvement in predicted properties over the MDS model. Use of Anderson-Darling GOFN confirms this finding and reveals a reduction factor (MDS model GOFN/Logarithmic model GOFN) for this measurement of 2.74 for strength and 2.23 for strain.

Table 27: Anderson-Darling goodness of fit number (GOFN) for Weibull tensile strength and fracture strain at different fibre length (Empirical model)

	Strength		*Fracture Strain*	
Fibre Length	***Linear Model GOFN***	***Logarithmic Model GOFN***	***Linear Model GOFN***	***Logarithmic Model GOFN***
6	24.64	1.08	39.19	1.06
10	3.64	1.69	22.46	4.01
20	0.94	0.83	5.72	4.82
30	1.59	1.21	6.12	0.88
50	4.28	1.18	12.13	1.03
100	8.45	0.48	11.46	0.53
150	13.18	1.38	12.27	0.62
200	3.97	0.21	5.42	0.36
250	4.08	2.96	0.71	0.60
300	5.81	1.04	7.47	0.46
Sum	***70.60***	**12.06**	***122.94***	**14.39**

4.4. Jute/Epoxy Composite

In order to triangulate these findings, data from other authors has been analysed. The jute fibre reinforced composite properties reported by different authors are presented in Table 28. The Krenchel model (Equation 30) was used to predict the elastic modulus of the composite using the reported fibre volume fraction, fibre orientation factor and the form of reinforcement used. The jute fibre modulus used in the model was 27.8 GPa taken as the average of all the experimentally measured readings given in Table 15 (excluding 55.5 and 45 GPa as they are estimated from the composites). The calculated composite moduli are reported in Table 29. In each case (except one) it is observed the calculated modulus is lower than the experimental modulus.

Assuming that the Fibre Area Correction Factor (FACF) for the other batches of the jute fibres used in [81, 84, 85, 95-98] is similar to that reported here (1.42) and calculating the composite modulus using Equation 47 (Table 29), it was observed that the error in the predicted composite modulus is reduced (for all but two cases [96]).

Table 28: Reported elastic properties of jute fibre reinforced composite

Matrix	Volume Fraction	Weight Fraction	Reinforcement form	OF	Modulus [GPa]	Strength [MPa]	Failure Strain [%]	Poisson's Ratio	Reference
Epoxy	40%	-	Fibre yarn	1*	15.0	160	-	-	[81]
Epoxy	35%	33%	-	1	15.0 ± 1.0	104 ± 6.3	0.69%	-	[95]
Polyester	24%	22%	-	1	12.2 ± 0.3	84 ± 5.2	0.69%	-	[95]
Polyester	13%	-	Sliver	1	10.3	73	-	-	[84]
Polyester	27%	-	Sliver	1	18.6	129	-	-	[84]
Polyester	31%	-	Sliver	1	20.0	171	-	-	[84]
Polyester	37%	-	Sliver	1	23.0	-	-	-	[84]
Polyester	43%	-	Sliver	1	26.7	214	-	-	[84]
Polyester	16%	-	Chopped Strand	0.385	5.2 ± 0.5	38 ± 5.8	0.73% ± 0.11%	-	[85]
Polyester	45%	-	Fabric (20x12)	0.625	7.0 ± 1.1	60 ± 2.8	-	0.25	[96]
Polyester	45%	-	Fabric (20x12)	0.375	3.5 ± 0.4	35 ± 3.3	-	0.22	[96]
Polyester	36%	-	Fabric (22x12)	0.647	9.0^	-	-	-	[97]
Polyester	36%	-	Fabric (22x12)	0.353	6.5^	-	-	-	[97]
Polyester	29.5%	-	-	1	16.8	119	-	-	[98]

* Quasi-unidirectional

^ Notched samples

Table 29: Estimated composite modulus using Krenchel and Equation 47 with the error in the estimated modulus

Matrix	Matrix Modulus	Volume Fraction	Reinforcement Form	Orientation Factor (OF)	Twist Angle	Twist - OF	Final OF	Modulus [GPa]	Krenchel [GPa]	Error	Equation 47 [GPa]	Error	Reference
Epoxy	3.3*	40%	Fibre yarn	1	23.7#	0.7	0.70	15.0	9.5	***-36.6%***	12.7	***-15.6%***	[81]
Epoxy	3.6	35%	-	1	0	1.0	1.00	15.0	11.7	***-22.1%***	15.6	***4.0%***	[95]
Polyester	4.1	24%	-	1	0	1.0	1.00	12.2	9.6	***-21.2%***	12.4	***1.3%***	[95]
Polyester	3.0	13%	Sliver	1	0	1.0	1.00	10.3	6.0	***-41.7%***	7.4	***-27.9%***	[84]
Polyester	3.0	27%	Sliver	1	0	1.0	1.00	18.6	9.3	***-49.7%***	12.3	***-33.5%***	[84]
Polyester	3.0	31%	Sliver	1	0	1.0	1.00	20.0	10.3	***-48.4%***	13.8	***-31.1%***	[84]
Polyester	3.0	37%	Sliver	1	0	1.0	1.00	23.0	11.8	***-48.6%***	16.0	***-30.4%***	[84]
Polyester	3.0	43%	Sliver	1	0	1.0	1.00	26.7	13.3	***-50.3%***	18.2	***-32.1%***	[84]
Polyester	3.0	16%	Chopped Strand	0.385	0	1.0	0.39	5.2	4.2	***-19.8%***	4.9	***-6.5%***	[85]
Polyester	1.4	45%	Fabric (20x12)	0.625	23.7^	0.7	0.44	7.0	6.1	***-13.4%***	8.3	***18.3%***	[96]
Polyester	1.4	45%	Fabric (20x12)	0.375	23.7^	0.7	0.26	3.5	3.9	***12.7%***	5.3	***50.8%***	[96]
Polyester	4.4	36%	Fabric (22x12)	0.647	23.7^	0.7	0.45	9.0	7.2	***-20.2%***	9.0	***0.2%***	[97]
Polyester	4.4	36%	Fabric (22x12)	0.353	23.7^	0.7	0.25	6.5	5.2	***-20.1%***	6.2	***-4.7%***	[97]
Polyester	2.8	29.5%	-	1	0	0	1	16.8	9.9	***-41.3%***	13.2	***-21.5%***	[98]

* Resin properties taken from Rudd et al [99] for the specific resin / hardener system quoted by Gassan et al [81].

Yarn twist angle was calculated from the specified twist per meter and tex assuming a circular cross-section for the yarn and an average density of 1350 kg/m^3.

^ The yarn twist angle is assumed to be similar to that of yarn used by Gassan et al [81].

5. Conclusion

The jute fibre cross-section was analysed using digital images. The fibre cross-section was modelled using different geometrical shapes (major circle, minor circle, ellipse, super ellipse, convex hull) and the fibre area was estimated for each individual case. The area distribution for each case was determined and it was observed for all the assumed shapes (except for the minor circle) that the area distribution showed a negative skew (the distribution peak shifts toward right) and the maximum peak drops when compared to true area distribution. This negative skew indicates that the method overestimates the fibre area. The drop in distribution peak indicates an increase in the range of the data. Any fibre area calculated using a method that over-estimates the fibre area will always underestimate the modulus and strength of the fibre.

The fibre cross-sectional area calculated assuming an elliptical cross-section gives a lower variation in the fibre area compared to circular cross-section. However, it over estimates the area when compared to true fibre area. Therefore using the ellipse will yield an underestimate of modulus and strength and hence will result in a safer mechanical design when the fibres are used as the reinforcement in a composite. The minimum elliptical area calculated from the two orthogonal projection widths (*A* and *B)* gives the area closest to the true fibre area.

Jute technical fibres from a single batch from South Asia were tested in tension at ten different gauge lengths between 6 mm and 300 mm with 50 or 100 tests at long (100 – 300 mm) or short (6 – 50 mm) gauge lengths respectively. The Young's modulus, strain to failure and ultimate tensile strengths were determined individually. The Young's modulus was found to be ~30 GPa while the strength and fracture strain fall from ~558 to ~153 MPa and ~1.79 to ~0.58 % respectively as the length increases from 6 mm to 300 mm. Weibull distribution parameters have been estimated for each fibre length using the Maximum Likelihood Estimate (MLE) method to quantify the variation. Point estimates, single parameter (standard) and Multiple Data Set (MDS) weak link scaling predictions were assessed using Anderson-Darling Goodness Of Fit Numbers. The author recommends the use of MDS weak link scaling for this problem. The weak link scaling should be performed with at least two points, preferably three and using fibre length at two extreme points and a third point near the mean fibre length.

Two empirical models (a linear and a Natural Logarithmic Interpolation Model (NLIM)) have been successfully developed to characterise the ultimate strength and fracture strain across the entire range of the fibre lengths tested (i.e. 6-300 mm). The logarithmic interpolation model for ultimate strength and fracture strain was found to produce a better fit to the point estimates (at the 10 distinct fibre lengths) than the linear model, but both models produce a better estimation for ultimate strength than for fracture strain. The NLIM produces a significant improvement in predicted properties over the MDS model. Use of Anderson-Darling GOFN confirms this finding and reveals a reduction factor (MDS model GOFN/Logarithmic model GOFN) for this measurement of 2.74 for strength and 2.23 for strain.

The commercial use of natural fibres as reinforcement for composites is constrained by a perceived high variability in strength. An examination of tensile test data from 785 individual tests reveals that the coefficient of variation (CoV) for failure strain is consistently lower than the CoV for fracture stress (strength). Hence, failure strain is the more consistent failure criterion as shown in Figure 39 and Figure 41. The use of optical microscopy to determine fibre "diameter" and hence cross-sectional area may explain this higher variation in strength, as the strength is normally calculated from an assumed Cross-Sectional Area (CSA) which probably is not the true CSA at the fibre fracture. The author recommends the use of failure strain as the key design criterion for natural fibre composites in order to improve reliability in the design of natural fibre reinforced composites.

Well characterised jute fibres have been used to manufacture unidirectional epoxy matrix composites. Three plates were manufactured with natural fibres and clear resin while one plate used dyed fibres in pigmented epoxy resin. The later samples were used for identification of the fibre orientation and fibre volume fraction. The data was successfully used to validate a model for the prediction of moduli and strength.

The tensile modulus and strength of jute fibre reinforced composites manufactured from well characterised fibres was measured experimentally. Six micromechanical models were used to predict the composite elastic modulus. Two micromechanical models were used to predict composite strength. For both mechanical properties, the inclusion of a fibre area correction factor to account for the non-circular cross-section of the fibre resulted in an improved prediction of the respective mechanical properties. For natural fibre composites, the rule of mixtures ($RoM_{||}$) should be

extended to become Equation 47 and the Kelly-Tyson equation should become Equation 48.

The close correlation between the prediction of the elastic modulus and the experimentally measured values suggest that the system chosen is compliant with the assumptions of the rule-of-mixtures. If the fibres are thus well bonded to the matrix, there is probably little benefit to be gained by the various processes being investigated by others for modification of the interface [100]. A well chosen resin system will eliminate the additional chemical/physical processes required for interface modification and hence reduce the cost and environmental burdens arising in the manufacture of natural fibre reinforced polymer matrix composites.

6. Future Work

In order to develop a better understanding of the micromechanics of natural fibre composites, the following future work is recommended:-

- Modelling the individual elementary cells of the technical jute fibres using Voronoi cell to characterise the fibre structure (the shape and area of individual fibre cell). The data can be further used to model the technical fibres to predict the fibre properties and understand the influence of the cell shape and size on the properties.
- The variation in the cross-section along the fibre length should be characterised; this will help to better understand the reason for the variation in the fibre mechanical properties and accurately predict the mechanical properties. It will also validate the applicability of the Fibre Area Correction Factor (FACF). The SkyScan 2011 [88] state-of-the-art x-ray nanotomograph (focal spot size less than 400 nm) would be an appropriate instrument for this task.
- The interface properties of the natural fibres and the matrix should be assessed. The contribution of the variation in the fibre cross-section to the interface strength should be evaluated.
- Measuring the Poisson's ratio of the fibres using optical microscopy would allow comparison of the experimental data for Poisson's ratio of the composite to rule of mixtures predictions.

- Develop a finite element model to predict the natural fibre composite mechanical properties based on the stochastic geometrical and mechanical properties of the individual constituents derived from experiments and compare it with rule of mixture predictions to validate the applicability of the micromechanics to the natural fibre composite.
- Confirm the applicability of strain as the key design criterion for fracture and of the fibre area correction factor, for a wide range of natural fibres and validate the methodology of deriving the composite properties.
- Investigate the use of compatible epoxidised bio-based resin system [101] for "green composites".

References

[1] P A Fowler, J M Hughes and R M Elias, Biocomposites: technology, environmental credentials and market forces, Journal of the Science of Food and Agriculture, 2006, 86 (12), 1781-1789.

[2] C. A. Farnfield and P. J. Alvey, Textile terms and definitions 7th edn, 1975, The Textile Institute, Manchester.

[3] MJ John and S Thomas, Biofibres and biocomposites, Carbohydrate Polymers, 2008, 71(3), 343-364.

[4] C Hill and M Hughes, Natural fibre reinforced composites opportunities and challenges, Journal of Biobased Materials and Bioenergy, 2010, 4, 148-158.

[5] J Summerscales, N Dissanayake, W Hall and AS Virk, A review of bast fibres and their composites. Part 1: fibres as reinforcements, Composites Part A: Applied Science and Manufacturing, 2010, 41 (10), 1329-1335.

[6] J Summerscales, N Dissanayake, W Hall and AS Virk, A review of bast fibres and their composites. Part 2: composites, Composites Part A: Applied Science and Manufacturing, 2010, 41 (10), 1336-1344.

[7] J F V Vincent, Structural Biomaterials, Macmillan, London. ISBN 0-333-26126-7.

[8] NPJ Dissanayake, J Summerscales, SM Grove, and MM Singh, Energy Use in the Production of Flax Fiber for the Reinforcement of Composites, Journal of Natural Fibers, October 2009, 6(4), 331-346.

[9] NPJ Dissanayake, J Summerscales, SM Grove, and MM Singh, Life cycle impact assessment of flax fibre for the reinforcement of composites, Journal of Biobased Materials and Bioenergy, September 2009, 3(3), 245-248.

[10] C Alves, P M C Ferrão, A J Silva, L G Reis, M Freitas, L B Rodrigues and D E Alves, Ecodesign of automotive components making use of natural jute fiber composites, Journal of Cleaner Production, March 2010, 18 (4), 313-327.

[11] 'Textile fibres - Determination of length and length distribution of staple fibres (by measurement of single fibres)' ISO 6989:1981(E).

[12] R C Gonzalez and R E Woods, Digital Image Processing, Prentice Hall, 2007, ISBN 013168728X.

[13] R C Gonzalez, R E Woods and S L Eddins, Digital Image Processing Using Matlab, Prentice Hall, 2004, ISBN 0130085197.

[14] Matlab 2008a, Image Processing Toolbox, http://www.mathworks.com/access/helpdesk/help/toolbox/images/adapthisteq.html

[15] W H Press, S A Teukolsky, W T Vetterling and B P Flannery, Numerical Recipes: The Art of Scientific Computing, Cambridge University Press, 2007, ISBN 0521880688.

[16] M Berg, M Krefeld, M Overmars and O Schwarzkopf, Computational Geometry: Algorithms and Applications, Springer, 2000, ISBN 3540656200.

[17] E W Weisstein, Superellipse, From MathWorld--A Wolfram Web Resource. http://mathworld.wolfram.com/Superellipse.html.

[18] D C Hanselman and B L Littlefield, Mastering MATLAB 7, Prentice Hall, 2004, ISBN 0131430181.

[19] S S Rao, Engineering Optimization: Theory and Practice, John Wiley and Sons, 1996. ISBN 0471550345

[20] 'Filament tensile strength and Modulus', Grafil Test Refrence101.13, Courtaulds Limited, Coventry UK, March 1980.

[21] 'Standard Test Method for Tensile Strength and Young's Modulus for High-Modulus Single-Filament Materials (Withdrawn 1998)', ASTM Standard D3379-75.

[22] P Kittl and G Diáz, Weibull's fracture statistics or probabilistic strength of materials: state of the art, Res Mechanica, 1998, 24 (2), 99-207.

[23] S. van der Zwaag, The concept of filament strength and the Weibull modulus, Journal of Testing and Evaluation, 1989, 17 (5), 292-298.

[24] S B Batdorf, Statistical fracture theories, In SM Lee (editor), International Encyclopedia of Composites volume 6, VCH Publishers, New York, 1991, pages 395-404. ISBN 0-89573-736-1 (v6), ISBN 0-89573-290-4 (set).

[25] SL Phoenix and IJ Beyerlein, Statistical strength theory for fibrous composite materials, Chapter 1.19 in T-W Chou (editor), Volume 1: Fibre Reinforcements and General Theory of Composites, pages 559-639 from A Kelly and C Zweben (editors), Comprehensive Composite Materials, Elsevier, Oxford, 2000. ISBN 0-08-043719-2 (v1), ISBN 0-08-042993-9 (set).

[26] J Andersons, R Joffe, M Hojo, S Ochiai, Glass fibre strength distribution determined by common experimental methods, Composite Science and Technology, 2002, 62 (1), 131-145.

[27] J Andersons, E Sparnins, R Joffe, L Wallstrom, Strength distribution of elementary flax fibres, Composite Science and Technology, 2005, 65 (3-4), 693-702.

[28] Y Paramonov and J Andersons, A family of weakest link models for fibre strength distribution, Composites Part A: Applied Science and Manufacturing, 2007, 38 (4), 1227-1233.

[29] A S Waltson and R L Smith, An examination of statistical theories for fibrous materials in the light of experimental data, Journal of Materials Science, 1985, 20 (9), 3260-3270.

[30] W A Curtin, Tensile strength of fiber-reinforced composites: III. Beyond the traditional Weibull model for fiber strengths, Journal of composite materials, 2000, 34 (15), 1301-1332.

[31] M Lienkamp and P Schwartz, A Monte Carlo simulation of the failure of a seven fiber microcomposite, Composites science and technology, 1993, 46 (2), 139-146.

[32] E A Elsayed, Reliability Engineering, Addison Wesley Longman, 1996 ISBN 0201634813

[33] Life Data Analysis Reference, ReliaSoft Publishing, 2005. Available on-line at: http://www.weibull.com/lifedatawebcontents.htm. (Accessed 22/08/08)

[34] I J Myung, Tutorial on maximum likelihood estimation, Journal of Mathematical Psychology, 2003, 47, 90-100.

[35] A A Griffith, The phenomena of rupture and flow in solids, Philosophical Transactions of the Royal Society of London Series A, 1921, 221, 163-198.

[36] J Nocedal .and S J Wright, Numerical Optimization, Springer, 2006. ISBN 0387303030

[37] J E Dennis and R B Schnabel, Numerical Methods for Unconstrained Optimization and Nonlinear Equations, Society for Industrial Mathematics, 1987. ISBN 0898713641

[38] K L Pickering and T L Murray, Weak link scaling analysis of high-strength carbon fibre, Composites Part A: Applied Science and Manufacturing, 1999, 30 (8), 1017-1021.

[39] K L Pickering, G W Beckerman, S N Alam and N J Foreman, Optimising industrial hemp fibre for composites, Composites Part A: Applied Science and Manufacturing, 2007, 39 (2), 461-468.

[40] R M Rowell and H P Stout, Jute and Kenaf, In: M Lewin and E M Pearce editors, Handbook of Fiber Chemistry, Marcel Dekker Inc. 1998, Chapter 7, ISBN 0824794710

[41] S N Chattopadhyay, N C Pan and A Day, Reuse of reactive dyes for dyeing of jute fabric, January 2006, Bioresource Technology, 97(1), 77-83.

[42] A Milner, The Ashford Book of Dyeing, Unicorn, 1998, ISBN 0908704887

[43] Contrast Ratio <http://www.w3.org/TR/2008/REC-WCAG20-20081211/#contrast-ratiodef> (January 2010).

[44] J P Marques de Sá, Applied Statistics Using SPSS, STATISTICA, MATLAB and R, Springer-Verlag Berlin Heidelberg, 2007, ISBN 978-3-540-71971-7

[45] B T Åström, Manufacturing of Polymer Composites, Chapman & Hall, London, 1997, ISBN 0748770763.

[46] C Williams, J Summerscales and S Grove, Resin Infusion under Flexible Tooling (RIFT): a review, Composites Part A: Applied Science and Manufacturing, 1996, 27A (7), 517–524.

[47] J Summerscales and T J Searle, Review: low pressure (vacuum infusion) techniques for moulding large composite structures, Proceedings of IMechE Part L: Journal of Materials: Design and Applications, 2005, L219 (1), 45–58.

[48] D Cripps, T J Searle and J Summerscales, Open mould techniques for thermoset composites. In: R Talreja and J -A Månson, Editors, Comprehensive Composite Materials Encyclopaedia, Polymer Matrix Composites vol. 2, Elsevier Science, Oxford (2000), 737–761 July, Chapter 21.

[49] M Feiler, W Dudenhausen, L Chatzigeorgiou, Manufacturing of primary aircraft structures with vacuum assisted resin infusion, Society of Manufacturing Engineers ICCM-14, 2003.

[50] Available from: <http://www.mcmc-uk.com/prod-data-sheet/sr-8100-infusion-uk.pdf> (January 2010).

[51] Plastics – Determination of tensile properties. BS EN ISO 527-1:1996.

[52] Plastics – Determination of tensile properties. BS EN ISO 527-4:1996.

[53] Standard test method for tensile properties of polymer matrix composite materials. ASTM Standard D3039-00.

[54] D F Adams, L A Carlsson and R Byron Pipes, Experimental Characterization of Advanced Composite Materials, CRC Press, 2002, ISBN 1587161001

[55] G C Mordan, Adhesives and Installation Techniques, In: A L Window editor, Strain Gauge Technology, Elsevier Applied Science, 1992, Chapter 2, ISBN 1851668640.

[56] K Scott and A Owens, Instrumentation, In: A L Window editor, Strain Gauge Technology, Elsevier Applied Science, 1992, Chapter 5, ISBN 1851668640.

[57] Standard test method for Poisson's ratio at room temperature. ASTM Standard E 132-04.

[58] K Zuiderveld, Contrast Limited Adaptive Histogram Equalization, In: P S Heckbert (editor), Graphic Gems IV, Academic Press Inc., 1994, 474-485.

[59] M W Hyer and A M Waas, Micromechanics of Linear Elastic Continuous Fiber Composites. In: A Kelly and C Zweben (editors), Volume 1: Fibre Reinforcements and General Theory of Composites, Elsevier Science, 2000, 345–375, Chapter 12.

[60] R M Jones, Mechanics of Composite Materials, CRC Press, 1998, ISBN 156032712X.

[61] J C Halpin and S W Tsai, Effect of Environment Factors on Composite Materials, AFML-TR-67-423, 1969.

[62] I M Daniel and O Ishai, Engineering Mechanics of Composite Materials, Oxford University Press, 2005, ISBN 019515097X.

[63] H L Cox, The elasticity and strength of paper and other fibrous materials, British Journal of Applied Physics, 1952, 3 (3), 72-79.

[64] M R Piggott, Load Bearing Fibre Composites, Pergamon Press, 1980.

[65] M J Folkes, Short Fibre Reinforced Thermoplastics, Research Studies Press, 1982.

[66] H Krenchel, Fibre Reinforcement, Akademisk Forlag, 1964.

[67] B Lamy and C Baley, Stiffness prediction of flax fibers-epoxy composite materials, Journal of Materials Science Letters, 1 June 2000, 19(11), 979-980.

[68] E Bodros and C Baley, Study of the tensile properties of stinging nettle fibres (Urtica dioica), Meterials letters, 2008, 62 (14), 2143-2145.

[69] A Kelly and W R Tyson, Tensile Properties of Fibre-Reinforced Metals: Copper/Tungsten and Copper/Molybdenum, Journal of the Mechanics and Physics of Solids, 1965, 13, 329-350.

[70] R T Potter, Strength of Composite, In: A Kelly editor, Concise Encyclopedia of Composite Materials, Pergamon, 1994, ISBN 0080423000.

[71] M Abramowitz and I A Stegun (Eds.). 'Handbook of Mathematical functions: with Formulas, Graphs, and Mathematical Tables', Dover Publications 1965. ISBN 0486612724.

[72] T B L Kirkwood, Geometric Means and Measures of Dispersion, Biometrics, 1979, 35 (4), 908-909.

[73] 'Carbon fibre - Determination of the tensile properties of single-filament specimen' BS ISO 11566:1996.

[74] M Smithson, Statistics and Confidence, SAGE Publication, 2000, ISBN 0761960309.

[75] M A Stephens, Tests Based on EDF Statistics. Goodness-Of-Fit Techniques (ed. M. A. S. Ralph, B. D'Agostino and M. Dekker), 1986, pp. 97-185. ISBN 0824774876.

[76] Z P Xia, J Y Yu, L D Cheng, L F Liu and W M Wang, Study on the breaking strength of jute fibres using modified Weibull distribution, Composites Part A: Applied Science and Manufacturing, 2009, 40(1), 54-59

[77] MK Sridhar, G. Basavarajappa, SG Kasturi and N. Balusubramanian, Evaluation of jute as a reinforcement in composites, Indian journal of textile research, 1982, 7, 87–92.

[78] Kh. M Mannan and M A I Talukder, Characterization of raw, delignified and bleached jute fibres by study of absorption of moisture and some mechanical properties, Polymer, May 1997, 38 (10), 2493-2500.

[79] K Krishnamoorthay, Handbook of Statistical Distribution with Application, Chapman and Hall, 2006, ISBN 1584886358.

[80] W J Roff and J R Scott, Fibres, Films, Plastics and Rubbers: A handbook of common polymers, London Butterworths, 1971, ISBN 040815960X.

[81] J Gassan and A K Bledzki, Possibilities for improving the mechanical properties of jute/epoxy composites by alkali treatment of fibres, Composite science and technology, 1999, 59 (9), 1303-1309.

[82] N Defoirdt, S Biswas, L D Vriese, L Q N Tran, J V Acker, Q Ahsan, L Gorbatikh, A V Vuure, I Verpoest, Assessment of the tensile properties of coir, bamboo and jute fibres, Composites Part A: applied science and manufacturing, 2010, 41 (5), 588-595.

[83] S S Tripathy, L D Landro, D Fontanelli, A Marchetti and G Levita, Mechanical properties of jute fibres and interfacial strength with an epoxy resin, Journal of applied polymer science, 2000, 75 (13), 1585-1596.

[84] P. J. Roe and M. P. Ansell, Jute-reinforced polyester composites, Journal of Materials Science, 1985, 20 (11), 4015-4020.

[85] R. A. Clark and M. P. Ansell, Jute and glass fibre hybrid laminates, Journal of Materials Science, 1986, 21(1), 269-276A K Bledzki and J Gassan, Composites reinforced with cellulose based fibres, Progress in polymer science, 1999, 24(2), 221-274.

[86] XW Xu and K Jayaraman, An image-processing system for the measurement of the dimensions of natural fibre cross-section, International Journal of Computer Applications in Technology, March 2009, 34(2), 115-121.

[87] EPSRC Engineering Instrument Pool - SkyScan 1174 CT Scanner, http://www.eip.rl.ac.uk/sectk.htm, accessed 16:30 on 29 October 2009.

[88] SkyScan2011 x-ray nanotomograph, http://www.skyscan.be/products/2011.htm, accessed 16:38 on 29 October 2009.

[89] EW Weisstein, Variation Coefficient, From MathWorld--A Wolfram Web Resource. http://mathworld.wolfram.com/VariationCoefficient.html, accessed 10:07 on 09 November 2009.

[90] C Baley, Analysis of the flax fibres tensile behaviour and analysis of the tensile stiffness increase, Composite Part A: Applied Science and Manufacturing, 2002, 33 (7), 939-948.

[91] R-B Adusumali, M Reifferscheid and H Weber, T Roeder, H Sixta, W Gindl, Mechanical Properties of Regenerated Cellulose Fibres for Composites, Macromolecular Symposia, 2006, 244(1), 119-125.

[92] S J Eichhorn and R J Young, Composite micromechanics of hemp fibres and epoxy resin microdroplets, Composite Science and Technology, 2004, 64 (5), 767-772.

[93] Y Xue, Y Du, S Elder, K Wang and J Zhang, Temperature and loading rate effects on tensile properties of kenaf bast fiber bundles and composites, Composites Part B: Engineering, 2009, 40(3), 189-196.

[94] I Krucinska, W Zurek and G Egbers, The influence of fibre irregularity on the tensile properties of carbon and glass fibres, Composite Science and Technology, 1995, 54 (2), 169-175.

[95] A N Shah and S C Lakkad, Mechanical properties of jute-reinforced plastics, Fibre Science and Technology, July 1981, 15(1), Pages 41-46.

[96] T M Gowda, A C B Naidu and R Chhaya, Some mechanical properties of untreated jute fabric-reinforced polyester composites, Composites Part A: applied science and manufacturing, 1999, 30 (3), 277-284.

[97] K S Ahmed, S Vijayarangan and A C B Naidu, Elastic properties, notched strength and fracture criterion in untreated woven jute-glass fabric reinforced polyester hybrid composites, Materials and design, 2007, 28 (8), 2287-2294.

[98] P Kumar, Mechanical Behaviour of Jute Fibres and Their Composites, Indian Journal of Technology, 1986, 24 (1), 29-32.

[99] C.D. Rudd, K.N. Kendall, C. Mangin, A.C. Long, Liquid Moulding Technology: A Guide to RTM, SRIM and Related Composites Processing Techniques, Woodhead Publishing, 1997, ISBN 1855732424.

[100] A Hernandez Michelena, W Hall and J Summerscales, A review of bast fibres and their composites. Part 3: the interface, in preparation.

[101] http://www.tech.plym.ac.uk/sme/mats324/suppliers.htm#bioresin

[102] L C Pardini, L G B Manhani, Influence of the testing gauge length on the strength, Young's modulus and Weibull modulus of carbon fibres and glass fibres, Materials Research, 2002, 5 (4), 411-420.

[103] H W Herring, Selected mechanical and physical properties of boron filaments, TN D-3202, NASA, 1966.

[104] A G Metcalf and G K Schmitz, Effect of length on the strength of glass fibres, Proceedings of the ASTM, 1964, 64, 1075-1093.

[105] W J Padgett, S D Durham and A M Mason, Weibull analysis of the strength of carbon fibres using linear and power law models for the length effect, Journal of Composite Materials, 1995, 29 (14), 1873-1884.

[106] N E Zafeiropoulos and C A Baillie, A study of the effect of surface treatments on the tensile strength of flax fibres: Part II. Application of Weibull statistics, Composites Part A: Applied Science and Manufacturing, 2007, 38 (2), 629-638.

[107] L S Sutherland and C G Soares, Review of probabilistic models of the strength of composite materials, Reliability Engineering and System Safety, 1997, 56, 183-196.

[108] G R Baran, J I Mccool, K G Boberick and H Q Zhang, Size effect in resin/glass composite flexure strengths, Journal of Oral Rehabilitation, 1999, 26, 775-780.

[109] B Bohannan, Effect of size on bending strength of wood members, FPL 56, US Forest Service Research Paper, 1966.

[110] J D Barrett, Effect of size on tension perpendicular to grain strength of Douglas-Fir, Wood and Fiber, 1974, 62 (2), 126-143.

[111] S B Batdorf and H L Heinisch, Weakest link theory reformulated for arbitrary fracture criterion, Journal of the American Ceramic Society, 1978, 61 (7-8), 355-358.

Appendices

A: papers published in the course of the research for this doctoral study (on CD ROM)

Appendix A1: A review of bast fibres and their composites. Part 1: fibres as reinforcements
Appendix A2: A review of bast fibres and their composites. Part 2: composites
Appendix A3: Physical characterisation of jute technical fibres: fibre dimensions
Appendix A4: Modelling tensile properties of jute fibres
Appendix A5: Failure strain as the key design criterion for fracture of natural fibre composites
Appendix A6: Multiple data set (MDS) weak-link scaling analysis of jute fibres
Appendix A7: Tensile properties of jute fibres

B: detailed technical annexes

Appendix B1: Maximise the likelihood method
Appendix B2: Confidence bounds on the Weibull parameters
Appendix B3: Anderson-Darling (AD) goodness of fit test
Appendix B4: Coefficient of variation for Weibull Distribution
Appendix B5: Dyeing jute fibres
Appendix B6: Specimen tensile test results
Appendix B7: Specimen axial Poisson's ratio
Appendix B8: Micrograph fibre volume fraction
Appendix B9: Micrograph fibre angle distribution parameters
Appendix B10: Fibre orientation factor calculated from fibre distribution
Appendix B11: Weibull plots of raw data
Appendix B12: Weibull distribution literature survey

Appendix B1: Maximum likelihood Estimate (MLE)

The two-parameter Weibull probability density function (PDF) is:

$$f(\sigma)=\frac{\beta}{\eta}\left(\frac{\sigma}{\eta}\right)^{\beta-1}e^{-\left(\frac{\sigma}{\eta}\right)^{\beta}} \tag{A1}$$

where β is the **shape parameter** (Weibull modulus) and η is the **scale parameter** (characteristic strength or strain).

Experimental results show some observed values are more likely to occur that other values. The *PDF* parameters are therefore estimated to maximise the likelihood of producing the observed experimental data [33].

The Likelihood function for the two-parameter Weibull *PDF* is,

$$L(\sigma|\beta,\eta)=\prod_{r=1}^{n}\left(\frac{\beta}{\eta}\left(\frac{\sigma_r}{\eta}\right)^{\beta-1}e^{-\left(\frac{\sigma_r}{\eta}\right)^{\beta}}\right) \tag{A2}$$

For computational convenience the log-likelihood function is used [32, 33],

$$\Lambda=n\times\ln\left(\frac{\beta}{\eta}\right)+\sum_{r=1}^{n}\ln\left(\frac{\sigma_r}{\eta}\right)^{\beta-1}-\sum_{r=1}^{n}\left(\frac{\sigma_r}{\eta}\right)^{\beta} \tag{A3}$$

The Weibull parameters are estimated by maximising the log-likelihood function using Newton's method [19, 36, 37]. The partial derivatives of Equation A3 are set equal to zero, namely,

$$\left\{\frac{\partial\Lambda}{\partial x_j}\right\}=0, \qquad x_j=\beta,\eta \tag{A4}$$

Using Taylor's series expansion we get Equation A5 [19], which can be iteratively solved for shape and scale parameter until convergence criterion is met.

$$[J_i]\{X_{i+1}\}=-\left\{\frac{\partial\Lambda_i}{\partial x_j}\right\}+[J_i]\{X_i\} \qquad x_j=\beta,\eta \tag{A5}$$

where, $[J_i]$ is the matrix of second partial derivatives (Hessian matrix) of the log-likelihood function. $\{X_i\}$ and $\{X_{i+1}\}$ are the initial and final vectors of the Weibull parameters.

$$\left\{\frac{\partial\Lambda_i}{\partial x_j}\right\} \tag{A6}$$

is vector of values of partial derivatives of the log-likelihood function for the initial value of Weibull parameters.

Appendix B2: Confidence bounds on the Weibull parameters

Confidence intervals characterise a range within which the point estimates of the Weibull parameters are likely to occur a given percentage of time [32, 74]. The uncertainty about the parameters is given by the confidence width (upper – lower estimate) of the parameters. A wide interval may suggest that more samples need to be tested to get improved estimates of the parameters [74]. Herein, The Weibull Fisher Matrix method [32, 33] is used to estimate the confidence bounds. The lower and upper bounds on the point estimates of the Weibull parameters are calculated using,

$$\beta_U = \beta \times \exp\left(\frac{z\sqrt{Var(\beta)}}{\beta}\right) \qquad \beta_L = \frac{\beta}{\exp\left(\frac{z\sqrt{Var(\beta)}}{\beta}\right)}$$

$$\eta_U = \eta \times \exp\left(\frac{z\sqrt{Var(\eta)}}{\eta}\right) \qquad \eta_L = \frac{\eta}{\exp\left(\frac{z\sqrt{Var(\eta)}}{\eta}\right)} \tag{A7}$$

For two sided confidence bound z is given by,

$$\frac{1-\delta}{2} = \frac{1}{\sqrt{2\pi}}\int_z^\infty e^{\frac{-t^2}{2}}dt = 1-\Phi(z) \tag{A8}$$

Where δ is the confidence level, subscript U and L identify the upper and lower bound for the Weibull parameters respectively, and β, and η are estimated Weibull parameters. The variance and covariance of Weibull parameters are estimated from the inverse of Fisher matrix [32, 33], namely

$$\begin{pmatrix} Var(\beta) & Cov(\eta,\beta) \\ Cov(\beta,\eta) & Var(\eta) \end{pmatrix} = \begin{pmatrix} -\frac{\partial^2\Lambda}{\partial\beta^2} & -\frac{\partial^2\Lambda}{\partial\eta\partial\beta} \\ -\frac{\partial^2\Lambda}{\partial\beta\partial\eta} & -\frac{\partial^2\Lambda}{\partial\eta^2} \end{pmatrix}^{-1} \tag{A9}$$

Appendix B3: Anderson-Darling (AD) goodness of fit test

The Anderson-Darling Goodness Of Fit Number (GOFN) is used to examine the fit of experimental data to the calculated Weibull distributions at each fibre length (point estimates).

The Anderson Darling GOFN number A, is calculated using Equation A10 [75], viz

$$A^2 = -n - (1/n)\sum_{i=1}^{n}(2i-1)\left[\ln(Z_i) + \ln(1 - Z_{n+1-i})\right] \quad \text{(A10)}$$

where, n is the number of samples and for a standard Weibull distribution Zi is,

$$Z_i = 1 - \exp\left\{-\left(\frac{\sigma_i}{\eta}\right)^{\beta}\right\} \quad \text{(A11)}$$

or for a Weibull distribution with weak link scaling Zi is,

$$Z_i = 1 - \exp\left\{-\frac{l}{l_0}\left(\frac{\sigma_i}{\eta}\right)^{\beta}\right\} \quad \text{(A12)}$$

In Equation A11 and A12, σ is the vector of experimental observation in ascending order.

Appendix B4: Coefficient of variation for Weibull Distribution

The mean of Weibull distribution is given by Equation A13 [33],

$$\mu = \eta \cdot \Gamma\left(\frac{1}{\beta}+1\right) \tag{A13}$$

where, η is the scale parameter and β is shape parameter. Γ is gamma function given by Equation A14.

$$\Gamma(n) = \int_0^\infty e^{-x} x^{n-1} dx \tag{A14}$$

The standard deviation of Weibull distribution is given by Equation A15 [33]

$$\sigma = \eta \cdot \sqrt{\Gamma\left(\frac{2}{\beta}+1\right) - \Gamma\left(\frac{1}{\beta}+1\right)^2} \tag{A15}$$

CoV for Weibull distribution is calculated by substituting equation of mean and standard deviation from Equation A13 and A15 respectively in Equation 52.

$$CoV = \frac{\sqrt{\Gamma\left(\frac{2}{\beta}+1\right) - \Gamma\left(\frac{1}{\beta}+1\right)^2}}{\Gamma\left(\frac{1}{\beta}+1\right)} \tag{A16}$$

Appendix B5: Dyeing jute fibres

Dry jute fibres were first weighed (75 grams) and then soaked in water for 15 minutes. The dye pot was prepared by adding warm water (45 °C) in plastic container using water to fibre ratio of 30:1 by weight. The dye power was mixed with cold water to make a smooth paste, which was then diluted and completely dissolved in the dye bath. Ratio of 1:25 was used for dye powder weight (3 grams) to fibre weight. The wetted jute fibres were added to the dye bath and stirred for 10 minutes. Glauber's salt (sodium sulphate) was then added to the dye bath in 3 equal parts at 5 minute intervals. The fibres were removed from the bath while adding Glauber's salt to the bath to properly mix the salt in the bath. After mixing the salt the fibres were again immersed in the bath. The weight ratio of 1.1:1 was used for the Glauber's salt (82.5 grams) to fibre. Dye was fixed to the fibres by adding soda ash (sodium carbonate) to the dye bath 10% weight of soda (7.5 grams) to fibre weight was used. The soda ash was dissolved in small quantity of warm water and then added to the dye bath (fibres were removed from the bath while soda ash solution was added). The fibres were left in the solution for 2 hours and the solution was stirred occasionally. After that, fibres were rinsed in cold water and were dried for 12 hours in warm air. While dyeing the fibres due care was taken to ensure minimum disturbance to the original fibre orientation.

Appendix B6: Specimen tensile test results

The specimen dimension, the tensile test results and the failure location for each specimen which failed within the gauge length are given in Table A.

Table A: Specimen tensile test results

Sample	*Width [mm]*	*Thickness [mm]*	*Modulus [GPa]*	*Strength [MPa]*	*Failure Strain [%]*	*Failure Location*
2c	25.23	2.91	9.19	131.1	1.61%	LGM
2d	25.21	3.57	6.70	88.3	1.42%	LGM
3e	25.39	4.42	8.89	98.4	1.20%	LGM
4b	25.05	2.97	6.90	92.6	1.41%	LGM
4c	25.22	3.04	7.90	94.6	1.24%	LGT
5a	25.14	3.15	8.98	104.9	1.26%	LGM
5b	25.16	3.44	8.04	-	-	LAT
5c	25.02	3.61	8.28	99.6	1.29%	LGM
5d	25.06	3.67	7.79	106.8	1.40%	LGB
5e	24.87	3.59	7.33	94.8	1.41%	LGM
5f	25.03	3.67	8.70	94.2	1.15%	LGT

LGM – **L**ateral failure in **G**auge length at **M**iddle of the gauge length.

LGT/B – Lateral failure in **G**auge length at **T**op/**B**ottom end of the gauge length.

LAT – **L**ateral failure **A**t tab near **T**op end.

Appendix B7: Specimen axial Poisson's ratio

The axial Poisson's ratio calculated for each specimen from the axial and transverse strain measured using strain gauges bonded on the opposite faces of the specimen is given in Table B.

Table B: Specimen axial Poisson's ratio

Sample	*Strain Gauge 1*	*Strain Gauge 2*	*Average*
2d	0.42*	-	-
3a	0.42	0.43	0.43
3b	0.38	0.42	0.40
3c	0.44	0.40	0.42
3e	0.38	0.46	0.42
3f	0.44	0.43	0.43
4a	0.43	0.49	0.46
4b	0.40	0.41	0.40
4d	0.45	0.39	0.42
4e	0.48	0.36	0.42
4f	0.44	0.41	0.43
5a	0.33	0.51	0.42
5b	0.43	0.38	0.40
5c	0.43	0.40	0.42
5d	0.39*	-	-
5e	0.48	0.40	0.44

*only one strain gauge reading was available therefore it was not included to calculate mean Poisson's ratio

Appendix B8: Micrograph fibre volume fraction

The estimated fibre volume fractions for each micrograph for each specimen are given in Table C.

Table C: Micrograph fibre volume fraction

	Sample No.					
Micrograph No.	***5a***	***5b***	***5c***	***5d***	***5e***	***5f***
1	15.94%	18.66%	22.97%	18.01%	20.15%	13.65%
2	15.41%	17.88%	15.24%	10.86%	14.38%	16.49%
3	21.93%	19.90%	17.29%	20.87%	22.41%	26.34%
4	14.46%	13.96%	20.55%	28.54%	16.01%	16.55%
5	19.69%	19.05%	25.71%	25.08%	15.92%	13.85%
6	-	19.01%	20.17%	22.03%	19.40%	23.87%

Appendix B9: Micrograph fibre angle

Note: that deviation from the intended direction is taken as a positive number as this better reflects the waviness of the fibres than reporting an average of angles with both positive and negative signs. In practice a positive angle viewed from the front will be a negative angle if viewed from back.

Table D: Micrograph fibre angle

Sample	*5a*		*5b*		*5c*		*5d*		*5e*		*5f*	
Micrograph No.	*Mean*	*SD*	*Mean*	*SD*	*Mean*	*SD*	*Mean*	*SD*	*Mean*	*SD*	*Mean*	*SD*
1	4.85	15.46	1.39	26.96	13.16	14.98	12.25	14.64	5.66	17.96	10.23	21.05
2	0.30	16.32	10.21	30.35	3.43	23.37	10.22	23.01	3.17	15.05	8.42	15.74
3	9.02	12.72	1.42	33.66	18.03	14.84	6.90	17.93	8.94	14.61	11.57	11.25
4	8.92	14.03	13.13	23.88	1.34	26.74	1.13	12.91	7.89	14.72	3.10	21.21
5	2.77	12.73	3.64	26.82	13.72	18.42	7.01	13.24	4.64	12.98	5.29	12.02
6	8.48	20.65	9.41	19.87	16.69	12.18	12.04	10.81	4.56	16.68	9.26	16.87
7	-	-	12.53	31.21	1.01	11.94	4.94	12.21	10.03	14.28	3.30	9.60
8	-	-	6.38	24.81	16.78	25.01	8.74	15.68	4.59	22.46	1.55	16.96

Appendix B10: Fibre orientation distribution factors

Table E: Micrograph fibre orientation distribution factors

	Sample No.					
Micrograph No.	***5a***	***5b***	***5c***	***5d***	***5e***	***5f***
1	0.87	0.72	0.81	0.82	0.83	0.76
2	0.87	0.65	0.76	0.74	0.88	0.84
3	0.87	0.63	0.75	0.82	0.85	0.86
4	0.86	0.71	0.72	0.91	0.86	0.79
5	0.91	0.72	0.77	0.88	0.90	0.91
6	0.78	0.78	0.79	0.86	0.85	0.82
7	-	0.63	0.92	0.91	0.85	0.94
8	-	0.74	0.67	0.84	0.77	0.86

Appendix B11: Weibull plots of raw data

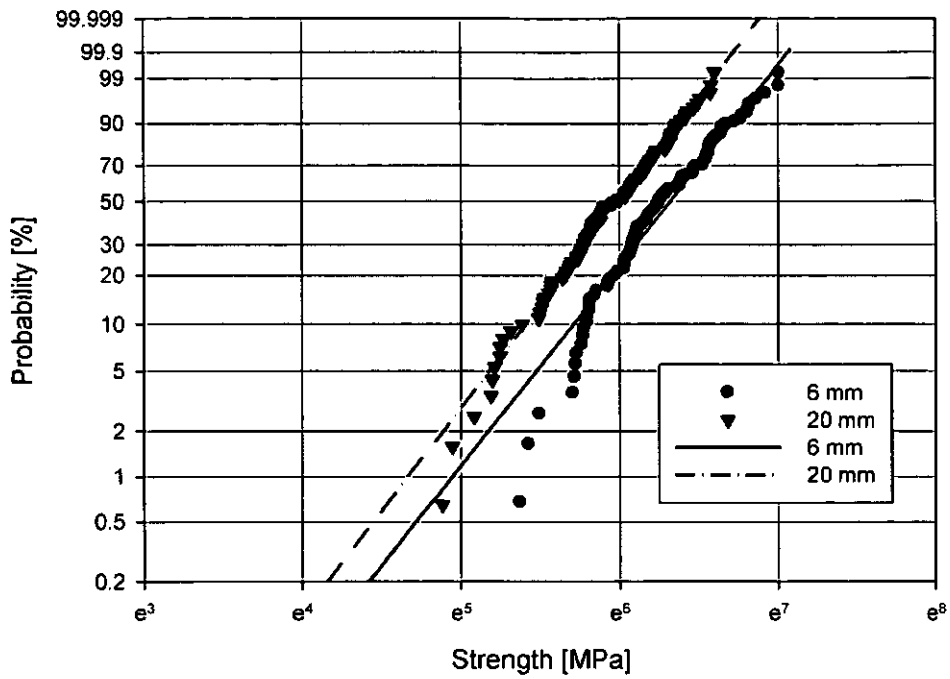

(a)

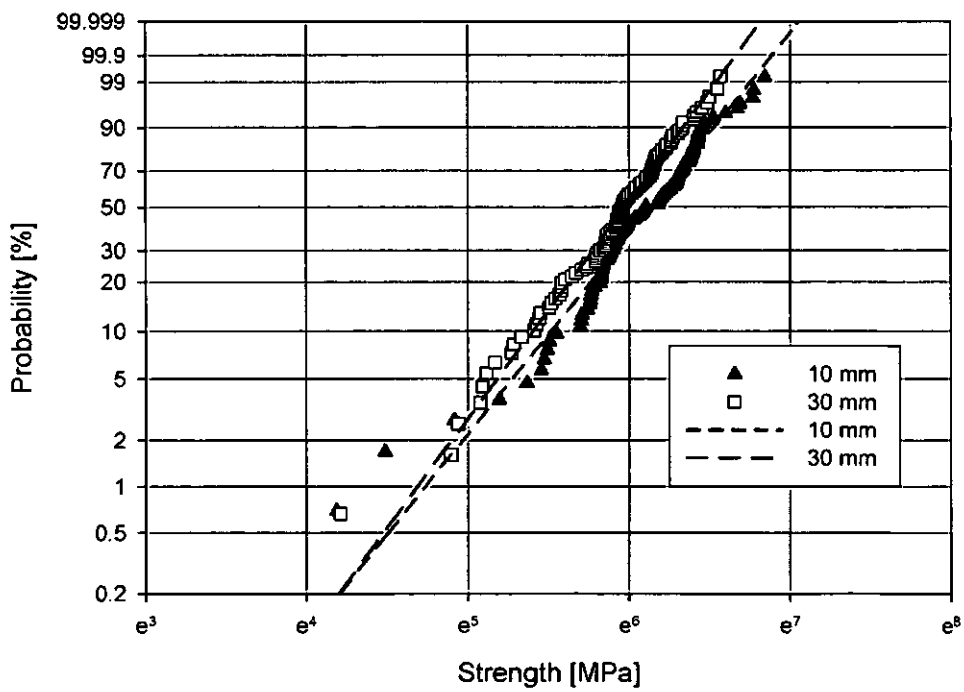

(b)

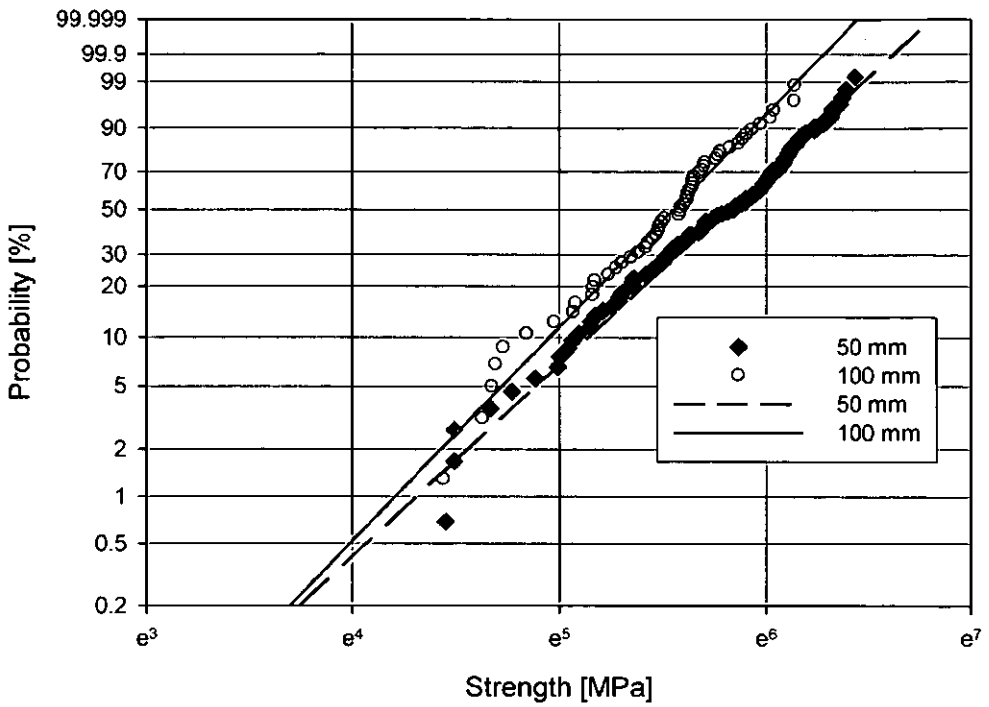
99.999
99.9
99
90
70
50
30
20
10
5
2
1
0.5
0.2
Probability [%]
e3
e4
e5
e6
e7
Strength [MPa]
50 mm
100 mm
50 mm
100 mm

(c)

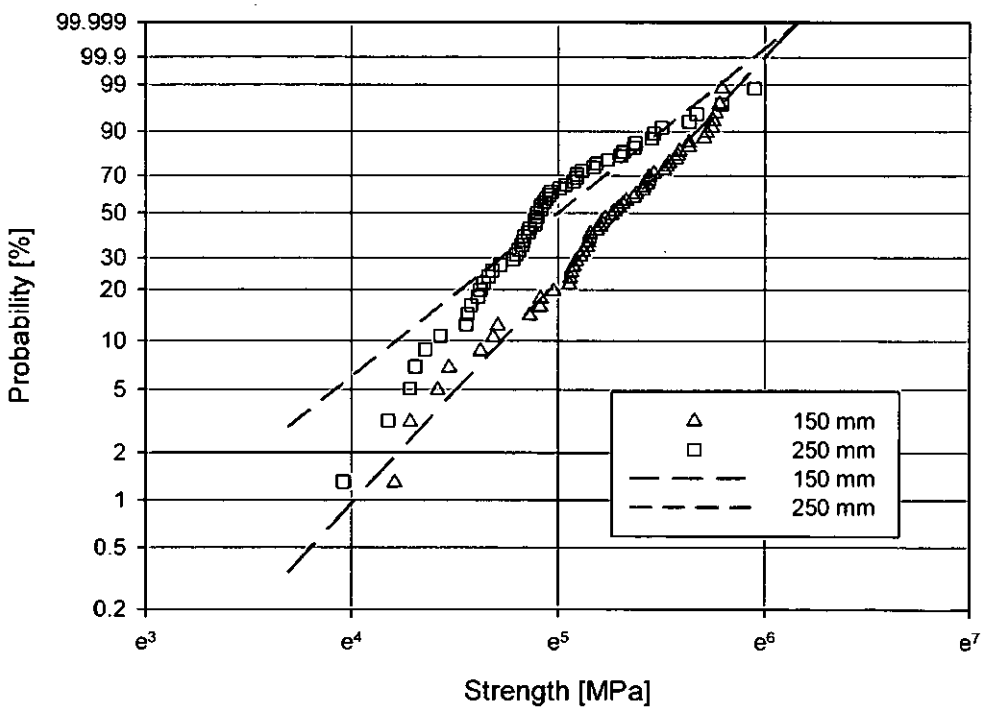
99.999
99.9
99
90
70
50
30
20
10
5
2
1
0.5
0.2
Probability [%]
e3
e4
e5
e6
e7
Strength [MPa]
150 mm
250 mm
150 mm
250 mm

(d)

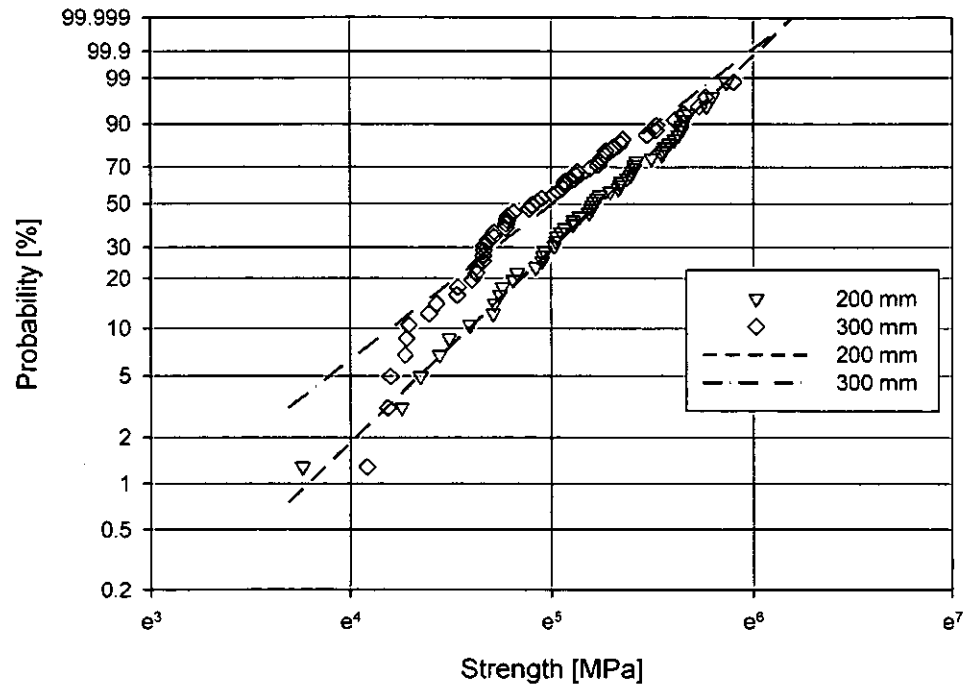

(e)

Figure B - 1: Weibull plots for fibre strength, (a) 6 – 20 mm, (b) 10 – 30 mm, (c) 50 – 100 mm, (d) 150 – 250 mm, (e) 200 – 300 mm

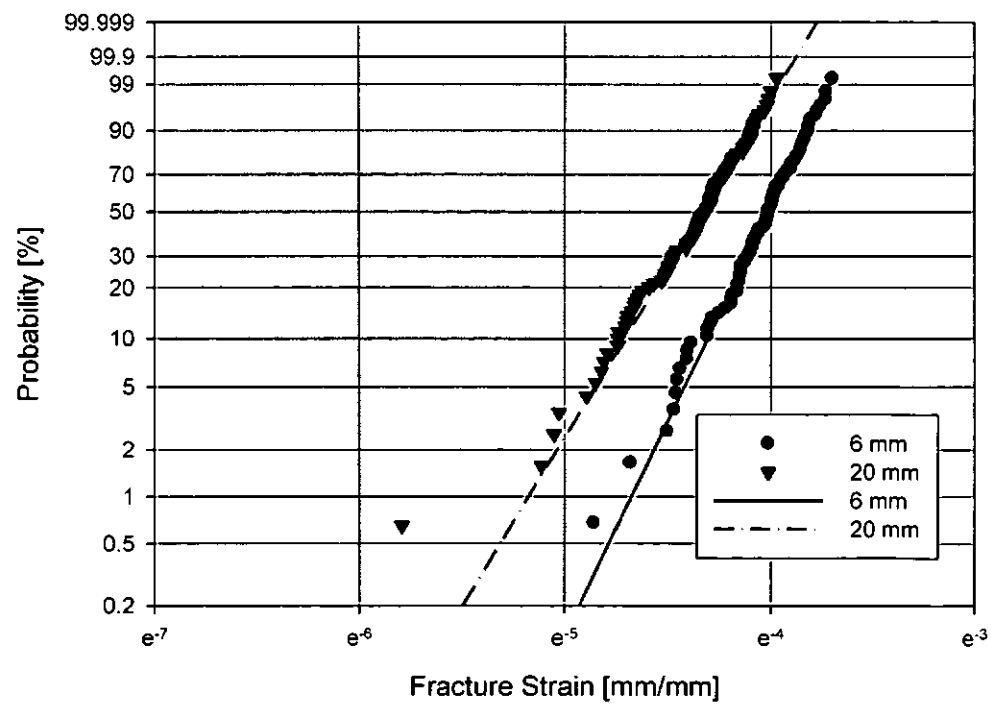

(a)

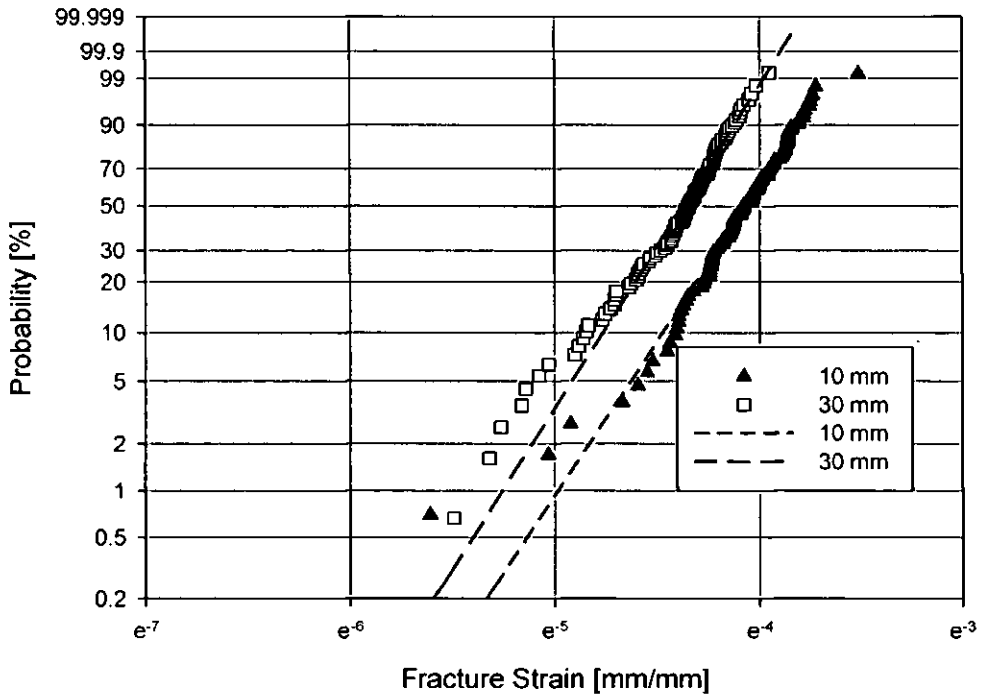
99.999
99.9
99
90
70
50
30
20
10
5
2
1
0.5
0.2
Probability [%]
e-7
e-6
e-5
e-4
e-3
Fracture Strain [mm/mm]
10 mm
30 mm
10 mm
30 mm

(b)

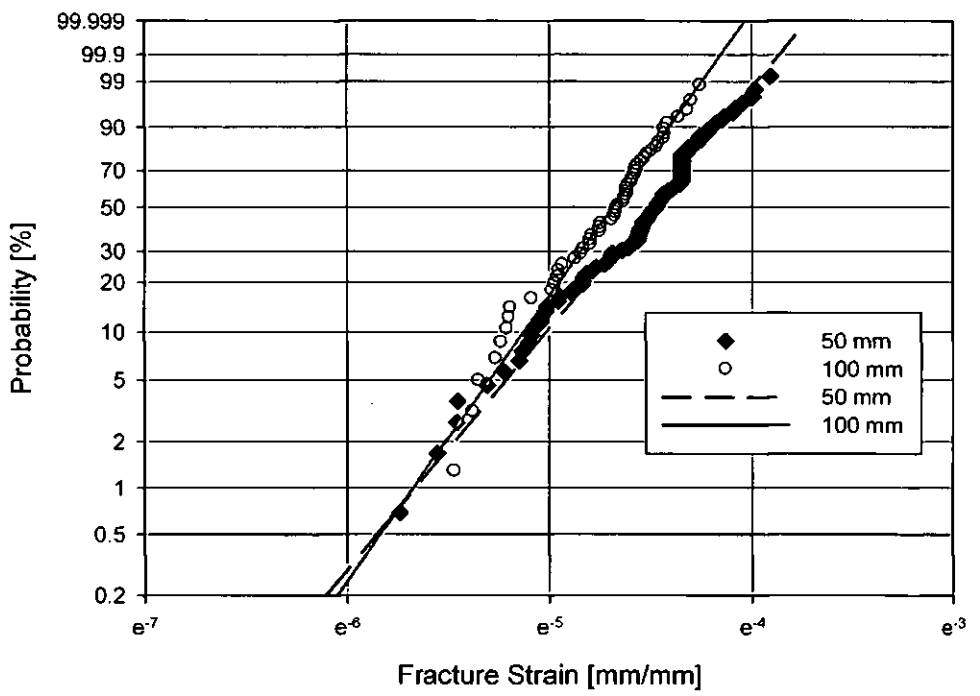
99.999
99.9
99
90
70
50
30
20
10
5
2
1
0.5
0.2
Probability [%]
e-7
e-6
e-5
e-4
e-3
Fracture Strain [mm/mm]
50 mm
100 mm
50 mm
100 mm

(c)

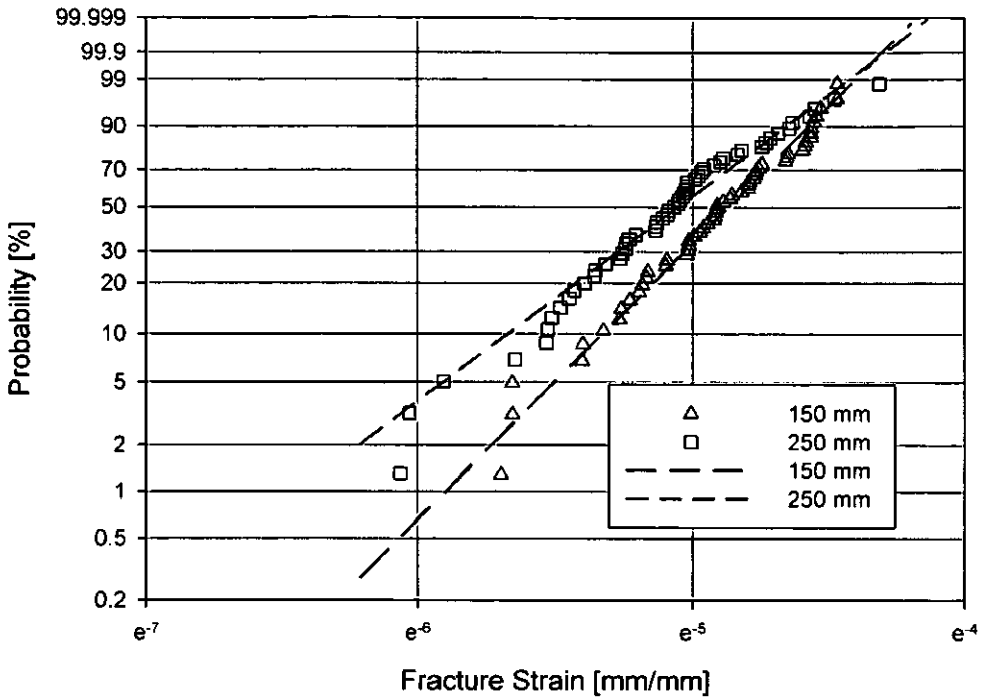

(d)

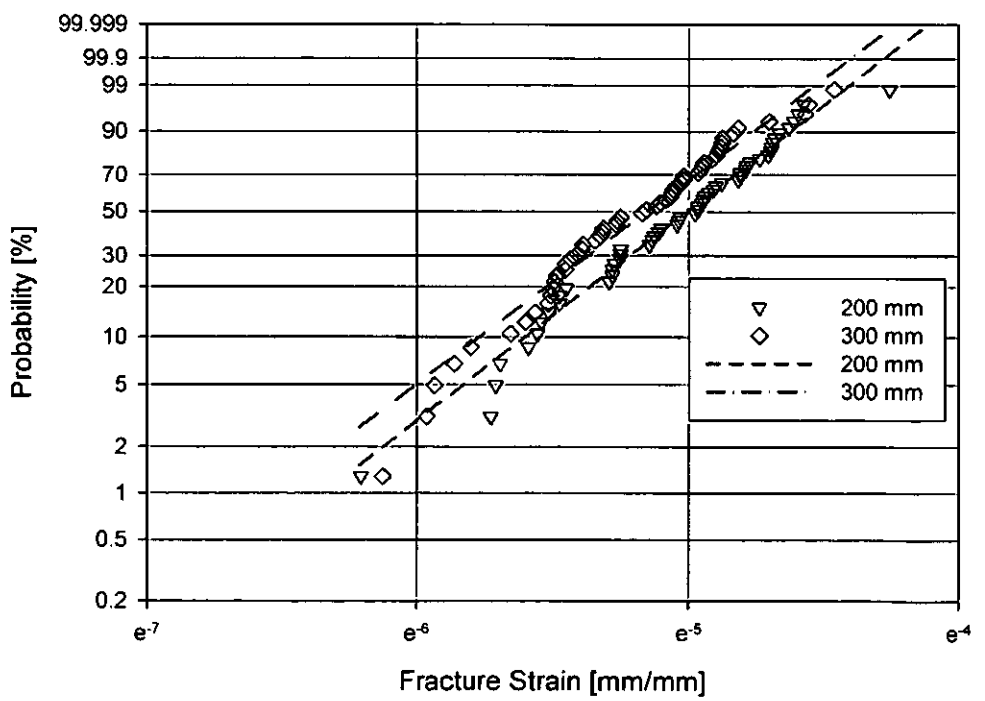

(e)

Figure B - 2: Weibull plots for fibre fracture strain, (a) 6 – 20 mm, (b) 10 – 30 mm, (c) 50 – 100 mm, (d) 150 – 250 mm, (e) 200 – 300 mm

Appendix B12: Weibull distribution literature survey

The probabilistic strength of a material is defined as the loading (stress/strain) which will lead to the failure of the material under normal environmental conditions for a given probability (relative frequency of occurrence). The probabilistic strength of a material is obtained by repeating identical experiments to generate a data set of the strength which is used to estimate the distribution parameters and then the probability of failure is derived from the distribution.

The Weibull distribution is widely used to model diverse life (failure) behaviours and to quantify the spread in the failure indicators of the tested subject (material, system, composite, etc) [32, 33]. Depending on the values of the Weibull distribution parameters (the shape parameter, β, and the scale parameter, η) the Probability Distribution Function (*PDF*) assumes different characteristic shapes to model different reliability and the failure rate. The general form of Weibull distribution *CDF* is given by Equation A17,

$$F(\sigma) = 1 - e^{-\left(\frac{\sigma}{\eta}\right)^{\beta}} \qquad \text{(A17)}$$

where β is the shape parameter (Weibull modulus), η is the scale parameter (characteristic failure limit) and σ is measured failure limit.

The composite reinforcement fibres exhibit high variability in the mechanical properties therefore to quantify the variation the probabilistic strength or fracture strain of synthetic [26, 38, 102-105] and natural fibres [27, 39, 68, 76, 82, 106] is modelled using the Weibull distribution. The probabilistic strength or fracture strain models developed for the reinforcement fibres have been further used to predict the composite strength [25, 107].

The Weibull distribution has been used to quantify the variation in the strength of the composite due to size effect i.e. the larger specimen will have lower fracture strength than a smaller specimen [108]. The same concept (size effect) has been used to model the strength of wood with Weibull distribution [109, 110].

The Weibull statistical fracture theory is also used to predict the probability of failure for a random stress state when failure statistics are known for a particular stress state (e.g. tension) [22, 24, 111]. The probabilistic theories are used to predict the strength of material/structure while performing safety assessment of a system.

There are different variations of the Weibull distribution models available to represent a number of physical problems. Weak-Link scaling [27] is one of the modified Weibull distributions which consider the deviation from the experimental tested size (length or volume) of the material to give the probability of failure at a specified size for a given load. The theory assumes that the total volume of the part/system can be conceptually divided into many volume elements and each volume has a small probability of failure and the probability of failure of the part as a whole is calculated by multiplying probability of survival of each element [104, 111]. Thus, a larger volume will have a lower probability of survival on average. The *CDF* of Weibull distribution with Weak-Link Scaling is given by Equation A18,

$$F(\sigma) = 1 - e^{-\frac{l}{l_0}\left(\frac{\sigma}{\eta_w}\right)^{\beta}} \tag{A18}$$

where η_w is the scale parameter (characteristic failure limit) for the Weibull distribution with weak link scaling, l is the designated size and l_0 is the reference size. For simplicity, the reference size is generally normalised to 1.

The Weak-Link scaling model does not always represent/quantify the experimental observations [29, 38, 105] therefore linear and power laws model were proposed by Padgett et al [105] to capture the effect of fibre gauge length on tensile strength. The scale parameter was assumed to be a function of fibre gauge length and the modified Weibull distribution function is given by Equation A19 and A20 for power law and linear model respectively,

$$F(\sigma) = 1 - e^{-l^{\gamma}\left(\frac{\sigma}{\eta_w}\right)^{\beta}} \tag{A19}$$

$$F(\sigma) = 1 - e^{-(l+\gamma)\left(\frac{\sigma}{\eta_w}\right)^{\beta}} \tag{A20}$$

Where l is the fibre gauge length and γ is a fitting parameter.

The Weibull distribution parameters for the model were estimated by maximum likelihood method [34, 105].

The Weibull distribution parameters are estimated using linear regression or maximum likelihood method [32-34]. Most authors [27, 102] use linear regression method as it is simple. The Weibull distribution parameters are estimated by rearranging Equation A17 to get Equation A21,

$$\ln\left(-\ln\left(1-F(\sigma)\right)\right) = \beta\ln\sigma - \beta\ln\eta \tag{A21}$$

The Equation A21 is in the form of,

$$y = bx - a \tag{A22}$$

Where,

$$y = \ln\left(-\ln\left(1 - F(\sigma)\right)\right)$$

$$b = \beta$$

$$a = \beta \ln \eta$$

Hence, the Weibull distribution parameters can be obtained from the plot of '*y*' against natural-logarithm of 'σ' failure limit. The $F(\sigma)$ is calculated using the medial rank position [27, 33] of the data points given by Equation A23.

$$MR = \frac{i - 0.3}{N + 0.4} \tag{A23}$$

Where, *i* is the failure order and *N* is the total number of samples.

The Weibull parameters are estimated from the slope and intercept of the plot using linear regression method.

The maximum likelihood method estimates the distribution parameters by maximizing the likelihood function based on the given data set [34]. Maximum likelihood method can be used to fit complex statistical models and error (or confidence) bound can be calculated for the distribution parameters [29]. Therefore maximum likelihood method was used to estimate Weibull distribution parameters for MDS weak-link scaling and the empirical model developed in section 2.3.3 and 2.3.4 respectively. The parameter estimation by maximum likelihood method is detailed in Appendix B1.

Zafeiropoulos and Baillie [106] in their work on flax fibres have shown that linear regression and maximum likelihood method give similar distribution parameters.